

DOE/MC/08383-26

**WELL TEST REPORT AND CO₂ INJECTION PLAN FOR THE LITTLE KNIFE
FIELD CO₂ MINITEST, BILLINGS COUNTY, NORTH DAKOTA**

**First Annual Report
September 1979—August 1980**

Work Performed for the Department of Energy
Under Contract No. DE-AC21-79MC08383

Date Published—November 1981

Gulf Oil Exploration and Production Company
Oklahoma City, Oklahoma



**National Energy Technology Laboratory
National Petroleum Technology Office
U.S. DEPARTMENT OF ENERGY
Tulsa, Oklahoma**

DISCLAIMER

This report was prepared as an account of work sponsored by an agency of the United States Government. Neither the United States Government nor any agency thereof, nor any of their employees, makes any warranty, expressed or implied, or assumes any legal liability or responsibility for the accuracy, completeness, or usefulness of any information, apparatus, product, or process disclosed, or represents that its use would not infringe privately owned rights. Reference herein to any specific commercial product, process, or service by trade name, trademark, manufacturer, or otherwise does not necessarily constitute or imply its endorsement, recommendation, or favoring by the United States Government or any agency thereof. The views and opinions of authors expressed herein do not necessarily state or reflect those of the United States Government.

This report has been reproduced directly from the best available copy.

**WELL TEST REPORT AND CO₂ INJECTION PLAN
FOR THE LITTLE KNIFE FIELD CO₂ MINITEST
BILLINGS COUNTY, NORTH DAKOTA**

**First Annual Report
September 1979—August 1980**

James E. Upton, *Principal Investigator*
Gulf Oil Exploration and Production Company
American First Tower
101 N. Robinson
P.O. Box 24100
Oklahoma City, Oklahoma 73124

John S. Miller, *Technical Project Officer*
Bartlesville Energy Technology Center
P.O. Box 1398
Bartlesville, Oklahoma 74005

Work Performed for the Department of Energy
Under Contract No. DE-AC21-79MC08383

Date Published—November 1981

UNITED STATES DEPARTMENT OF ENERGY

TABLE OF CONTENTS

	<u>Page</u>
ABSTRACT.....	1
HISTORY OF PROJECT.....	1
INTRODUCTION.....	2
DRILLING, COMPLETION, AND WELL TESTING PROCEDURES.....	3
Zabolotny Injection Well No. 1.....	3
Observation Wells.....	7
Zabolotny Observation Well No. 1.....	7
Zabolotny Observation Well No. 2.....	10
Zabolotny Observation Well No. 3.....	11
FOUR WELL MULTI-WELL PULSE TEST.....	13
RESERVOIR GEOLOGY.....	15
Lithology.....	15
Reservoir General.....	17
Reservoir Specific.....	17
Structure.....	18
Pore and Throat System.....	19
EQUIPMENT AND INSTRUMENTATION.....	21
CO ₂ Injection System.....	21
Water Injection System.....	22
Fluid Sampling System.....	22
SIMULATION MODELS.....	23
CO ₂ -WATER INJECTION SCHEME.....	23
SCHEDULE.....	26
ACKNOWLEDGEMENTS.....	26
REFERENCES.....	27

LIST OF FIGURES

	<u>Page</u>
Figure 1	Index map of the Williston Basin.....29
Figure 2	Top of Mission Canyon Formation structure map.....30
Figure 3	Little Knife CO ₂ minitest pattern.....31
Figure 4	Little Knife CO ₂ minitest location.....32
Figure 5	Casing and tubing settings in injection well no. 1.....33
Figure 6	Pressure history curve for injection well no. 1.....34
Figure 7	Modified tubing setting in injection well no. 1.....35
Figure 8	Wellhead schematic of injection well no. 1.....36
Figure 9	Wellhead schematic of observation wells.....37
Figure 10	Casing and tubing setting in observation well no. 1.....38
Figure 11	Pressure history curve for observation well no. 1.....39
Figure 12	Casing and tubing settings in observation well no. 2.....40
Figure 13	Pressure history curve for observation well no. 2.....41
Figure 14	Casing and tubing settings in observation well no. 3.....42
Figure 15	Pressure history curve for observation well no. 3.....43
Figure 16	Four well multi-well pulse test response at observation well no. 1.....44
Figure 17	Four well multi-well pulse test response at observation well no. 2.....45
Figure 18	Four well multi-well pulse test response at observation well no. 3.....46
Figure 19	Idealized depositional setting of Mission Canyon Formation at Little Knife Field.....47
Figure 20	Injection well no. 1 sonic log.....48
Figure 21	North-south structural fence diagram of zones A, B, C and D of the Mission Canyon Formation through cored wells in Little Knife Field.....49
Figure 22	Type log of Mission Canyon Formation at Little Knife Field.....50

LIST OF FIGURES

	<u>Page</u>
Figure 23	Stratigraphic fence diagram of zones C and D of the Mission Canyon Formation through all minitest wells..... 51
Figure 24	Close-up view of the reservoir rock in the Little Knife CO ₂ minitest..... 52
Figure 25	Photomicrographs of the reservoir rock in the Little Knife CO ₂ minitest in injection well no. 1..... 53
Figure 26	Photomicrographs of the reservoir rock in the Little Knife CO ₂ minitest in observation well no. 1..... 55
Figure 27	Photomicrographs of the reservoir rock in the Little Knife CO ₂ minitest in observation well no. 2..... 56
Figure 28	Core slabs of minitest reservoir rock from injection well no. 1 (9,817-9,819 feet)..... 58
Figure 29	Whole core porosity and permeability compared to lithology in each minitest well..... 59
Figure 30	Surface lineaments mapped throughout portions of Montana, western North Dakota and northwesternmost South Dakota..... 60
Figure 31	Surface lineaments from landsat photographs and aerial photographs in central and northern portions of Little Knife Field..... 61
Figure 32	Aerial view of nearest surface lineament next to the Little Knife CO ₂ minitest..... 62
Figure 33	Surface outcrop fractures measured at observation well no. 3..... 63
Figure 34	Fractures measured from oriented cores in the minitest project interval..... 64
Figure 35	Blocks of Sentinel Butte Formation illustrating surface fracture separation..... 65
Figure 36	Outcroppings of Sentinel Butte Formation, at observation well no. 3, where surface fracture strike directions and fracture separations were measured..... 66
Figure 37	Generalized illustration representing the average trends of fractures, not individual fractures, through the minitest area..... 67

LIST OF FIGURES

	<u>Page</u>
Figure 38	Generalized illustration of the various pore types and associated throats in porous beds of Mission Canyon Formation.....68
Figure 39	Scanning electron micrographs (SEM) of relief pore casts from porous beds of Mission Canyon Formation at Little Knife Field.....69
Figure 40	Average calculated pore throat radii and percent of throats, from core analysis, across the perforated interval in injection well no. 1.....70
Figure 41	Average calculated pore throat radii and percent of throats, from core analysis, across the perforated interval in observation well no. 1.....71
Figure 42	Average calculated pore throat radii and percent of throats, from core analysis, across the perforated interval in observation well no. 2.....72
Figure 43	Average calculated pore throat radii and percent of throats, from core analysis, across the perforated interval in observation well no. 3.....73
Figure 44	Pore-to-throat size ratios and pore-to-throat coordination numbers for porous beds of the Mission Canyon Formation.....74
Figure 45	Representative individual samples of pore throat radii and percent of throats compared to the amount of porosity and permeability developed in injection well no. 1.....76
Figure 46	Representative individual samples of pore throat radii and percent of throats compared to the amount of porosity and permeability that is developed in observation well no. 1.....77
Figure 47	Representative individual samples of pore throat radii and percent of throats compared to the amount of porosity and permeability that is developed in observation well no. 2.....78
Figure 48	Representative individual samples of pore throat radii and percent of throats compared to the amount of porosity and permeability that is developed in observation well no. 3.....79
Figure 49	Layout of surface equipment at the Little Knife CO ₂ minitest site.....80

LIST OF FIGURES

	<u>Page</u>
Figure 50 CO ₂ injection system for the Little Knife CO ₂ minitest.....	81
Figure 51 Zabolotny Injection Well No. 1 looking to the west.....	82
Figure 52 Fifty (50) ton capacity liquid CO ₂ truck.....	82
Figure 53 Line heater downstream of injection pump.....	83
Figure 54 CO ₂ gas meter shed downstream of the line heater.....	83
Figure 55 Manifold system at back of CO ₂ storage tanks.....	84
Figure 56 Water injection system for the Little Knife CO ₂ minitest.....	85
Figure 57 Salt water filter building and associated tanks.....	86
Figure 58 Zabolotny Injection Well No. 1 looking to the east.....	86
Figure 59 Fluid sampling system for the Little Knife CO ₂ minitest.....	87

APPENDICES*

1. Zabolotny Injection Well No. 1 log suite.
2. Gulflog computation summary-Zabolotny Injection Well No. 1.
3. Core analysis report-Zabolotny Injection Well No. 1.
4. Fracture detection: Core vs. logs comparison Little Knife CO₂ project.
5. Temperature log Zabolotny Injection Well No. 1.
6. Results of water injection from cased hole log analysis in the Zabolotny Injection Well No. 1, Little Knife Field CO₂ pilot test, North Dakota.
7. Dual spacing thermal neutron decay time (TDT log)-Zabolotny Injection Well No. 1.
8. Zabolotny Observation Well No. 1 log suite.
9. Gulflog computation summary-Zabolotny Observation Well No. 1.
10. Core analysis report-Zabolotny Observation Well No. 1.
11. Interim report Little Knife CO₂ minitest project multiwell pulse test report Little Knife, North Dakota.
12. Dual spacing thermal neutron decay time (TDT log)-Zabolotny Observation Well No. 1.
13. Zabolotny Observation Well No. 2 log suite.
14. Gulflog computation summary-Zabolotny Observation Well No. 2.
15. Core analysis report-Zabolotny Observation Well No. 2.
16. Dual spacing thermal neutron decay time (TDT log)-Zabolotny Observation Well No. 2.
17. Zabolotny Observation Well No. 3 log suite.
18. Gulflog computation summary-Zabolotny Observation Well No. 3.
19. Core analysis report-Zabolotny Observation Well No. 3.
20. Dual spacing thermal neutron decay time (TDT log)-Zabolotny Observation Well No. 3.
21. Logging results on Zabolotny Observation Wells 1, 2 and 3.
22. Reservoir and formation characterization Little Knife CO₂ minitest project.

APPENDICES

23. Depositional facies, diagenesis and reservoir character of the Mission Canyon Formation (Mississippian) of the Williston Basin at Little Knife Field, North Dakota.
24. Semi-log plot of pore throat radii (microns) vs. percent of throats (48 analyses, 12 from each well).
25. Special core analysis-Zabolotny Injection Well No. 1.
26. Special core analysis-Zabolotny Observation Well No. 1.
27. Special core analysis-Zabolotny Observation Well No. 2.
28. Special core analysis-Zabolotny Observation Well No. 3.
29. Little Knife Field CO₂ minitest water injection simulation, Billings County, North Dakota.
30. Design of a CO₂-water injection program for the Little Knife CO₂ flood minitest.

*APPENDICES ARE AVAILABLE FROM THE TECHNICAL PROJECT OFFICER, JOHN MILLER, AT THE BARTLESVILLE ENERGY TECHNOLOGY CENTER, BARTLESVILLE, OKLAHOMA.

WELL TEST REPORT AND CO₂ INJECTION PLAN

FOR THE

LITTLE KNIFE FIELD CO₂ MINITEST

BILLINGS COUNTY, NORTH DAKOTA

By

Robert L. Nettle
Robert F. Lindsay
John B. Desch

Gulf Oil Exploration and Production Company
American First Tower
101 N. Robinson
P. O. Box 24100
Oklahoma City, Oklahoma 73124

ABSTRACT

Gulf Oil Exploration and Production Company in conjunction with the Department of Energy is conducting a field test of the CO₂ miscible displacement process. The project is being conducted in the Mission Canyon Formation (lower Mississippian), a dolomitized carbonate reservoir which is currently in the middle stage of primary depletion. Location of the field is in west-central North Dakota at the approximate center of the Williston Basin. Four wells were drilled in an inverted four-spot configuration within the five-acre minitest. The central well is the injection well surrounded by three non-producing observation wells. Oriented cores were obtained from each well for detailed reservoir characterization and laboratory testing. In addition, pulse and injectivity tests were obtained. Results from these tests were used to upgrade two reservoir simulation models. Various parameters within the models were modified to determine the most efficient injection plan. A WAG-type injection sequence involving alternate slugs of water and CO₂ will be employed. The test is designed to establish the incremental recovery, over waterflooding, by a miscible CO₂ flood in an oil reservoir.

HISTORY OF PROJECT

The United States Department of Energy on August 7, 1978, issued request for proposal number EW-78-R-21-8383 entitled "Minitests of Carbon Dioxide Miscible Flooding Process". The Little Knife CO₂ minitest proposal was submitted after personnel from Gulf Science and Technology and Gulf Oil Exploration and Production Company verified that the CO₂ process was applicable. The cost-sharing contract was awarded on July 17, 1979. The project is anticipated to be completed in July, 1982.

Prepared for DOE under Contract No. DE-AC21-79MC08383

A "Site Selection and Drilling Report" was presented to the DOE, as provided in the contract. Following acceptance of this report on August 10, 1979, an application was presented before the North Dakota Industrial Commission in August for approval of the project. Commission approval was granted on September 20. Under the National Environmental Policy Act of 1969 an environmental assessment was prepared and requests were then filed with the State of North Dakota and Billings County. Permission to drill the four minitest wells was given in September. The remainder of the first project year was utilized for design, laboratory work, and drilling of one injection well and three observation wells. The first five months of the second project year involved surface facility construction and preparation for fluid injection.

INTRODUCTION

Little Knife Field is located near the central portion of the Williston Basin (Fig. 1). The field is isolated within a broad, low lying, northward plunging anticlinal nose (Fig. 2). Closure on the east, north and west is created by the gentle fold with stratigraphic entrapment the mechanism for closure to the south. The primary recovery mechanism in the reservoir is by fluid expansion with limited edgewater drive.

The Little Knife CO₂ minitest is a non-producing, five-acre field trial of the CO₂ miscible displacement process in a heterogeneous carbonate reservoir. The minitest center is 1,800 feet from the north line and 2,460 feet from the west line of Section 3, T.144N. R.98W. (Fig. 2). The test pattern consists of a single injection well offset by three observation wells arranged in an inverted four-spot configuration (Fig. 3 and 4). Initially, two wells were drilled, cored, completed and tested. Based on the analysis of the core and well test data the remaining two wells (observation no. 2 and observation no. 3) were located as shown.

The minitest will involve time-lapse logging to monitor saturation changes as alternate slugs of water and CO₂ pass the observation wells. The test is designed to give the following information:

1. Reduction in original oil saturation due to water injection.
2. Reduction in waterflood residual oil saturation due to alternate CO₂/water injection.
3. Extent of gravity segregation within the porous zone.
4. Effect of stratification and crossflow.
5. Influence of reservoir heterogeneity on fluid injection performance.

This information is needed to assess the potential for a full-scale fluid-injection project in the Mission Canyon. Vertical and areal conformance of the injected slug will be determined in addition to the displacement efficiency. The volume of displaced oil that can actually

be recovered will not be measured directly in the field. In lieu of actual production data the day-to-day evaluation of project performance will make use of a composition numerical reservoir-simulation model¹.

DRILLING, COMPLETION AND WELL TESTING PROCEDURES

Zabolotny Injection Well No. 1

Zabolotny Injection Well No. 1 was spudded on December 5, 1979. A continuous directional survey was run to locate the bottom of the surface hole. Surface casing was then run and cemented without difficulty. Drilling continued and coring depth was reached on December 28. The interval from 9,680-9,880 feet was cored. Coring operations were completed on January 1, 1980, and the hole was drilled to a total depth of 10,150 feet. Solids removal equipment was utilized in the drilling fluid program in all wells to reduce formation damage in order to obtain high quality, open-hole logs. The coring fluid and cement slurry programs were also designed accordingly.

The open-hole logging suite for the injection well consisted of the following (Appendix 1):

1. Dual Laterolog-Micro-SFL with Gamma Ray and Caliper (DLL/MSFL).
2. Compensated Neutron-Formation Density with Gamma Ray and Caliper (CNL/FDC).
3. Borehole Compensated Sonic with Gamma Ray and Caliper (BHC).
4. Wave Forms-Variable Density (Wave Forms/VDL).
5. Fracture Identification Log with Gamma Ray (FIL).
6. Continuous Directional Survey (CDR).
7. Gyroscopic Multi-Shot Survey.

The gyroscopic multi-shot survey was run to total depth to compare with the continuous directional survey. Agreement between the two directional surveys was excellent. The multi-shot survey was used in the observation wells because it was judged to be more accurate.

The open-hole log calculations across the perforated interval 9,824-9,839 feet are:

$$\begin{aligned} S_w &= 23.1\% \\ S_o &= 76.9\% \\ \emptyset &= 20.0\% \end{aligned}$$

Whole core porosity analysis across the same interval is:

$$\emptyset = 19.5\%$$

Log and core calculations on a foot-by-foot basis from this well are listed in Appendices 2 and 3.

The fracture identification log (FIL) and wave forms-variable density log (wave forms-VDL) were both run to detect fractures in the Mission Canyon and were compared to oriented cores taken from the same interval. A fair comparison was obtained between oriented core fracture directions and fracture directions calculated from the logs. A summary of oriented core fracture directions and log calculated fracture directions, corrected for depth discrepancies, is presented in Appendices 3 and 4.

Compared to the surface location the bottom-hole location (at reservoir depth), in the injection well, has a horizontal drift of 80 feet to the northwest, on an azimuth of 288° (Fig. 3).

After the well was circulated and cleaned up, a combination string of production casing was run and cemented. The casing is 5-1/2" OD, L-80, R-III, 8rd, LT&C. The weight below the DV collar is 23.0#/ft. and the weight above it is 17.0#/ft. (Fig. 5).

A completion rig was moved in on January 23, after the location was cleaned and covered with scoria. A cement bond log-variable density log with gamma ray (CBL-VDL-GR log) found good bonding throughout the Mission Canyon. A base thermal neutron decay time log with gamma ray and casing collar locator (TDT), was run with five passes made to measure statistical variation. The casing was perforated at 9,824-9,839 feet, at a density of four shots per foot with 90-degree phasing, using the DLL/MSFL log for depth control. A perforation washer, with a mechanical collar locator, was run and each foot of perforations was swabbed and/or flowed until positive fluid entry was assured. The wellbore was cleaned by circulating with filtered salt water. The work string was laid down, and the production tubing string was run and set (Fig. 5).

The tubing is 2-7/8" OD, 6.5#/ft., C-75, R-2, CS-CB, Hydril, coated internally with TK-2. Premium threads were used in order to get a bubble-tight seal. If any CO₂ were to leak into the casing, which is loaded with water, a severe corrosion problem would be likely. The tubing was coated for the same reason. The coating recommendation resulted from testing and prior field usage. Both Gulf and consulting service company personnel concurred on the coating. The various tubing nipples on the bottom of the packer assembly were run for a corrosion study. The nipples have been weighed and will be reweighed after they are recovered at the end of the test. The nipples are isolated by special couplings so there will be no galvanic corrosion. The reentry guide was put on so that logging tools would be less likely to hang and/or damage the nipples. The landing nipples are made of Inconel 718. This was one of the most corrosion-resistant materials tested. There are two landing nipples in the packer assembly and two in the tubing string. This arrangement permits testing various components for leaks and provides a safe means for working on the well, should the need arise.

The packer and seal assembly have several features that are necessary. The packer has Nitrile packing elements and Viton O-rings. The seals are made of bonded Viton. These materials are

used to combat the effects of CO₂. Additional seal units were used to allow the tubing to stretch and contract, depending on the type and temperature of the fluid being injected.

Only one PTS concentric chamber was run in the injection well. Two had been planned but "tight" spots in the casing made it advisable to run only one. The chamber is made of J-55 stock and is coated internally with TK-2. Capillary tubing, .094"OD, was run from the chamber to the surface. The capillary tubing is strapped to the 2-7/8" OD tubing, above and below every connection, and is connected directly to a recorder on the surface which gives a continuous reading and an intermittent printout of the chamber pressure. The pressure history for the injection well is shown in Figure 6. The capillary tubing is loaded with helium and a correction for this is made. Shortly after the chamber was hooked up, it became apparent that "tight" spots had damaged the system. The tubing was pulled and the chamber was relocated in the string such that it was above the "tight" spots (Fig. 7).

The contacted components of the casing fittings of the injection well are coated with D-trim which is corrosion resistant in the presence of H₂S (Fig. 8). The tree has an Inconel-clad bore, which is NACE rated for an H₂S atmosphere. The difference in design is possible because the fluid in the casing will be static. The well test procedure for the injection well consisted of: 1) a temperature survey, 2) log-inject-log tests, and 3) two pulse tests. The log portion of the log-inject-log test utilized the TDT log². The TDT log is a pulsed neutron tool that uses a neutron generator (minitron), which is a particle accelerator, to generate neutrons. The decay rate of the neutrons is a direct relationship of the neutron absorbers surrounding the tool. When the formation contains chlorine, or traces of boron and/or lithium, the absorption rate is faster than formations without these elements. The absence of chlorine in hydrocarbons allows a distinction to be made between porous rocks containing oil and gas and those containing salt water, as well as determining their porosity and water saturation. By knowing the tools response to the formation, injected fluids, and formation fluids, the residual oil saturation after waterflooding can be determined. In addition, the interval affected by the injected fluids can also be detected. As stated above, a base TDT log was run before the casing was perforated. This log observed the TDT response to filtrate contamination by drilling and completion fluids.

Fifteen days later, the casing was perforated and approximately 100 barrels of oil produced with the perforation washer. Following this, a second TDT log was run to observe the dissipation of mud filtrate and other formation damage as the formation returned to original conditions. Next, 100 barrels of filtered produced salt water were injected at a rate of 30 barrels/hour. Temperature surveys were run during injection, at 23 minutes, 105 minutes, 165 minutes, and 225 minutes after injection. These surveys indicated that the injected fluid was confined to the project interval, with the majority entering into approximately the center 10 feet (Appendix 5). This injection profile was in good agreement with the forecast from the open-hole logs which showed that portion of the project interval to be most porous.

After completing the temperature surveys, a third TDT log was run, 50 barrels of filtered salt water were injected, and a fourth TDT

log was run. Flushing had not stabilized so an additional 50 barrels were injected and a fifth TDT log run. When run no. 5 was compared to run no. 4 no change in sigma was apparent, thus indicating the end of oil flushing due to water injection.

The TDT residual oil analysis was determined by comparing run no. 2 and run no. 5, and resulted in a volumetric weighted average of 41.1 percent residual oil across the perforated interval. The open-hole log analysis resulted in a volumetric weighted average of 42.4 percent, with fairly uniform flushing. The results of communication analysis indicated that some fluid communication occurred during injection to the zone from 9,806-9,824 feet, located directly above the perforations. Fluids, however, were confined within the interval 9,806-9,839 feet, the basal portion of zone C and top portion of zone D, with no migration through the bottom or top of this interval. A detailed description of the procedure and analysis can be found in Appendix 6. The TDT logs are located in Appendix 7.

The injection well was used as the injector for multi-well pulse tests initially involving the first two wells and later involving all four wells. Results of the two pulse tests are presented later in this report.

Three CO₂ residual oil saturation tests were completed in core plugs from the injection well. The plugs were taken from a one foot interval at 9,823-24 feet for the first test, at 9,826-27 feet for the second test, and at 9,814-15 feet for the third. The existing slim-tube apparatus was modified to allow mounting of the reservoir core plugs at the outlet of the slim-tube and thus determine the residual oil to CO₂-water flow. The plugs were restored to connate water saturation, displaced with water (waterflood), and then flooded with a CO₂-oil miscible bank developed in a slim-tube at 245°F and 3,500 psi.

Water was not injected simultaneously with CO₂ in the first test. Average porosity and permeability of the core plugs was 23% and 7 md, respectively. Final saturations after the miscible bank and 1.2 core pore volumes of CO₂ were flowed were:

$$\begin{aligned} S_o &= 3\% \text{ PV} \\ S_w &= 20\% \text{ PV} \\ S_{CO_2} &= 77\% \text{ PV} \end{aligned}$$

A 1.5 to 1 water/CO₂ ratio was used in the second test. Average porosity and permeability of the plugs was 21.7% and 5.3 md, respectively. Final saturations were:

$$\begin{aligned} S_o &= 3.1\% \text{ PV} \\ S_w &= 61.5\% \text{ PV} \\ S_{CO_2} &= 35.4\% \text{ PV} \end{aligned}$$

For the third test, a 3 to 1 water/CO₂ ratio was used. Average porosity and permeability of the core plugs was 26% and 12.6 md, respectively. Final saturations were:

$$\begin{aligned} S_o &= 0.8\% \text{ PV} \\ S_w &= 63.5\% \text{ PV} \\ S_{CO_2} &= 35.7\% \text{ PV} \end{aligned}$$

A material balance on the slim-tube tests confirmed that multiple contact miscibility was achieved at test conditions in each test. Very low residual oil saturations (0.8-3.1% PV) observed for the various water/CO₂ ratios are more than satisfactory.

Observation Wells

Zabolotny Observation Well No. 1 was spudded on January 18, 1980, followed by Zabolotny Observation Well No. 2, on May 15, and Zabolotny Observation Well No. 3, on July 5. The solids removal equipment, coring fluid, and cement slurry programs employed in drilling the observation wells were the same as those used in the injection well.

These three observation wells required additional drilling time because directional surveys were run and the wells had to be turned so that the bottom-hole locations were evenly spaced from the injection well bottom-hole location. Even though all of the wells were drilled with the same bottom-hole assemblies, bit weights, rotating speeds at comparable depths, the same rig and mud specifications, each drilled differently. Each observation well had to be oriented in a different direction (Fig. 3).

There are only minor differences between the completions of the injection and observation wells. All observation wells are equipped with two PTS concentric chambers. The pressures are checked in both chambers and a fluid gradient is calculated. The type of fluid in the bottom of the well is then known. One chamber also serves as a back-up as well as a means of injecting chemical down-hole, if necessary. Gas-lift mandrels with wireline retrievable gas-lift valves are employed in the observation wells. These valves will be needed when injected water reaches the observation wells because there will not be enough formation pressure to initiate flow. The wells will be gas-lifted in order to obtain samples. The coating used in the observation wells is TK-7, as opposed to TK-2 in the injection well. Prior field experience at the Sacroc CO₂ project was the basis for the coating recommendations. The wellheads, on the observation wells, contain the same metallurgy as the injection well wellhead, the only difference is the valve arrangement (Fig. 9).

Zabolotny Observation Well No. 1

Coring depth for observation well no. 1 was reached on February 21, 1980. The interval from 9,737-9,853 feet was cored. Coring was completed on March 5 and the hole was drilled to a total depth of 10,213 feet. The open-hole logging suite was run and consisted of the following (Appendix 8):

1. Dual Laterlog-Micro-SFL with Gamma Ray and Caliper (DLL/MSFL).
2. Compensated Neutron-Formation Density with Gamma Ray and Caliper (CNL/FDC).
3. Borehole Compensated Sonic with Gamma Ray and Caliper (BHC).

4. Wave Forms-Variable Density with Gamma Ray (Wave Forms/VDL).
5. Fracture Identification Log with Gamma Ray (FIL).
6. Gyroscopic Multi-Shot Survey.

Open-hole log calculations across the perforated interval 9,809-9,824 feet are:

$$\begin{aligned} S_w &= 23.0\% \\ S_o &= 77.0\% \\ \phi &= 19.3\% \end{aligned}$$

Whole core porosity analysis across the same interval is:

$$\phi = 19.5\%$$

Log and core calculations on a foot-by-foot basis from this well are listed in Appendices 9 and 10.

Compared to the surface location the bottom-hole location (at reservoir depth), in observation well no. 1, has a horizontal drift of 94 feet to the west-southwest, on an azimuth of 258° (Fig. 3). This bottom-hole location is 258 feet from the injection well bottom-hole location (at reservoir depth), to the northeast on an azimuth of 49°.

A combination string of production casing was run and cemented after the well was circulated and cleaned up. The casing program in the observation wells is slightly different from the injection well. Below the DV collar the casing is 5-1/2" OD, 23#/ft, N-80, R-III, 8rd, LT&C and above the DV collar the casing is 5-1/2" OD, 17#/ft, L-80, R-III, 8rd, LT&C (Fig. 10).

A workover rig was moved in on March 17 to begin completing the well. The CBL-VDL-GR log response was almost the same as that from the injection well. A base TDT log was run from PBTd of 10,126 feet to 9,600 feet. The casing was perforated from 9,809-9,824 feet, at a density of one shot per foot with 0-degree phasing. The perforation washer was utilized to swab each foot of perforations until oil production was verified. A bit was run to plugged-back total depth (PBTd) and the well was circulated with filtered salt water. The work string was pulled, the production tubing string was run, and the PTS chambers were hooked-up to the recorder. The pressure history for observation well no. 1 is shown in Figure 11. Figure 10 illustrates the tubing setting in observation well no. 1.

As part of a reservoir and formation characterization program, a multiwell pulse test was conducted in April and May, 1980³. The injection well and observation well no. 1 were used in this test.

Background pressure data had to be collected prior to the test. A plug choke was run and set in the landing nipple above the PTS chambers so that wellbore effects would be minimized. The bottom-hole pressures in the observation well indicated that the plug was leaking so the tubing was loaded with water. The leak continued so

the plug was pulled. The tubing was gas-lifted using nitrogen but the well would not flow. Coiled tubing, with a special end fitting to protect the tubing coating, was run and the tubing was unloaded to a depth of about 9,000 feet. The well would not flow. The casing was reperforated from 9,809-9,824 feet on April 30, 1980, using a 2" OD gun loaded with 6.5-gram charges. Density was one shot per foot with 0-degree phasing. The well was opened and flowed for clean-up.

By injecting filtered salt water into the injection well, at a rate of 1,964 BWPD for two hours, a pulse was created in the reservoir that was monitored in the observation well. The initial response from this pulse arrived at the observation well in 30 minutes and peaked in 175.8 minutes, with a maximum amplitude of 17.600 psi. The pressure system used a 0-15,000 psia quartz sonde which was totally electronic. It has a sensitivity (ability to detect a change in pressure) of 0.001 psi. The analysis of the response provided the following: 1) transmissibility= 3,587 md-ft/cp, 2) diffusivity ($k/u\phi c$)= 40.703×10^6 md-psi/cp, and 3) storage capacity (ϕch)= 88.138×10^{-6} ft/psi. The primary conclusions from the analysis of the pulse test are:

1. Fluid communication did exist between the Zabolotny Injection Well No. 1 and Zabolotny Observation Well No. 1.
2. There was no fracture continuity between the wells.
3. The effective hydraulic thickness of the project interval includes the perforated interval and a dolomitized lobe above. The interval has an average thickness of 26.0 feet between the injection well and observation well.
4. The project interval of the Mission Canyon in the minitest area (9,806-9,839 feet) will confine fluids within itself, i.e., no vertical migration of fluids through its top or base.

Additional information is contained in Appendix 11.

As the pulse test was being completed, the observation no. 1 wellhead was damaged which necessitated killing the well with filtered salt water. The capillary tubing and wellhead were repaired but the gas-lift valves would not work. The tubing string had to be pulled and the valves replaced.

As a result of these incidents, the log-flow-log test was delayed approximately one month. As previously mentioned, the first TDT log was run prior to perforating the casing. Since that time, a total of 1,168 barrels of fluid had been produced. The log-flow-log test procedure was then carried out as follows:

TDT log Run No. 2
Flow 29 barrels of fluid

TDT log Run No. 3
Flow 32 barrels of fluid

TDT log Run No. 4
Flow 98 barrels of fluid

TDT log Run No. 5

The well was flowed in order to clean the perforations, dissipate formation damage, and re-establish, as nearly as possible, original fluid saturations around the wellbore. By monitoring saturation changes with the TDT log, it was determined that the saturation did return to near original. A copy of the TDT logs can be found in Appendix 12.

The surface locations for the remaining two observation wells were relocated to their present surface positions after the pulse test and oriented core data from the injection well and observation well no. 1 were analyzed (Fig. 3).

Zabolotny Observation Well No. 2

Drilling of observation well no. 2 progressed smoothly during the months of May and June. Coring depth was reached on June 23 and the interval from 9,775-9,893 feet was cored. Coring was completed on the 26th, and the hole was drilled to a total depth of 10,150 feet. The following logs were run (Appendix 13):

1. Dual Laterolog-Micro-SFL with Gamma Ray and Caliper (DLL/MSFL).
2. Compensated Neutron-Formation Density with Gamma Ray and Caliper (CNL/FDC).
3. Borehole Compensated Sonic with Gamma Ray and Caliper (BHC).
4. Gyroscopic Multi-Shot Survey.

The fracture identification log (FIL) and wave forms-variable density log (waveforms-VDL) were both run in the injection well and observation well no. 1. Sufficient data was obtained for comparison with the oriented cores, therefore these logs were deleted from the log suite.

Open-hole log calculations across the perforated interval 9,855-9,871 feet are:

$$\begin{aligned} S_w &= 24.9\% \\ S_o &= 75.1\% \\ \phi &= 20.3\% \end{aligned}$$

Whole core porosity analysis across the same interval is:

$$\phi = 20.9\%$$

Log and core calculations on a foot-by-foot basis from this well are listed in Appendices 14 and 15.

Compared to the surface location the bottom-hole location (at reservoir depth), in observation well no. 2, has a horizontal drift of 298 feet to the northwest, at an azimuth of 298° (Fig. 3). This bottom-hole location is 250 feet from the injection well bottom-hole location (at reservoir depth), to the southwest on an azimuth of 208°.

After the well was circulated and cleaned up, a combination string of production casing was run. The 5-1/2" OD casing was set at 10,149 feet and cemented with the same composition used in the two previous wells (Fig. 12).

After the drilling rig was moved out, the location was cleaned and a workover rig was moved in. The DV collar was drilled and a bit, casing scraper, and string mill were run to bottom. The CBL-VDL-GR log indicated a good cement bond. A base TDT log was run and the casing was perforated from 9,855-9,871 feet, at a density of one shot per foot with 0-degree phasing. A perforation washer was run and each perforation was straddled and produced. The packer assembly was run on tubing and set. The work string was laid down. The production string was run and landed (Fig. 12). The down-hole equipment and wellhead are essentially the same as those described in observation well no. 1. The pressure history for observation well no. 2 is shown in Figure 13.

After the base TDT log was run, a total of 1,057 barrels of fluid were produced. The log-flow-log test was then performed as follows:

TDT log Run No. 2
Flow 127 barrels of fluid

TDT log Run No. 3
Flow 468 barrels of fluid

TDT log Run No. 4
Flow 198 barrels of fluid

TDT log Run No. 5

A copy of the TDT logs can be found in Appendix 16. Analysis of run no. 5 showed that the well did clean-up and the saturations did return to near original.

Zabolotny Observation Well No. 3

Observation well no. 3 was drilled without encountering any difficulties. Coring depth was reached on August 15, and four cores were cut from 9,758-9,894 feet. The hole was deepened to a TD of 10,150 feet and the following logs were run (Appendix 17):

1. Dual Laterolog-Micro-SFL with Gamma Ray and Caliper (DLL/MSFL).
2. Compensated Neutron-Formation Density with Gamma Ray and Caliper (CNL/FDC).

3. Borehole Compensated Sonic with Gamma Ray and Caliper (BHC).
4. Circumferential Micro-Sonic with Gamma Ray and Caliper (CMS).
5. Gyroscopic Multi-Shot Survey.

Open-hole log calculations across the perforated interval 9,837-9,852 feet are:

$$\begin{aligned} S_w &= 27.5\% \\ S_o &= 72.5\% \\ \phi &= 19.3\% \end{aligned}$$

Whole core porosity analysis across the same interval is:

$$\phi = 19.5\%$$

Log and core calculations on a foot-by-foot basis for this well are listed in Appendices 18 and 19.

Compared to the surface location the bottom-hole location (at reservoir depth), in observation well no. 3, has a horizontal drift of 70 feet to the north, on an azimuth of 7° (Fig. 3). This bottom-hole location is 283 feet from the injection well bottom-hole location (at reservoir depth), to the northwest on an azimuth of 330°.

The casing was set at a depth of 10,143 feet. The string is 5-1/2" OD, 23#/ft, N-80, R-III, 8rd, LT&C on bottom and 5-1/2" OD, 17#/ft, L-80, R-III, 8rd, LT&C, on top with the DV collar at approximately 6,921 feet (Fig. 14). The casing was cemented in two stages, with the same composition that was used in previous wells.

After the drilling rig was moved out, the location was cleaned and covered with scoria. A workover rig was moved in and the DV collar was drilled. Following this, a bit, casing scraper, and string mill were run to bottom. The well was circulated with filtered, produced salt water. A casing collar log (CCL-N-GR) was run from PBSD of 10,015 feet to 8,500 feet and a CBL-VDL-GR log from PBSD to 4,600 feet. The log showed excellent bonding throughout the Mission Canyon section. A base TDT log was run and the casing was perforated at 9,837-9,852 feet with a 4" OD casing gun loaded with 22-gram charges at a density of one shot per foot with 0-degree phasing. The perforation washer was run and each perforation was flowed with approximately 20 barrels of fluid swabbed and/or flowed during each setting. The packer assembly was run on tubing and the packer set. The assembly was tested to 1,600 psi. The work string was laid down and the production string was run and landed (Fig. 14). The pressure recording system was purged with helium and tested. The pressure history for observation well no. 3 is shown in Figure 15. The well was gas-lifted using nitrogen, but it would not flow. Coiled tubing was run to a depth of 9,000 feet, and the production tubing was unloaded with nitrogen. The well still would not flow continuously. The casing was then re-perforated on October 9, 1980, using a 2-1/8" HSC gun loaded with four shots per foot and

90-degree phasing. The well was shot in an under-balanced condition and it started flowing immediately.

The log-flow-log test was performed once flow had stabilized. After perforating a total of 1,375 barrels of fluid was produced. The log-flow-log test was then performed as follows:

TDT log Run No. 2
Flow 126 barrels of fluid

TDT log Run No. 3

Analysis of the TDT logs showed that the well had not cleaned up. It was decided to run the pulse test and then resume the log-flow-log test. The pulse test was concluded in late November and the log-flow-log procedure for observation no. 3 proceeded as follows:

Flow 520 barrels of fluid

TDT log Run No. 4
Flow 392 barrels of fluid

TDT log Run No. 5

Analysis of the last run showed that the saturations around the wellbore had finally normalized. A copy of the TDT logs can be found in Appendix 20. A summary of the logging results from the log-flow-log test performed in all three observation wells is contained in Appendix 21.

FOUR WELL MULTI-WELL PULSE TEST

A multi-well pulse test involving the four minitest wells was conducted on November 15, 1980. Three days of unhindered background pressure had been recorded in the three observation wells prior to the test. The test was conducted by pumping filtered salt water into the injection well for two hours while the response to this "pulse" was monitored downhole in the three observation wells. A pulse response was recorded at each observation well. The single pulse was started at 12:10 + .25 hours and stopped at 14:10 + .00 hours, at an average injection rate of 2,297.5 BWPD. In addition, drawdown/buildup tests were conducted in each observation well and static reservoir pressures were recorded in all four wells. The objective for this test was to determine if a preferential direction to flow exists through the project interval in the minitest area.

The maximum response from the pulse arrived at observation well no. 1 (258 feet away) in 175.0 minutes with a maximum amplitude of 21.180 psi (Fig.16). Analysis of the response provided the following: 1) transmissibility= 3,482.5 md-ft/cp, 2) diffusivity ($k/u\phi c$)= 39.578 x 10⁶ md-psi/cp, 3) storage capacity (ϕch)= 87.990 x 10⁻⁶ ft/psi, 4) effective hydraulic thickness= 25.2 ft., 5) effective permeability= 29.3 md, and 6) storage= 33,610 res. bbl/acre.

The maximum response from the pulse arrived at observation well no. 2 (the nearest well 250, feet away) in 175.98 minutes, with a

maximum amplitude of 15.835 psi (Fig. 17). Analysis of the response provided the following: 1) transmissibility= 4,712 md-ft/cp, 2) diffusivity ($k/u\phi c$)= 37.638 x 10⁶ ft/psi, 3) storage capacity (ϕch)= 125.19 x 10⁻⁶ ft/psi, 4) effective hydraulic thickness= 36.5 ft., 5) effective permeability = 27.4 md, and 6) storage= 47,820 res. bbl/acre.

The maximum response from the pulse arrived at observation well no. 3 (the farthest well, 283 feet away) in 217.5 minutes, with a maximum amplitude of 16.010 psi (Fig. 18). Analysis of the response provided the following: 1) transmissibility= 3,189.6 md-ft/cp, 2) diffusivity ($k/u\phi c$)= 32.054 x 10⁶ md-psi/cp, 3) storage capacity (ϕch)= 99.507 x 10⁻⁶ ft/psi, 4) effective hydraulic thickness= 29.4 ft., 5) effective permeability= 23.0 md, and 6) storage= 38,010 res. bbl/acre.

The following conclusions have been derived from results of this test:

1. All three observation wells are in good fluid communication with the injection well.
2. There are no continuous high permeability channels or fractures connecting the injection well with any of the three observation wells.
3. There was no evidence of a free gas saturation within the confines of the four-well minitest pattern.
4. In situ effective permeabilities representing the average value between the injection well and each of the observation wells were quite similar, the maximum being 29 md and the minimum being 23 md.
5. Effective hydraulic thicknesses contacted by the pulse wave between the wells varied from 25 to 36 feet.
6. Several injection-temperature surveys in the injection well show that injected water is not migrating out of the project interval near the wellbore.
7. The pulse test hydraulic thicknesses correlate well with the combined electric log gross thickness of the project interval. The hydraulic thickness between the injection well and observation well no. 2 is slightly greater than the log thicknesses.
8. The in situ effective storage values between the three observation wells varied from a low of 34,000 res. bbl/acre (injection well to observation well no. 1) to a high of 48,000 res. bbl/acre (injection well to observation well no. 2).
9. Pressure drawdown/buildup tests were performed on each of the observation wells with some of the transmissibilities being less than those from the pulse test. This difference is an indication that there is some local confinement of

fluid flow near the wellbore by low porosity/permeability streaks. This confinement apparently "comes and goes" when traversing interwell distances, resulting in the higher pulse test transmissibilities.

10. All of the observation wells had a severe skin damage value probably due to drilling fluid invasion, low perforation density, invasion of cement into porous intervals and micro-fractures near the wellbore.

Additional information about the test is contained in Appendix 22.

RESERVOIR GEOLOGY

The Mission Canyon Formation (lower Mississippian) at Little Knife Field is 465 feet thick and is interpreted as a regressive carbonate sequence, analogous to the lime mud-to-sabkha cycle of Wilson⁵. Most of the carbonates were deposited in a subtidal setting by three sub-environments or facies. Upsection, these sub-environments are: 1) open marine, 2) a transitional setting between the open marine and shallow protected shelf and 3) a protected shelf of restricted marine. Intertidal rocks directly overlie and pass laterally into the uppermost subtidal beds. These, in turn, have lagoonal beds interfingering with them upsection and are overlain by rocks of supratidal origin which cap the Mission Canyon and form the primary seal across the field (Fig. 19).

Lithology

Key beds were located throughout the Mission Canyon section and were used to divide the formation into six informal zones (Fig. 20). Lithologies of these six zones, A through F, within the Mission Canyon at Little Knife Field are:

1. Zone A is a 60-foot cap of thin to thick bedded anhydrite, including: 1) chicken-wire mosaic, 2) thin-bedded mosaic, 3) laminated to medium bedded, 4) ropey displacive, and 5) burrowed replacive (most nomenclature is after Maiklem⁶). Both a dolomite matrix and laminated interbeds of dolomite are associated with the anhydrite beds. At the base of the zone and into uppermost portions of zone B, pseudomorphs of anhydrite after selenite gypsum crystals, anhydrite porphyroblasts, and localized laminated crusts are present. Interpreted depositional setting is supratidal.
2. Zone B is 70 feet thick and forms part of the reservoir interval. It is separated into:
 - a) An upper interval varying from 5-40 feet in thickness consisting of interbedded, thin, porous, and discontinuous, lenticular dolomitized skeletal wackestones. They are partly replaced by anhydrite, which was later leached and set between thin to thick beds of dense cemented grainstones. Constituents

included peloids, clotted and lumped micrite, ooids, pisolites, calcispheres and skeletal detritus. Interpreted depositional setting of the skeletal wackestones is shallow, nearshore subtidal while the wackestone/ grainstones are part of an intertidal barrier.

- b) The lower two thirds of the zone is dolomitized burrowed, sparsely skeletal, pelletal wackestone/ packstones. The carbonates were partially replaced by anhydrite and then leached and form an upper reservoir. Interpreted depositional setting is restricted shallow marine.
3. Zone C is 65 feet thick and also forms a portion of the reservoir interval. It is medium to thick bedded and mostly dense at its top becoming more porous progressively lower in the section. Upper portions are slightly dolomitized to dolomitized pelletal wackestones grading downwards into skeletal wackestones with some replacement by anhydrite. Dense beds have sparse amounts of intercrystal pore occlusion by chert. Upper portions of the zone have rare quartz silt laminations beneath porous upper reservoir intervals, set in dense dolomite. The lower porous portion forms part of a lower reservoir. Depositional setting is restricted marine to transitional marine.
 4. Zone D is 50 feet thick, forming the lowest portion of the reservoir interval. It is a medium to thick bedded interval of partially dolomitized, burrowed, skeletal wackestones. The facies exhibits some anhydrite replacement and leaching. The uppermost portion of the zone forms the major portion of a lower reservoir. Depositional setting is the seaward portion of a protected shelf and transitional into the open marine.
 5. Zone E is 50 feet thick and is composed of thick bedded sparsely dolomitized to dolomitized skeletal, mudstone/ wackestones with irregular shaped incipient siliceous nodules. Porosity intervals in this zone are non-hydrocarbon bearing. Depositional setting is restricted to transitional marine.
 6. Zone F is 170 feet thick and composed of medium to thick bedded alternating mudstones and skeletal wackestone/ grainstone. The basal 10-15 feet is slightly argillaceous, interlaminated skeletal packstones and pelletal packstones which form a transitional zone of contact from the Mission Canyon into the underlying Lodgepole Limestone. This zone is also non-hydrocarbon bearing. Depositional setting is open marine.

Hydrocarbon bearing porosity is isolated within beds deposited in both transitional open to restricted marine and restricted marine settings, in zones B, C and D of the Mission Canyon. These beds were partially-to-completely dolomitized to form fine-grained, sucrosic

dolomite (Fig. 22). A field-wide study of Little Knife discussing the overall depositional settings, diagenesis and reservoir character is included in Appendix 23.

Reservoir General

Beds utilized for the CO₂ minitest project interval are located at the base of zone C and at the top of zone D, a total thickness of 31 feet (Fig. 20 and 21). These beds form the mid-to-basal portion of the reservoir interval within the field. They were deposited within a transitional open to restricted marine setting by an epeiric sea which occupied the Williston Basin, with large volumes of lime mud being deposited (Figs. 19 and 22). Higher wave energy, perhaps storms, washed skeletal fragments of crinoid columnals from more seaward open marine areas, back shoreward, into the low-energy outer portions of the protected shelf to mix with finer accumulating carbonate muds. These skeletal fragments interfinger many times downsection with the carbonate muds and represent cyclic carbonate deposition (Fig. 21). These skeletal fragments, once deposited, were thoroughly mixed with finer carbonate muds by burrowing organisms, homogenizing the sediment. The end result was a sedimentary deposit of uniform, though low, permeability within which contemporaneous solutions began to slowly migrate through. Landward, to the east, upon subaerial portions of the Mission Canyon depositional system, a coastal sabkha existed. Evaporation upon tidal flats enriched waters with respect to calcium, magnesium and sulfate ions. These brine solutions probably moved through the outer fringes of the sabkha precipitating out gypsum or anhydrite, with calcium ions withdrawn out of the system, causing a dramatic increase in the Mg²⁺/Ca²⁺ ratio to begin to dolomitize the subtidal sediments (Butler⁷). Apparently these enriched solutions were able to prograde out predominantly in a lateral and downward manner into subtidal sediments, similar to what Jacka and Franco⁸ postulate to have happened to Permian sediments along shelf areas of the Permian Basin. Within the subtidal sediments calcium sulfate, in the form of anhydrite, preferentially partially replaced crinoid fragments leaving carbonate mud unaffected. As anhydrite replacement came to a close, the muddy carbonate was then dolomitized. Dolomitization began at a much slower rate, partially dolomitizing the finer carbonate muds (Bathurst⁹, p. 531-532). Once both anhydrite replacement and dolomitization had ceased, porous beds of partially dolomitized skeletal wackestones resulted. Later, the replacing anhydrite was partially leached away, enhancing overall porosity to leave the final end product of diagenetic modifications-porous, sucrosic, calcareous dolomite.

Reservoir Specific

Reservoir rock characteristics in the project interval are similar in each well (Fig. 23). The lower half (15-16 feet) is composed of highly porous and permeable rock that is partially dolomitized (70%), originally skeletal wackestone (skeletal limestone) (Fig. 24, 25, 26 and 27). A stylolite is located just above this bed throughout the minitest area, reducing porosity for approximately one foot (Fig. 28). This stylolitized horizon serves as a marker on sonic logs to divide the Mission Canyon into zone C

(above) and zone D (below). The upper half of the project interval is formed by two beds of rock. The intermediate bed is dolomitic limestone, containing low amounts of porosity and permeability. The uppermost bed is calcareous dolomite, which contains fair to good amounts of porosity and permeability. In observation well no. 3 only dolomitic limestone is present. This lack of a bed of calcareous dolomite is due to less dolomitization affecting uppermost portions of the project interval at this location. A comparison of porosity and permeability to lithology by whole core analysis, in all four wells, is illustrated in Fig. 29.

Structure

Little Knife Field is located within a broad, low lying anticlinal nose plunging gently to the north (Fig. 2). Beds dip to the west at approximately one-half degree and to the east at approximately one-quarter degree. Closure across the field is less than 100 feet. Several slight structurally higher portions of the field are separated by low saddles along the axis of the field, at approximately twenty foot differences. Closure is structural to the north, east and west with stratigraphic entrapment southward.

Regionally, western North Dakota, eastern Montana, and northwesternmost South Dakota are divided by a series of northwest and northeast trending surface lineaments. These lineaments tend to form elongate, slightly rhombic blocks. Little Knife Field is located within the center of the junction of the northeast trending Yellowstone block and the northwest trending Watford block (Thomas¹⁰) (Fig. 30). In central and northern portions of the field surface lineaments were mapped using Landsat and aerial photographs (Hodgson¹¹) (Fig. 31). Both northeasterly and northwesterly trends, similar to regional trends, are present within the field (Fig. 32).

Surface outcrop fractures in the Sentinel Butte Formation, next to observation well no. 3, were measured by one of the authors (Fig. 33). Sixty-nine apparent strikes were obtained which revealed a predominance of fractures in a northwesterly direction, maximum value N.70-80°W., and a northeasterly direction, maximum value N.60-70°E. Oriented cores were obtained in each of the four minitest wells, with strike and dip of all fractures recorded. Strikes of the fractures within the minitest interval revealed slightly differing fracture orientations from well to well (Fig. 34). Average fracture strike directions from the cores tend to be in either a northwesterly (N.67°W.) or northeasterly (N.69°E.) direction, similar to surface outcrop fractures.

Fracture separation (distance from one fracture to the next parallel fracture) could not be determined from cores. Surface outcrops were used to study fracture separation, assuming they will be similar to the subsurface. Surface fracture separation was found to vary from one to six feet. Surface cover limited the extent of the study area (Figs. 35 and 36).

Cores reveal the vertical continuity of individual fractures to be approximately eighteen to twenty-four inches. Each individual fracture consists of small interconnected, vertical, hairline en

echelon planes. No lateral offset has been observed where fractures transect skeletal fragments, ooids or pisolites.

The fracture identification log (FIL) and wave forms variable density log (wave forms-VDL) were both run in the first two wells drilled. A comparison of fracture directions taken from the oriented cores to those calculated fracture directions obtained from logs revealed a fair comparison, with fracture detection by the logs appearing slightly pessimistic but generally good. The FIL was, however, rated superior to the Wave Forms-VDL as the best source of fracture information from logs¹¹.

Because the fractures observed propagate only short distances vertically, it is felt that their lateral continuity may also extend for short distances. Multi-well pulse testing revealed no major contribution by fractures, but did calculate higher average permeabilities. These average permeabilities were approximately twice the permeabilities measured from whole core analysis and are interpreted to be due to the slight affect of short non-continuous fractures dispersed somewhat uniformly across the minitest area (Fig. 37).

Pore And Throat System

Four types of pores are present in porous beds of the Mission Canyon at the minitest location (Fig. 38). Moldic pores are the largest, produced by leaching of anhydrite which replaced skeletal fragments, and measure 150 to 30 microns wide (Fig. 39). These large moldic pores are connected by pore throats to other pores and pore throats associated with intercrystal pores between dolomite crystals. Polyhedral pores are the largest intercrystal pores. Each pore is surrounded by several dolomite crystal faces and form a complex polyhedral shape 50 to 10 microns wide. Tetrahedral pores are intermediate sized intercrystal pores, where individual dolomite crystals began to impinge other dolomite crystals, reducing the pore size to a small tetrahedral shape 10 to 3 microns wide. Interboundary-sheet pores are the smallest and narrowest pores, found between individual dolomite crystals where pore space has been reduced to a thin, linear, approximately one micron width. All of these intercrystal pore types are similar to those described by Wardlaw¹² and Wardlaw and Taylor¹³.

Permeability development is dominated by two pore throat radii sizes in the Mission Canyon: 1) interboundary-sheet throat radii, 0.8 microns, and 2) larger throat radii, 1.5-3.5 microns, connecting tetrahedral, polyhedral and moldic pores (Figs. 40, 41, 42 and 43). Both sizes of pore throats contribute to permeability development. Narrow interboundary-sheet pores/throats though forming only small amounts of total porosity, contribute to overall permeability development.

The relation of pore-to-throat size ratios are highly variable, ranging from 40:1 when larger polyhedral pores are well developed, down to 4:1 when not well developed (Fig. 44). An average pore-to-throat size ratio is approximately 5-10:1. The average pore-to-throat coordination number (the average number of throats connected to each pore) is 3 to 5 in two dimensional view (Fig. 44).

When pore throat radii size is compared to the amount of porosity and permeability that is developed, by mercury injection capillary pressure curves, five (5) throat radii vs. porosity and permeability relationships are found to exist (Figs. 45, 46, 47 and 48). At one (1) md of permeability (1.0, 0.7, and 0.9, actual measurements), averaging 0.8 md, the associated amounts of porosity vary between 13.0-8.3%, averaging 10.7%. The average maximum amount of pore throat radii associated with these porosities and permeabilities is 0.6 microns in size (kurtosis) and rarely develops to 0.8 microns. Below one (1) md of permeability a gap tends to exist segregating permeabilities into two end member groupings. One group is near one (1) md, as stated above. Another group is near 0.1-0.2 md (0.1, 0.2, 0.3 and 0.1 md, actual measurements), averaging 0.16 md, with porosity ranges from 9.9-2.5%, averaging 6.2%. No permeabilities between 0.7-0.3 md were encountered out of forty-eight samples that were run. Pore throat radii associated with this lowest range of porosity and permeability average 0.21 microns in size. These are pore throats associated with beds of such low porosity and permeability that they do not hold or contribute to the fluid flow of hydrocarbons.

Above permeabilities of one (1) md the associated amounts of porosity and pore throat radii can be divided into three groups or relationships. The first group is isolated between one (1) and seven (7) md permeability, averaging 3.5 md, and porosity ranges of 10-17.2%, averaging 13.6%. Within this group similar pore throat radii characteristics have been recognized. Pore throat radii, for this group, range between 0.6-2 microns with maximum development of throat radii at 0.8 microns, and on rare occasions throat radii extend to 1.3 microns. Next, an intermediate group exists between 7 and 48 md of permeability, averaging 22.3 md, with associated porosity ranges between 17.3-21.4%, averaging 19.6%. This group of porosities and permeabilities are related to pore throat radii that disperse into two maximum size ranges of throat radii, with low amounts of throat radii between them (polymodal, after Pettijohn¹⁴). The smaller throat radii are 0.8 microns in size (secondary maximum) while the larger throat radii are 1.8-2.5 microns (maximum) and are much more common. Hence, the abrupt shift from permeabilities of one (1) and seven (7) md to much higher values of permeability, up to 48 md, occurs. The final group contains the highest amounts of both permeability and porosity measured. Permeabilities range between 48 and 146 md, averaging 85.4 md, and porosity ranges between 21.8 and 27.6%, averaging 24.1%. Pore throat radii associated with this group have only one size range present (maximum percentage) at 2.5 microns. One slope of the histogram decreases downward into large throat radii up to 5 microns, forming as much as 10% of all throat radii. The smaller 0.8 micron throat radii, present in the other two groups, are reduced to only a few rare throats. Forty-eight (48) pore throat radii measurements were made, 12 from each well, and are illustrated in Appendix 24, 25, 26, 27, and 28. Mercury capillary pressure curves from which these above measurements were made are also included in Appendix 25, 26, 27 and 28, along with standard whole core analysis in Appendix 3, 10, 15, and 19.

EQUIPMENT AND INSTRUMENTATION

Fig. 49 illustrates the layout of the minitest site. The water filter and associated pumps and tanks, along with the water transfer pump, are located at Central Tank Battery No. 2. The rest of the equipment is located at the test site. The test site equipment is designed to operate primarily with propane fuel. Only a limited amount of electrical power is available.

The trailer is the central point of the operation. It serves as the instrumentation center, office, and storage area.

The equipment and instrumentation used in the project are separated into four systems. Foremost is the hardware used in the well completions as previously described. The other three systems are: 1) the carbon dioxide injection system, 2) the water injection system, and 3) the fluid sampling system.

CO₂ Injection System

The CO₂ injection system consisted of storage, metering, pumping and vaporizing sections (Figs. 50 and 51). All were located at the minitest site. All equipment upstream of the liquid meter was furnished by the CO₂ supplier.

The CO₂ was transported in a liquid state by truck to the minitest site from near Brandon, Manitoba (Fig. 52). It was stored as a liquid. The storage tanks had a vaporizing system, which is not shown in Fig. 50. A refrigeration system was not installed because the CO₂ injection phase should be completed during the winter. It is anticipated that the ambient winter temperature will be sufficiently low to prevent significant CO₂ loss.

The storage section had a capacity of 200 tons. This is approximately 1/2 of the volume of one cycle of CO₂ injection. This ensured that the injection pattern would not be altered or interrupted by delays in getting CO₂ to the test site.

CO₂, in a liquid state, was vaporized in the line heater (Fig. 53). Numerous safety relief valves provided vents in case liquid CO₂ was trapped and began to vaporize. All vessels were equipped with safety relief valves, even though they are not illustrated.

The metering system consisted of both a liquid and a gas meter (Fig. 54). Metered volumes were compared to delivered volumes. The accuracy of each meter as well as the convenience of computing standard volumes will be determined.

The pumping system was comprised of two pumps, a charge pump and an injection pump. The charge pump ensured that liquid was being supplied to the injection pump (Fig. 55). The injection pump consisted of a triplex pump driven by an internal combustion engine.

The line heater used to vaporize the CO₂ was leased. The CO₂ could not be injected as a liquid without freezing the packer fluid and possibly rupturing the casing and/or collapsing the tubing.

The gaseous CO₂ was heated above 60°F in order to avoid hydrate formation when it contacted water.

The estimated capital cost to install this system was \$70,000 of which \$55,000 was for tangible items. Operating expenses, excluding CO₂ but including equipment rentals, are estimated at \$18,000/month. The CO₂ will cost \$85/ton. Total project usage of CO₂ is estimated at 2,000 tons, so the raw material cost should be about \$170,000.

Water Injection System

The water injection system consisted of two main segments (Fig. 56). The first segment is the filtering system which was located at Central Tank Battery No. 2. The second segment is the injection pump which was located at the test site. A fiberglass line connected the two.

Water for the project was produced formation water from Central Tank Battery No. 2. A 30-day test was conducted and the water density remained essentially constant, so there should be no quality control problems.

The main component of the filter section was the filter unit (Fig. 57). It was an upflow, graded sand unit. Two tanks and pumps were necessary in order to backwash or regenerate the filter. Gas was added to the flow stream during the backwash cycle. The entire system was enclosed and a gas blanket was maintained in the tanks.

Tracers were used during the waterflood preflush (isopropanol) and with the water during the WAG (n-propanol). Both were injected in concentrations of .05% by volume (approximately 25 gal/day.).

The water injection pump was a triplex pump, powered by an internal combustion engine. The unit was skid-mounted and enclosed in an insulated structure (Fig. 58).

The tanks were leased. All other equipment was purchased. The estimated capital expenditure was \$245,000, of which \$210,000 is for tangible items. Operating expenses are estimated to be \$15,000/month.

Fluid Sampling System

The heart of the fluid sampling system was a three-phase metering separator (Fig. 59). The nominal rating of the unit was 1,000 BPD and 2 MMCFPD at 200 psi. The vessel itself was rated at 250 psi. The horizontal 24" OD x 10' vessel was equipped with standard instrumentation: 1) back-pressure valve and control, 2) relief valve, 3) pressure gauge, 4) thermometer, and 5) gauge glass. In addition, there were level controls for both oil and water and meters for gas, oil, and water. A downstream fluid sampler was attached. Only a small amount of fluid was produced from each observation well to collect representative samples to be analyzed for tracers, CO₂ content, and fluid composition. The entire unit was skid-mounted and enclosed in a steel structure. The building was insulated and the unit was equipped with catalytic heaters to prevent freezing.

The normal flow pattern was from the well being sampled, to the manifold, through the separator, and into the tanks. The separator could be by-passed in the event that there was insufficient wellhead pressure to buck the back-pressure of the separator. Flow from the wells could be initiated and/or maintained by gas-lift. The liquid was collected in the 400 barrel tanks then hauled to Central Tank Battery No. 2. Two tanks were used to check the meters. These tanks also simplified the transfer of the fluids to the tank battery.

The estimated capital cost to install this system was \$75,000 of which \$60,000 was for tangible items. Estimated normal operating expense was \$3,000/month. The majority of this amount was for tank rental and hauling. During the latter stages of the minitest the observation wells will probably have to be gas-lifted to collect fluid samples. This added an estimated \$10,000/month to the operating expenses. The high cost stems from using nitrogen as the gas-lift medium.

SIMULATION MODELS

In order to predict current and future technical performance of the minitest, and as a means of incorporating the large amount of data accumulated from the logs, cores, and well tests, two simulation models were developed: 1) a black-oil simulator, in a three dimensional mode, and 2) a compositional simulator, in one dimensional, two dimensional, and three dimensional modes.

The three dimensional black-oil simulator was used to characterize the reservoir, history match production, and compute the amount and rate of water injection needed to maintain pressure in the minitest area. Those wells surrounding the project area provided: 1) core analysis, 2) open-hole logs, 3) semi-annual bottom-hole pressures, and 4) production performance, and were used as a base for reservoir characterization. As the four minitest wells were drilled and additional core analysis and log data became available, the black-oil model was updated.

The compositional simulator in a one dimensional mode was used to match the slim-tube results of the three CO₂ residual oil saturation tests. By matching the miscibility test data, the one dimensional mode was utilized to determine a very rough estimate of the slug design. The two dimensional mode then expanded on this estimate to refine the slug design for optimizing oil recovery by CO₂ and water injection. The three dimensional mode will be used to monitor the performance of the minitest, obtain a better reservoir characterization and compute the sweep efficiency in the minitest area. Also, the model will be used to predict the expansion of the CO₂ test to a field-wide application. It is believed that an adequate simulation model will contribute significantly to interpretation and extrapolation of test results.

CO₂-WATER INJECTION SCHEME

A study of the water injection phase of the minitest was completed using the three dimensional, three-phase black oil simulator (Appendix 29). The study was designed to investigate the water injection requirements for repressurization and the effects of

injection on the reservoir. Several prediction cases were run to simulate the effects of various injection plans on the minitest area. These cases included two injection start-up dates and two different future production performance schedules.

The following observations were made, based on the results of the study:

1. The pressure in the minitest area will be raised above the calculated minimum CO₂ miscibility pressure of 3,400 psig, if water injection is begun on either October 1, or September 1, 1980.
2. A water injection rate of 1,150 STB/D, for fifteen (15) days, will adequately repressure the pilot area if the above dates are observed.
3. The current rate of reservoir fluid withdrawal will not adversely affect the pilot area if the aforementioned injection plan is utilized.
4. Water injection in the minitest area will not strongly affect the average reservoir pressure in the D-zone of Little Knife Field.

A two dimensional cross-sectional compositional simulator study was performed to develop the water and CO₂ (WAG) portion of the test (Appendix 30). Following a 15 percent pore volume of preflush water, the WAG injection scheme will commence and then be followed by drive water alone.

The optimum CO₂-water injection method will be strongly dependent on reservoir properties. The WAG ratio that gives the best mobility control will depend on the extent to which water and CO₂ will segregate in the reservoir. This will be dependent on capillary, gravity, and viscous force interactions across the minitest interval and layers of stratification. The optimum CO₂ volume to be injected will depend on: 1) CO₂ storage behind the CO₂-water front, 2) trapping of CO₂ by the drive water, 3) the extent to which stratification causes bypassing, and 4) on fingering and dispersive mixing at the CO₂-oil front (the simulator does not adequately represent these last two effects).

Work to optimize these parameters involved choosing a base case injection scheme, using likely values for the parameters. Each parameter was then varied from the base case value and the sensitivity of recovery and process performance to it was determined by simulation results. Three different WAG ratios were analyzed. They were: 1) 1:1, 2) 0:1, and 3) 3:1 (reservoir barrels of water/reservoir barrels of CO₂). The following results were observed:

1. Although ultimate recovery is more or less the same for all the CO₂ floods, breakthrough of injected fluids is earliest for the 3:1 WAG ratio and latest for the 1:1 WAG ratio. For CO₂ alone, breakthrough is slightly earlier than for the 1:1 WAG ratio. On this basis, we would prefer

the 1:1 WAG ratio. The improvements that a 1:1 WAG ratio flood gives over CO₂ alone are 2.3 percent PV more oil and a small improvement in breakthrough time. This would appear to be worth the extra effort involved in carrying out a WAG type flood.

2. Ultimate recoveries after about one (1) hydrocarbon pore volume (HCPV) total fluid injection (800-1,000 days) are high for all the CO₂ flood simulations: a) 76.5 percent original oil in place (OOIP) for the 1:1 WAG ratio, b) 74.2 percent OOIP for CO₂ alone, and c) 77.5 percent OOIP for the 3:1 WAG ratio, compared with 41.2 percent OOIP for a waterflood. Cumulative CO₂:oil ratios at this time are all low, about 1 MSCF/bbl. It should be realized that these CO₂ flood predictions in a cross-sectional model not allowing for areal sweep and capture efficiency effects, and other effects such as viscous fingering and dispersive mixing, will be optimistic. Also, some oil that is attributed to the CO₂ flood could have been recovered by primary and secondary methods. However, the fact that gravity segregation of CO₂ and water, and gravity override of oil by CO₂ do not seem to be important, even for the assumed $K_v/K_h = 1$, is a positive factor. Bypassing of oil because of permeability stratification appears to be limited. Overall, vertical sweep efficiency appears to be good.

Conclusions of the two dimensional, cross-sectional simulator study are:

1. The simulator represents CO₂-Little Knife crude oil behavior and the development of multiple contact miscibility in slim-tubes.
2. Residual oil saturation is low above the minimum miscibility pressure and does not depend on CO₂-water ratio.
3. A 1:1 water-CO₂ ratio appears, on the basis of breakthrough time, to be the best of those investigated. Recovery in the cross-sectional model after one (1) HCPV total fluid injection is 57.2 percent PV or 76.5 percent OOIP. (These numbers include primary and secondary oil and are not corrected for areal sweep and capture efficiencies.)

The following information was used to determine the project injection sequence:

1. Pattern Pore Volume (PV) = 779 M ft³
= 139 M Bbl
2. Hydrocarbon Pore Volume (HCPV) = 587 M ft³
= 105 M Bbl
3. Injection Rates: Water - 1,150 BPD
CO₂ - 40 tons/day

4. Reservoir Volume Factors: Water - 1.04 R Bbl/Bbl
 CO₂ - 74.1 R ft³/ton

SCHEDULE

	Volume	Time
Pre-flush Water	15% PV 20,000 Bbl	17 days
CO ₂	5% HCPV 400 tons	10 days
Water	5% HCPV 5,000 Bbl	4 days
CO ₂	5% HCPV 400 tons	10 days
Water	5% HCPV 5,000 Bbl	4 days
CO ₂	5% HCPV 400 tons	10 days
Water	5% HCPV 5,000 Bbl	4 days
CO ₂	5% HCPV 400 tons	10 days
Water	5% HCPV 5,000 Bbl	4 days
CO ₂	5% HCPV 400 tons	10 days
Water	100% PV 134,000 Bbl	<u>116 days</u>
		199 days

Actual flood-out injection will end when there is no change in TDT log response in the observation wells.

Fluid injection is expected to commence in early December, 1980 and will follow as close as possible the above schedule. Data acquisition during the injection period will be performed as follows:

1. Monitor injection pressure and injection rate continuously.
2. Record bottom-hole pressure in each well continuously.
3. Sample fluid from observation wells periodically to check for tracers and fluid composition.
4. Sample fluid from offset producing wells once a month.
5. Run TDT logs in each observation well until response is noted, then increase frequency as required.

ACKNOWLEDGEMENTS

Thanks is given to the various members of Gulf Oil Corporation for their assistance in preparing this report.

REFERENCES

1. White, T. M. and Lindsay, R. F.: "Enhanced Oil Recovery by CO₂ Miscible Displacement in the Little Knife Field, Billings County, North Dakota," DOE 5th Sym. Enhanced Oil & Gas Recovery & Improved Drilling Tech. (1979) V. 2, N-5/1-19.
2. Svor, T. R. and Price, J. M.: "Results of Water Injection From Cased-Hole Log Analysis in the Zabolotny Injection No. 1 Well," Gulf Science and Technology Tech. Memorandum No. 445STL084 (August 1980).
3. Kingelin, G. F., Cleland, R. B. and Barrett, D. L.: "Little Knife CO₂ Minitest Project, Multiwell Pulse Test Report," Gulf Science and Technology Tech. Memorandum No. 444TL207 (May 1980).
4. Hickey, M. C., Hurd, T. A., Kingelin, G. F. and Larsen, W. K.: "Reservoir and Formation Characterization-Little Knife CO₂ Minitest Project," Gulf Science and Technology Tech. Memorandum No. 445TM093 (March 1981).
5. Wilson, J. L.: "Carbonate Facies in Geologic History," Springer-Verlag (1975) 471.
6. Maiklem, W. R., Bebout, D. G. and Glaister, R. P.: "Classification of Anhydrite-A Practical Approach," Can. Petro. Geol. Bull. (1969) V.17, N.2, 194-233.
7. Butler, G. P.: "Modern Evaporite Deposition and Geochemistry of Coexisting Brine, the Sabkha, Trucial Coast, Arabian Gulf," J. Sed. Petrology (1969) V. 39, 70-89.
8. Jacka, A. D. and Franco, L. A.: "Deposition and Diagenesis of Permian Evaporites and Associated Carbonates and Clastics on Shelf Areas of the Permian Basin." Fourth Sym. on Salt: Northern Ohio Geol. Soc. (1974) V. 1, 67-89.
9. Bathurst, R. G. C.: "Carbonate Sediments and their Diagenesis," Elsevier, Amsterdam (1975) 650.
10. Thomas, G. E.: "Lineament-Block Tectonics: Williston-Blood Creek Basin," Amer. Assoc. Petro. Geol. Bull. (1974) V. 58, N.7 1305- 1322.
11. Hodgson, R. A.: "Little Knife Fracture Study Preliminary Report," Gulf Science and Technology Tech. Memorandum No. 4224DC80 (July 1978).
12. Bigelow, E. L.: "Fracture Detection: Core Vs. Log Comparison, Little Knife CO₂ Project," Gulf Science and Technology Tech. Memorandum No. 4453KR03-27 (May 1980).
13. Wardlaw, N. C.: "Pore Geometry of Carbonate Rocks as Revealed by Pore Casts and Capillary Pressure," Amer. Assoc. Petro. Geol. Bull. (1976) V. 60, N. 2, 245-257.

14. Wardlaw, N. C. and Taylor, R. P.: "Mercury Capillary Pressure Curves and the Interpretation of Pore Structure and Capillary Behavior in Reservoir Rocks," Can. Petro. Geol. Bull. (1976) V. 24, N. 2, 225-262.
15. Pettijohn, F. J.: "Sedimentary Rocks," Harper & Row (1957) 718.
16. Rasor, R. W., Haulenbeek, R. B., Avenshine, R. A. and Thakur, G. C.: "Little Knife CO₂ Minitest Water Injection Simulation," Gulf Science and Technology Company Report No. 445RL029 (July 1980).
17. Proctor, R. M. and Macauley, G.: "Mississippian of Western Canada and Williston Basin," Amer. Assoc. Petro. Geol. Bull. (1968) V. 52, N. 10, 1956-1968.
18. Wittstrom, M. D. Jr. and Hagemeyer, M. E.: "A Review of Little Knife Field Development, North Dakota," Williston Basin Symposium, Montana Geol. Soc. (1978) 361-368.
19. Wittstrom, M. D. Jr. and Hagemeyer, M. E.: "A Review of Little Knife Field Development," Oil & Gas J. (1979) V. 77, N. 6, 86-92.
20. Carlson, C. G. and Anderson, S. B.: "Sedimentary and Tectonic History North Dakota Part of Williston Basin," Amer. Assoc. Petro. Geol. Bull (1965) V. 49, N. 11, 1833-1846.
21. Habicht, J. K. A.: "Paleoclimate, Paleomagnetism and Continental Drift," Amer. Assoc. Petro. Geol. Studies in Geol. (1979) N.9, 31.
22. Lindsay, R. F. and Kendall, C. G. St. C.: "Depositional Facies, Diagenesis and Reservoir Character of the Mission Canyon Formation (Mississippian) of the Williston Basin at Little Knife Field, Billings, Dunn and McKenzie Counties, North Dakota," Soc. Econ. Paleo Mineral. Core Workshop No. 1 (1980) 79-104.
23. Irwin, M. L.: "General Theory of Epeiric Clear Water Sedimentation," Amer. Assoc. Petro. Geol. Bull. (1965) V.49, N.4, 445-459.
24. Lindsay, R. F. and Kendall, C. G. St. C.: "Depositional Facies, Diagenesis and Reservoir Character of the Mission Canyon Formation (Mississippian) of the Williston Basin at Little Knife Field, North Dakota," Casebook Examples of Carbonate Petroleum Reservoirs, Springer-Verlag (in press).
25. Nettle, R. L., Lindsay, R. F. and Desch, J. B.: "Enhanced Oil Recovery by CO₂ Miscible Displacement in the Little Knife Field, Billings County, North Dakota," DOE/BETC/IC Annual Report-Enhanced Oil Recovery (1980) V. 3, G-4/1-15.

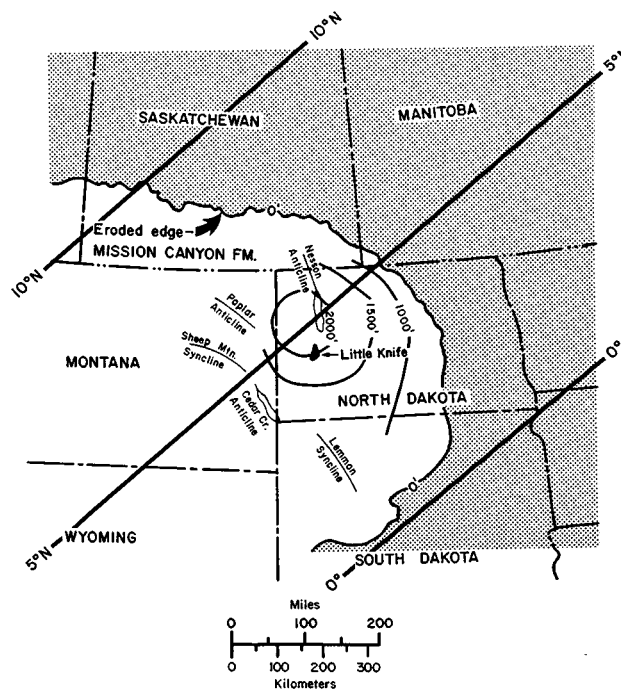


Fig. 1-Index map of Williston Basin, including: a) eroded edge of Mission Canyon Formation (Proctor and Macauley, 1968), b) major surface and subsurface structural features (Wittstrom and Hagemeyer, 1978, 1979), c) isopach thickness of Madison Group (Carlson and Anderson, 1965), and d) the generalized paleolatitude during the Carboniferous (Habicht, 1979).

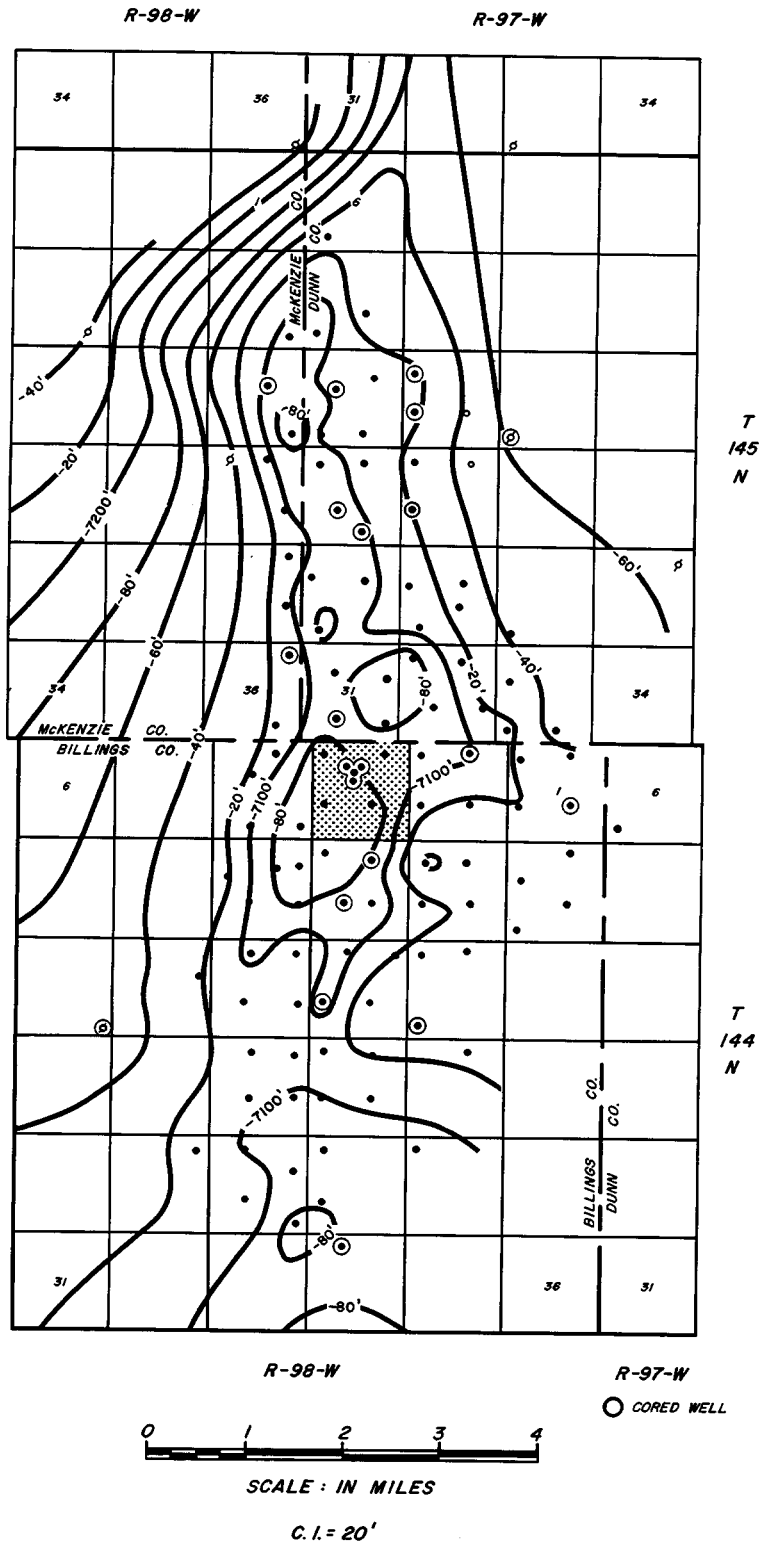


Fig. 2-Top of Mission Canyon Formation structure map, Little Knife Field. Black dots represent well locations. Circled wells are cored. Inverted four spot within stippled section is the CO₂ minitest project location. Structure map is contoured on a subsea datum. Modified after Lindsay and Kendall²².

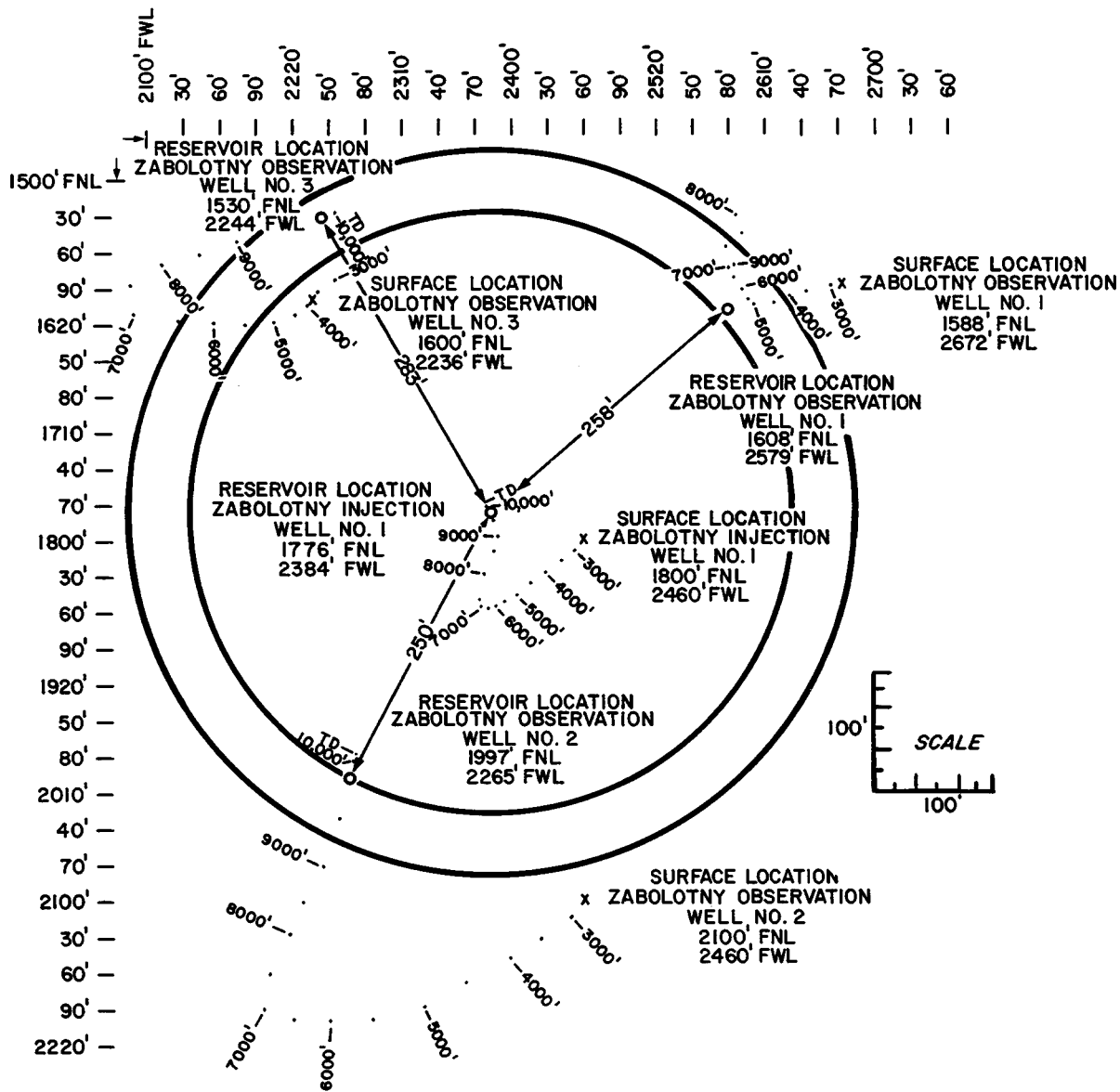


Fig. 3—Little Knife CO₂ minitest pattern, an inverted four spot, in Sec. 3, T144N, R98W, Billings County, North Dakota. The outer circle is 600 feet in diameter, inner circle is 500 feet in diameter. Center of the circle is the reservoir location of the central injection wellbore. Surface and reservoir locations of the wellbore, as well as the direction each well drilled is calculated and plotted from gyroscopic multi-shot surveys run in each well. Depth marks are noted from 3,000 feet to TD at 500-foot intervals.

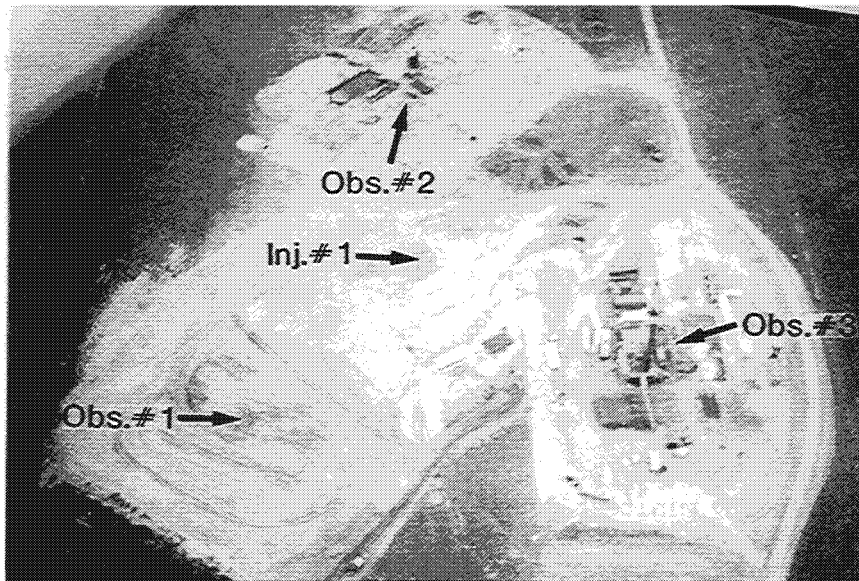


Fig. 4-Little Knife CO₂ minitest location. View in both photos is directly south. Upper photo illustrates the low lying country side, under cultivation, surrounding the minitest location. Bottom photo is a close-up view of the minitest location, with each of the four wells labeled. Gulf Zabolotny Observation Well No. 3 is in the process of having open hole logs run, after reaching TD.

ZABOLOTNY INJECTION #1 TUBING SETTING

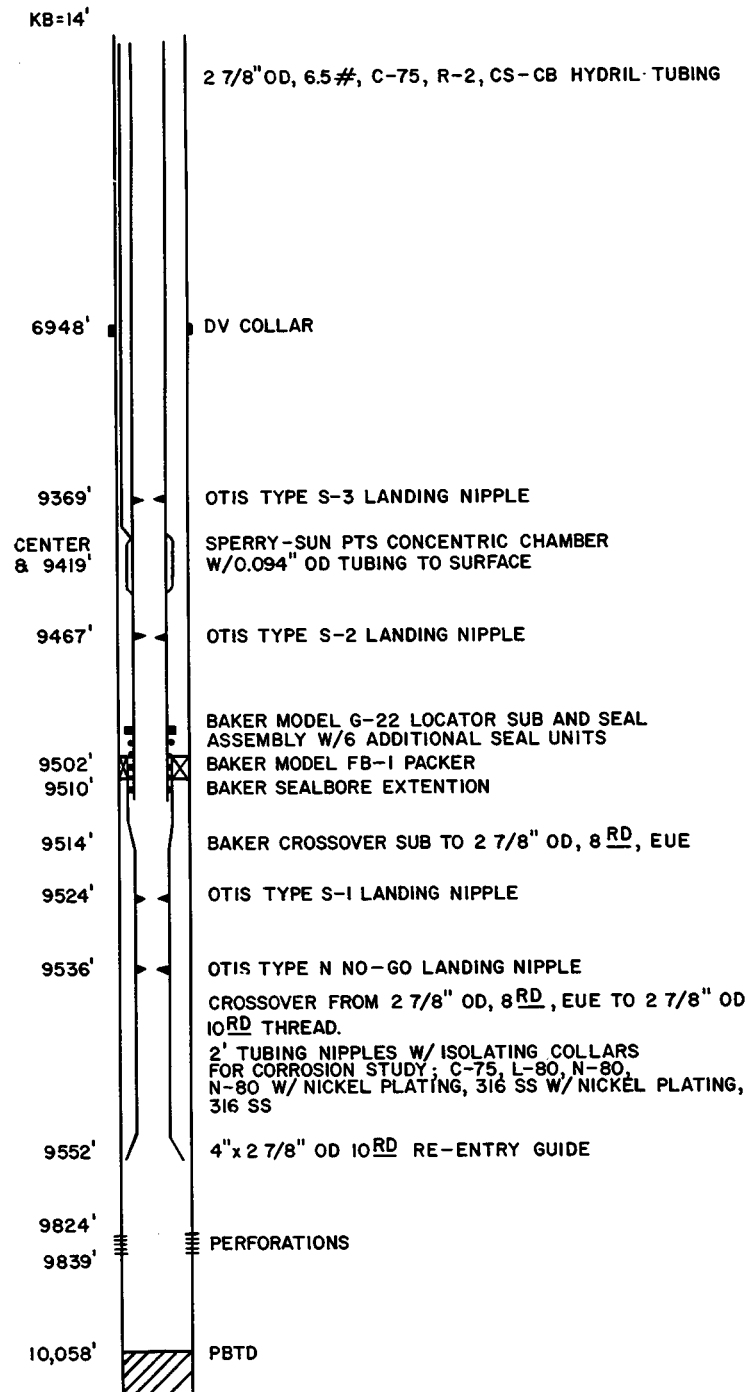


Fig. 5-Casing and tubing settings in the Zabolotny Injection Well No. 1. The casing is 5 1/2" OD, L-80, R-III, 8rd, LT&C. The weight below the DV collar is 23.0#/ft. and the weight above is 17.0#/ft. The tubing is 2-7/8" OD, 6.5#/ft., C-75, R-2, CS-CB, Hydril, coated internally with TK-2.

ZABOLOTNY INJECTION #1

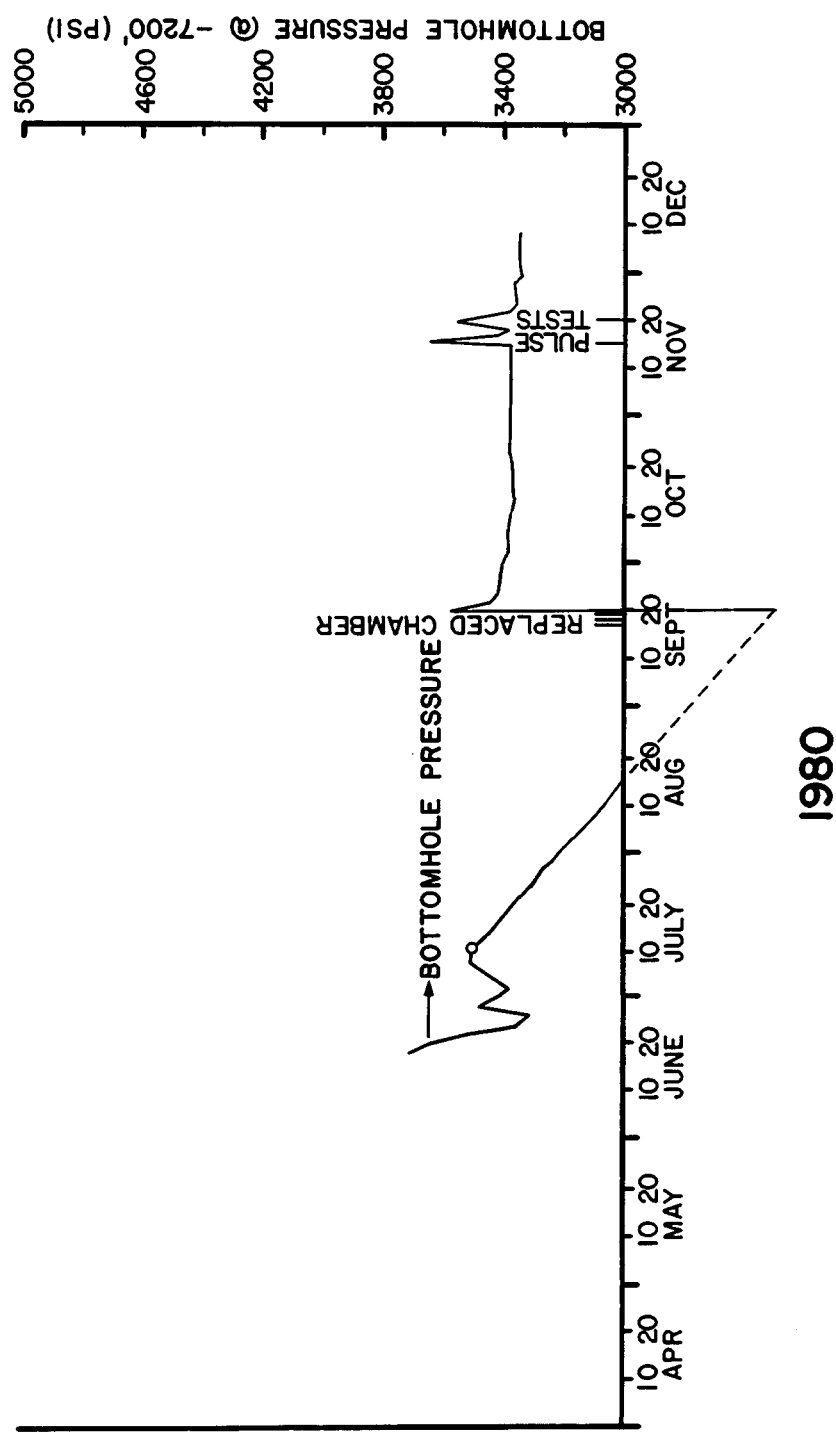


Fig. 6 -Pressure history curve for Zabolotny Injection Well No. 1. All recorded pressures are gradient corrected to a common datum of -7,200 feet.

ZABOLOTNY INJECTION # 1

TUBING SETTING

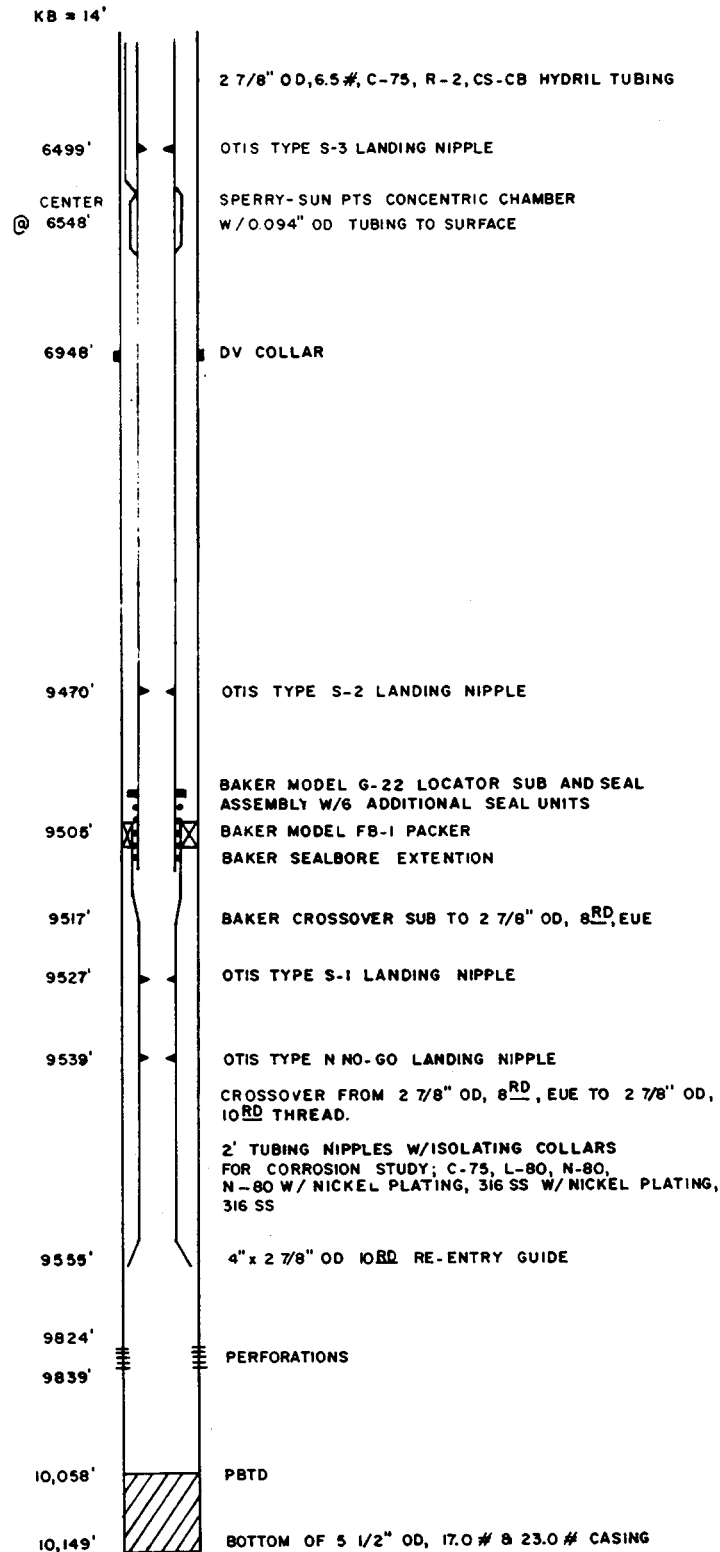


Fig. 7-Modified tubing setting to avoid "tight" spots in Zabolotny Injection Well No. 1.

WELLHEAD SCHEMATIC INJECTION WELL

BOTTOM HEAD CONNECTION TO BE 2 7/8" HYDRIL CS-CB
THREADED PIN.

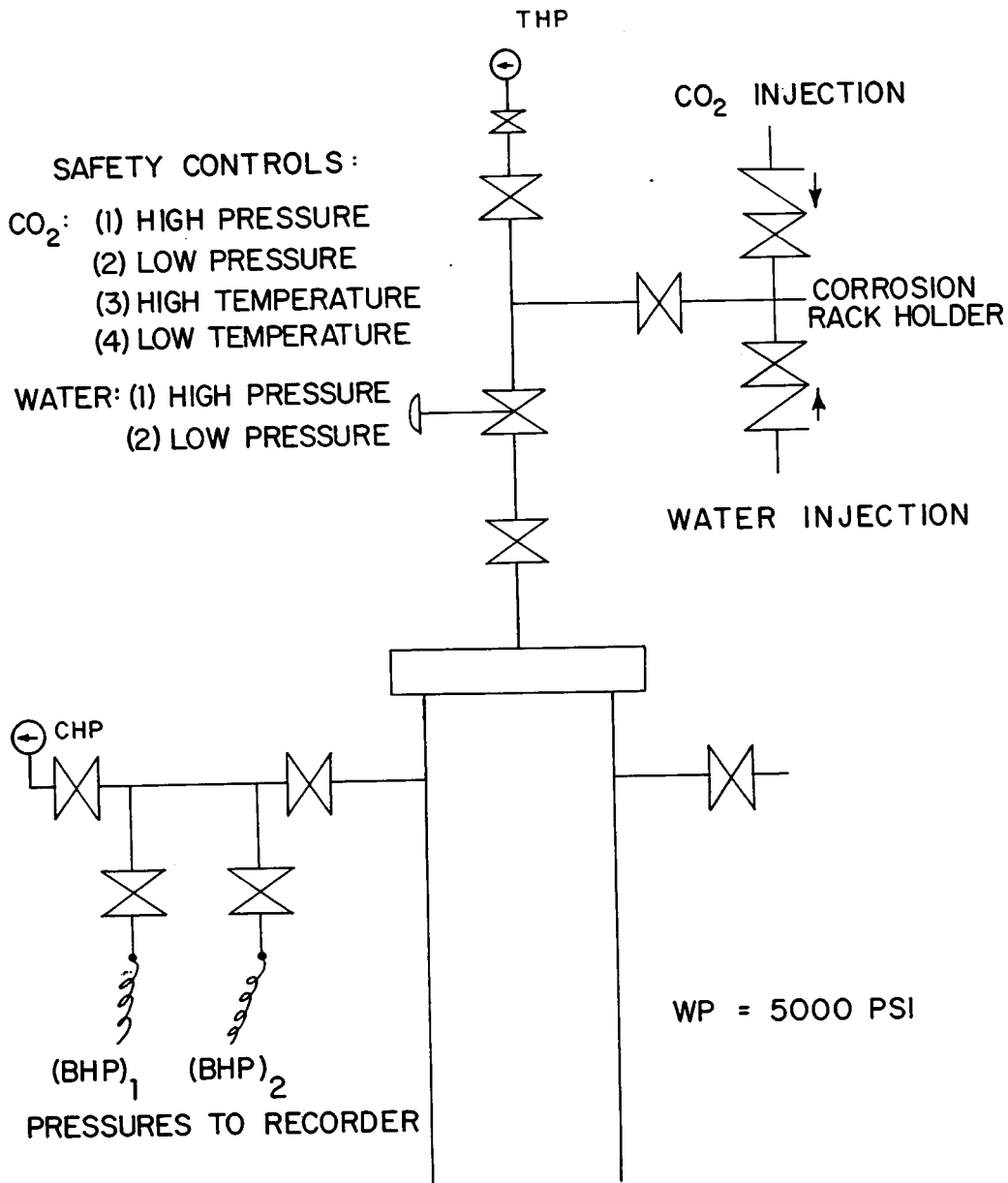


Fig. 8-Wellhead schematic of the Zabolotny Injection Well No. 1. The wellhead casing fittings are coated with D-trim, which is H₂S corrosion resistant, and has an Inconel-clad bore, NACE rated for H₂S atmospheres.

WELLHEAD SCHEMATIC OBSERVATION WELL

BOTTOM HEAD CONNECTION TO BE 2 $\frac{7}{8}$ " HYDRIL CS-CB
THREADED PIN.

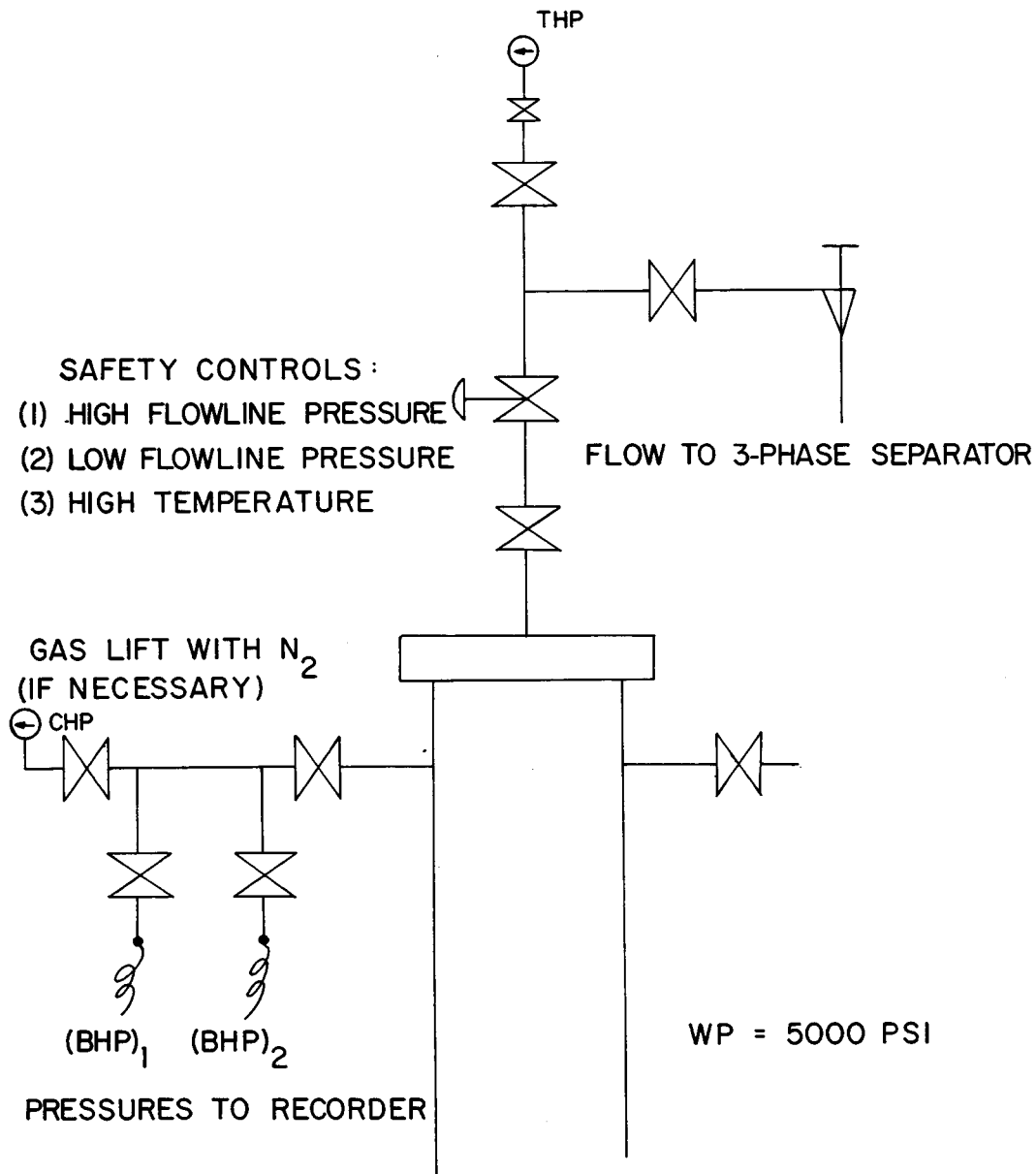


Fig. 9—Wellhead schematic of the Zabolotny Observation Wells. Each wellhead contains the same metallurgy as the Zabolotny Injection Well No. 1 wellhead with the only difference between them being the valve arrangement.

ZABOLOTNY OBSERVATION #1 TUBING SETTING

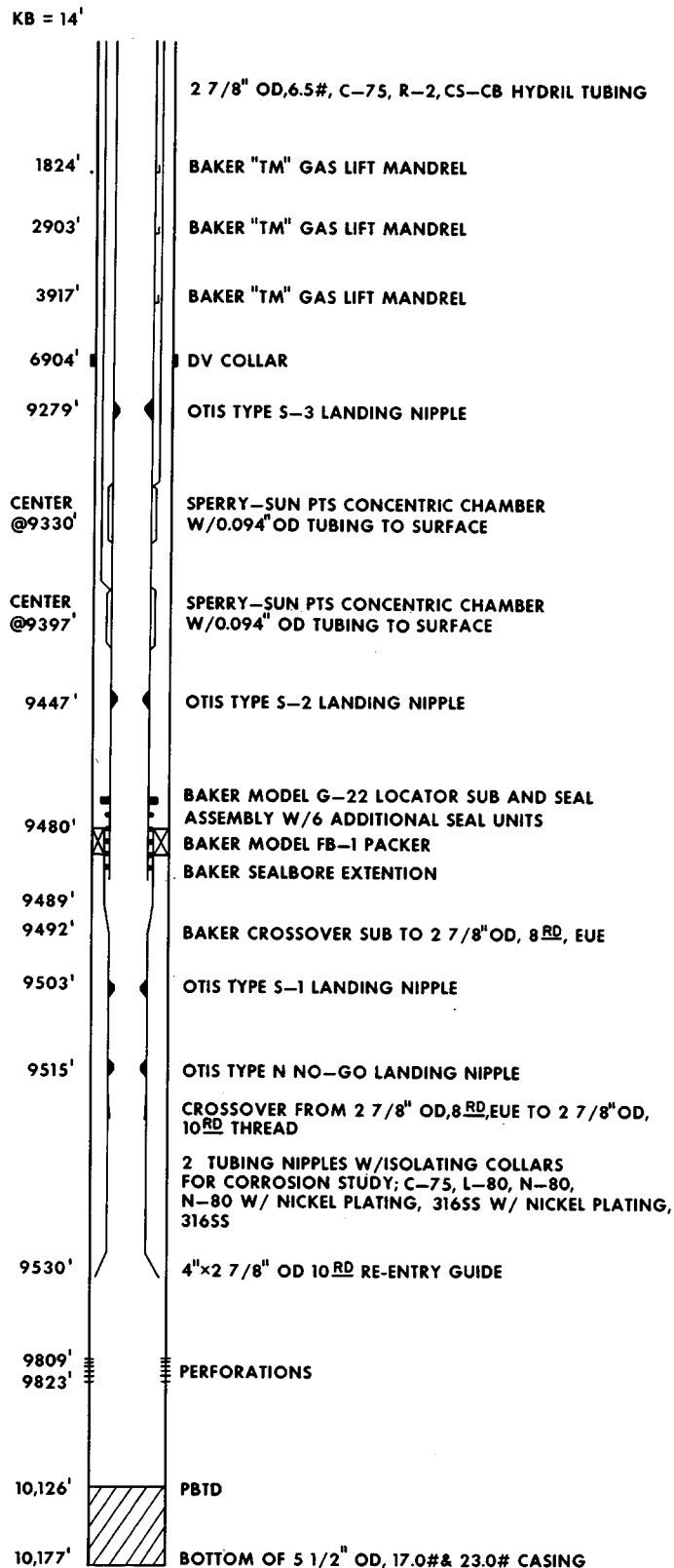
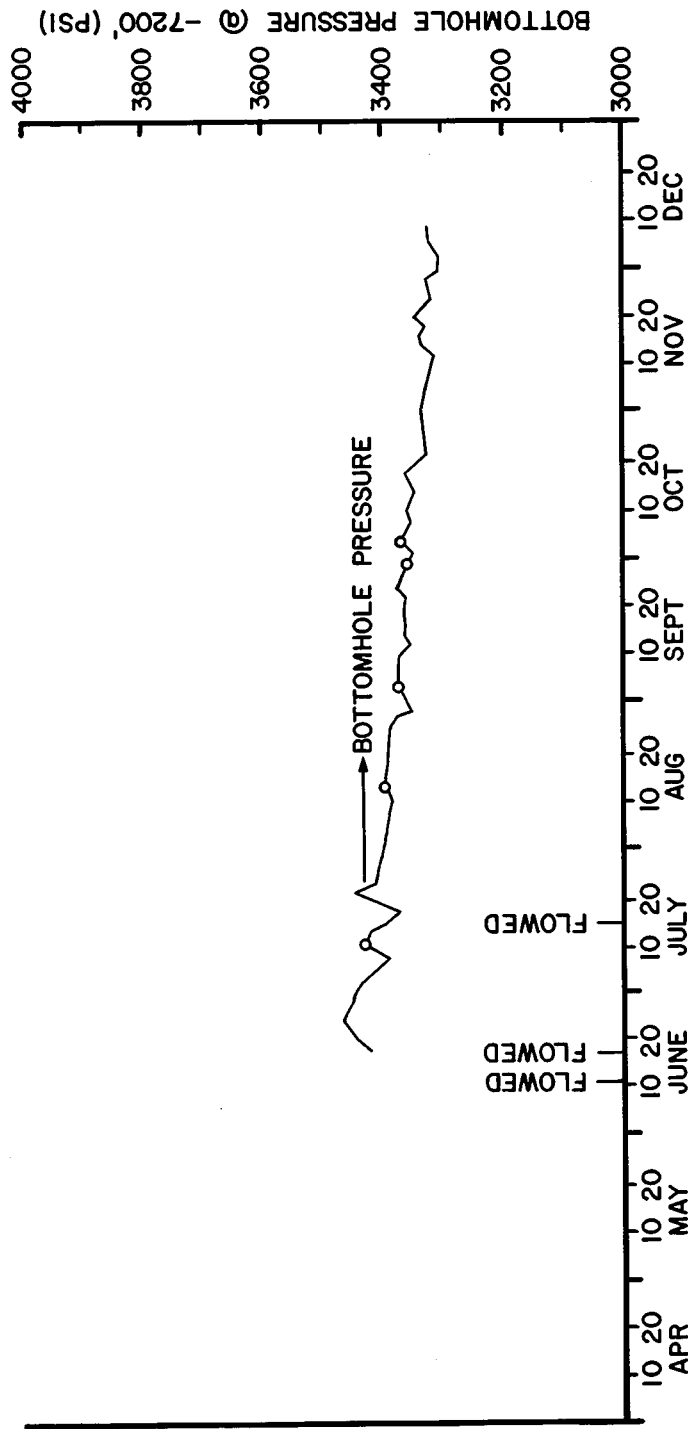


Fig. 10-Casing and tubing settings in the Zabolotny Observation Well No. 1. The casing is 5 1/2" OD, 23#/ft., N-80, RIII, 8rd, LT&C below the DV collar and 5 1/2" OD, 17#/ft., L-80, RIII, LT&C above the DV collar. The tubing is 2 7/8" OD, 6.5#/ft., C-75, R-2, CS-CB, Hydril, coated internally with TK-7.

ZABOLOTNY OBSERVATION #1



1980

Fig. 11 -Pressure history curve for Zabolotny Observation Well No. 1. All recorded pressures are gradient corrected to a common datum of -7,200 feet.

ZABOLOTNY OBSERVATION #2

TUBING SETTING

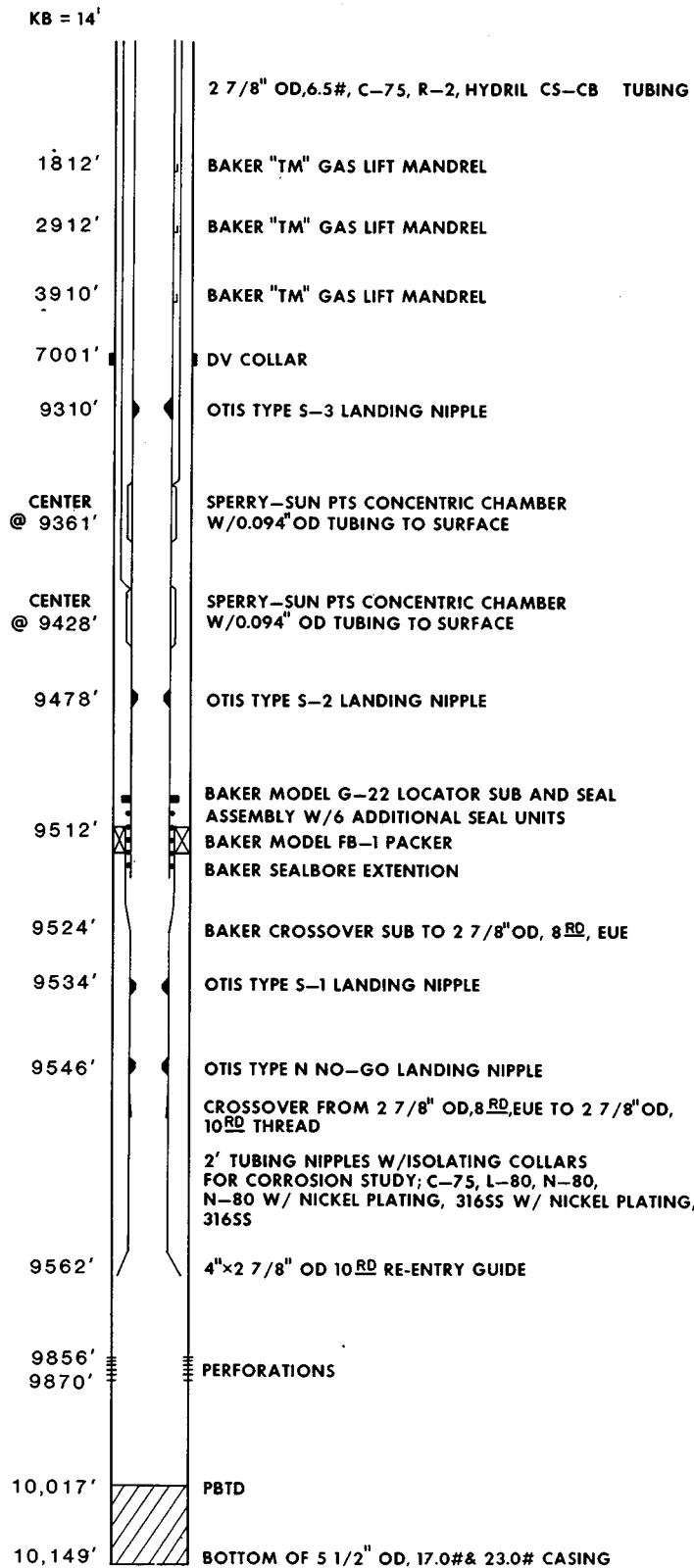
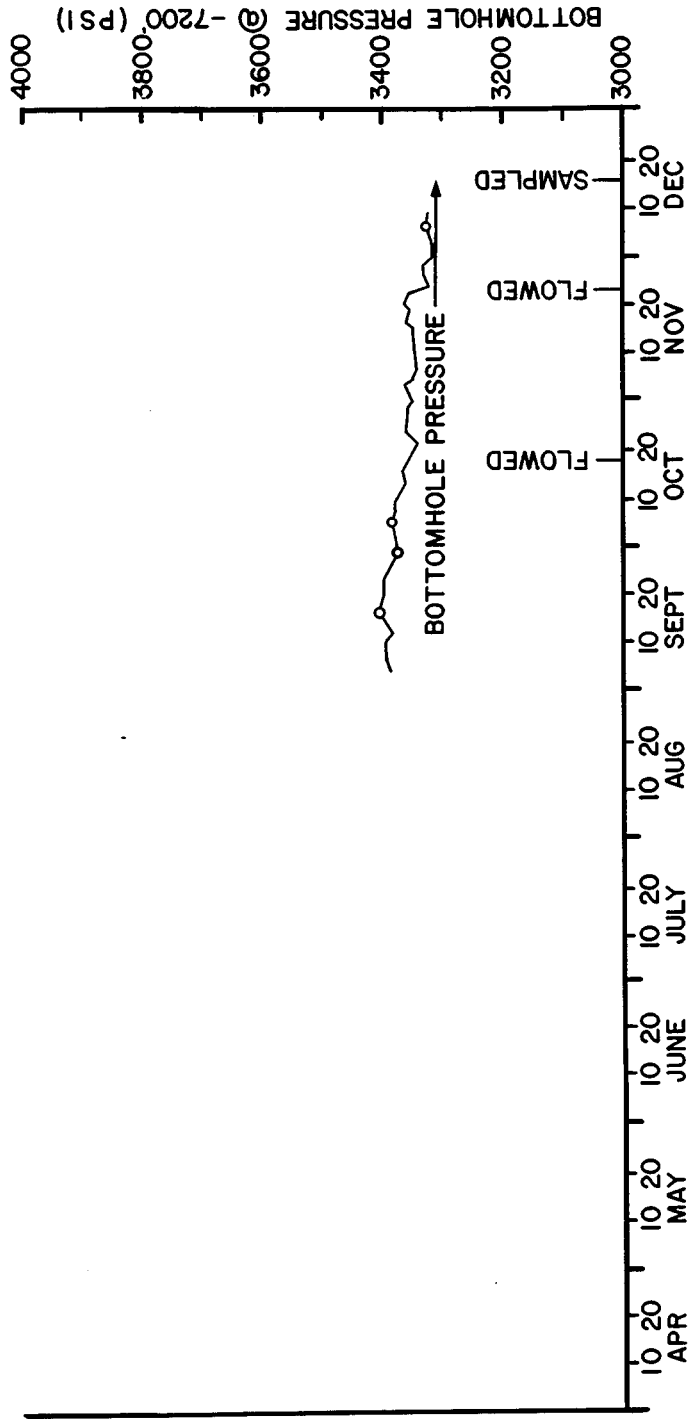


Fig. 12-Casing and tubing settings in the Zabolotny Observation Well No. 2. The casing is 5 1/2" OD, 23#/ft., N-80, R-III, 8rd, LT&C below the DV collar and 5 1/2" OD, 17#/ft., L-80, R-III, LT&C above the DV collar. The tubing is 2 7/8" OD, 6.5#/ft., C-75, R-2, CS-CB, Hydril, coated internally with TK-7.

ZABOLOTNY OBSERVATION #2



1980

Fig. 13 -Pressure history curve for Zabolotny Observation Well No. 2. All recorded pressures are gradient corrected to a common datum of -7,200 feet.

ZABOLOTNY OBSERVATION #3 TUBING SETTING

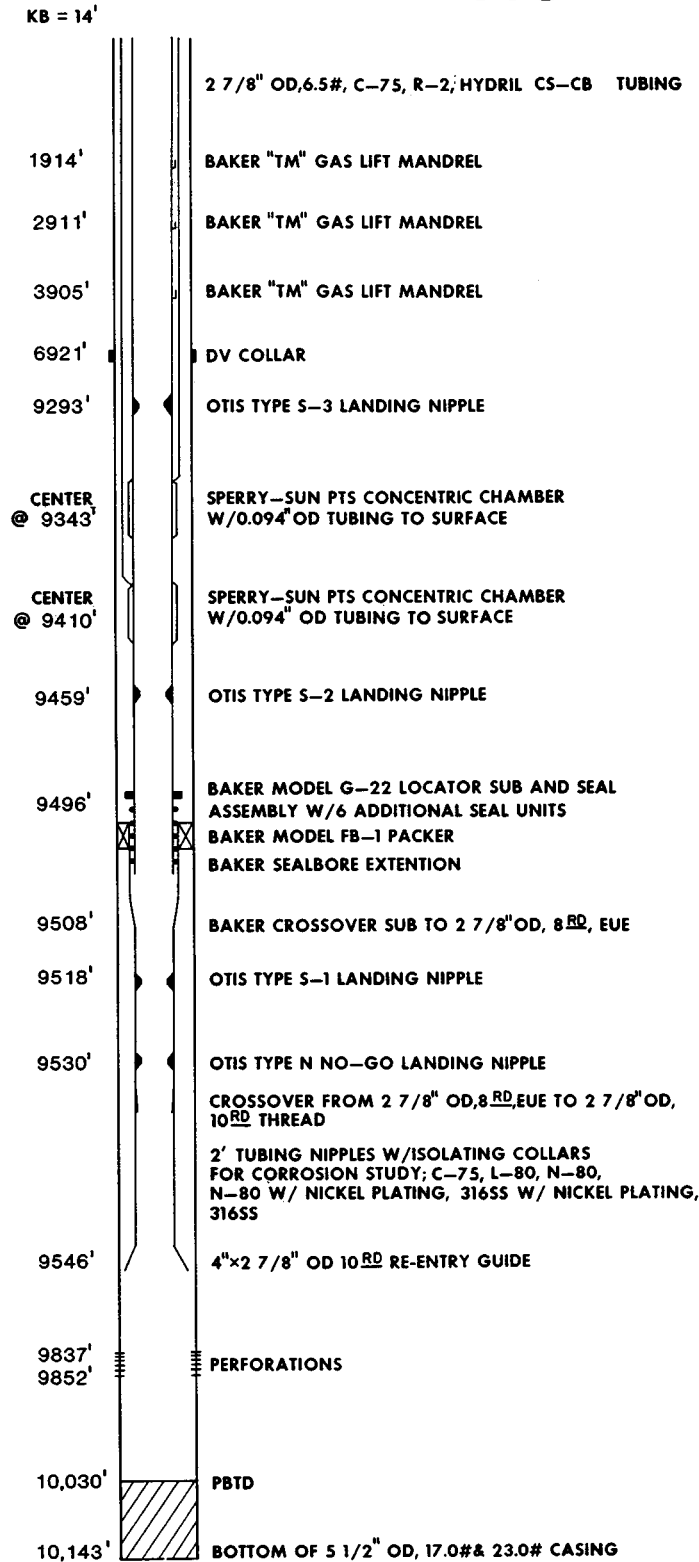
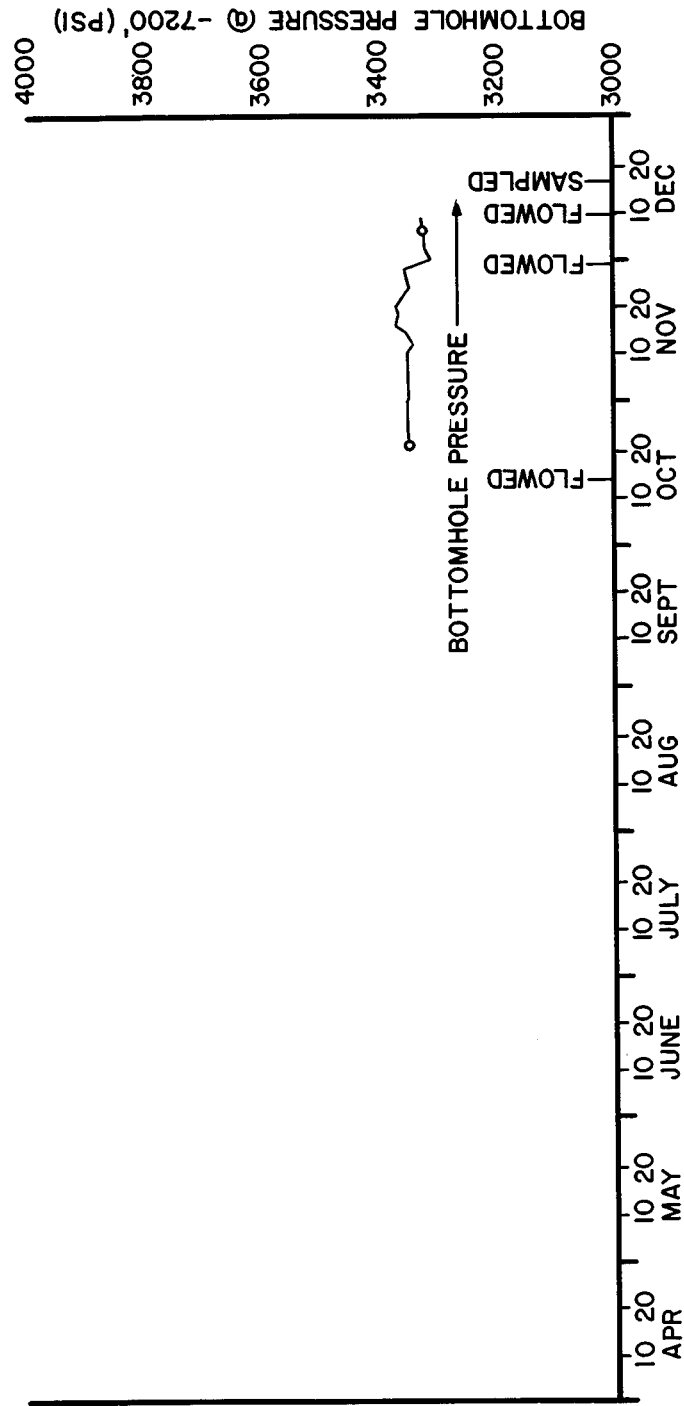


Fig. 14-Casing and tubing settings in the Zabolotny Observation Well No. 3. The casing is 5 1/2" OD, 23#/ft., N-80, R-III, 8rd, LT&C below the DV collar and 5 1/2" OD, 17#/ft., N-80, R-III, LT&C above the DV collar. The tubing is 2 7/8" OD, 6.5#/ft., C-75, R-2, CS-CB, Hydril, coated internally with TK-7.

ZABOLOTNY OBSERVATION #3



1980

Fig. 15 -Pressure history curve for Zabolotny Observation Well No. 3. All recorded pressures are gradient corrected to a common datum of -7,200 feet.

ZABOLOTNY OBSERVATION WELL NO. 1

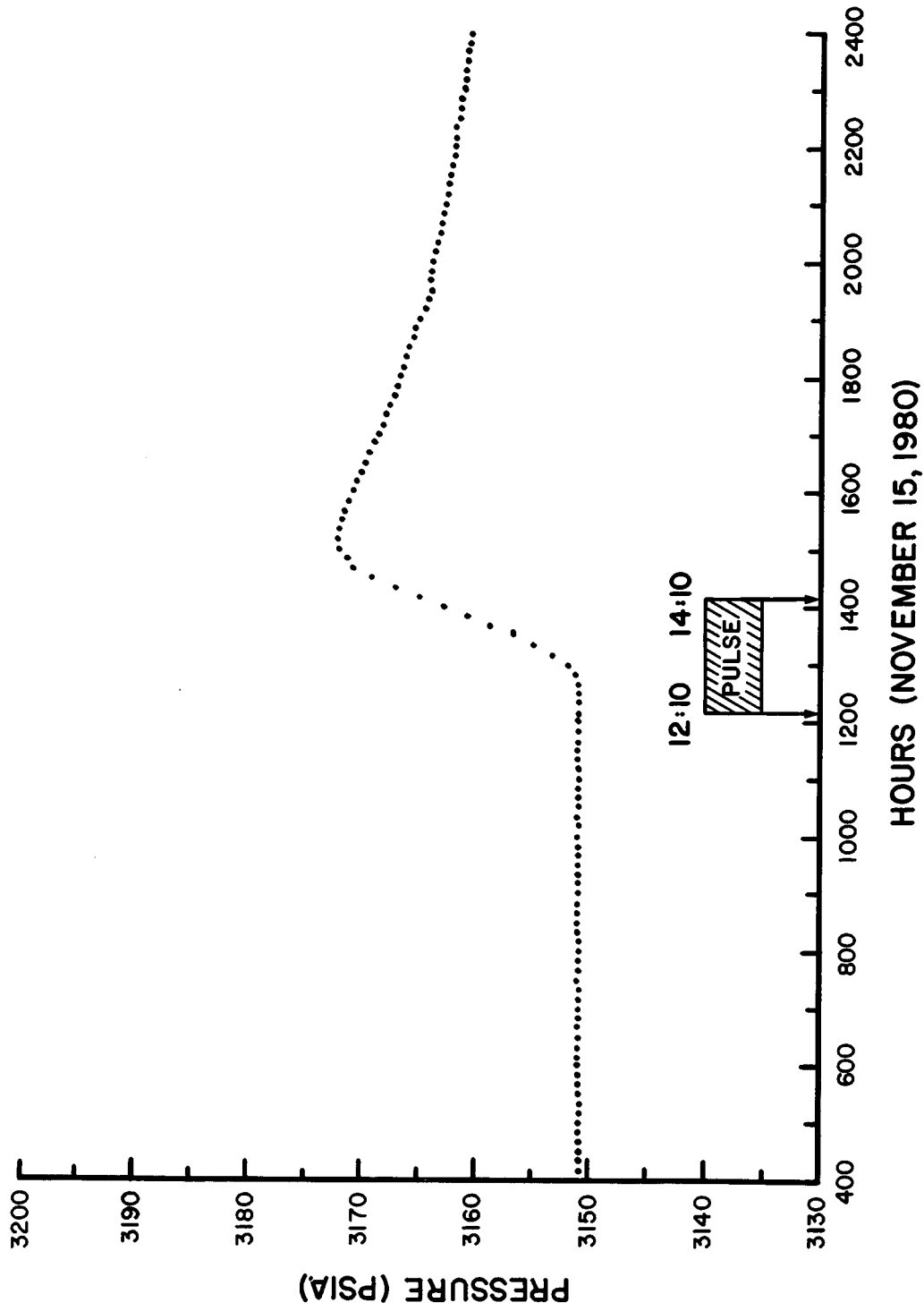


Fig. 16-Four well multi-well pulse test response recorded at Zabolotny Observation Well No. 1. Pressure (psia) at the surface recorded from the bottom PTS chamber (not helium corrected).

ZABOLOTNY OBSERVATION WELL NO. 2

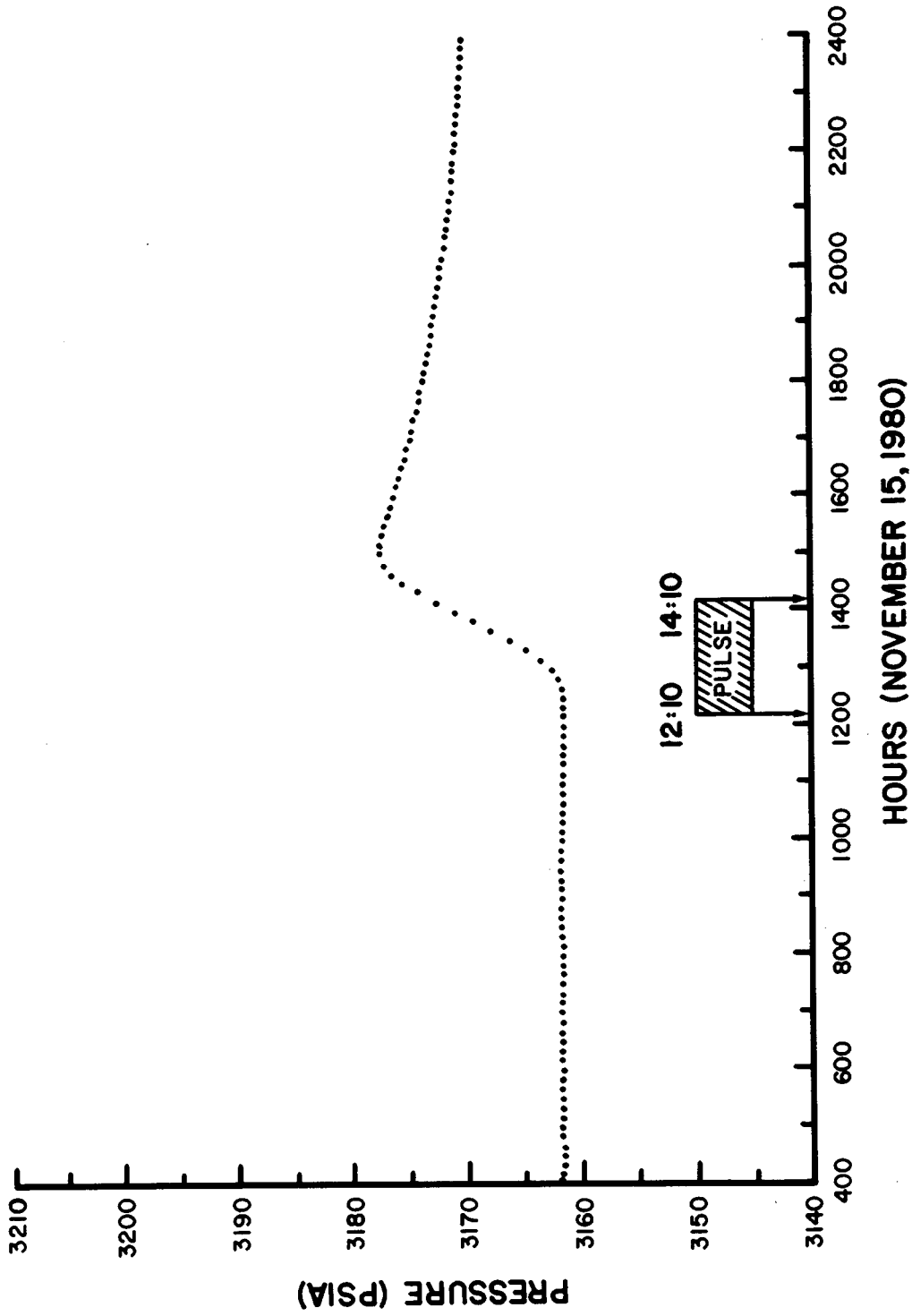


Fig. 17-Four well multi-well pulse test response recorded at Zabolotny Observation Well No. 2. Pressure (psia) at the surface recorded from the bottom PFS chamber (not helium corrected).

ZABOLOTNY OBSERVATION WELL NO. 3

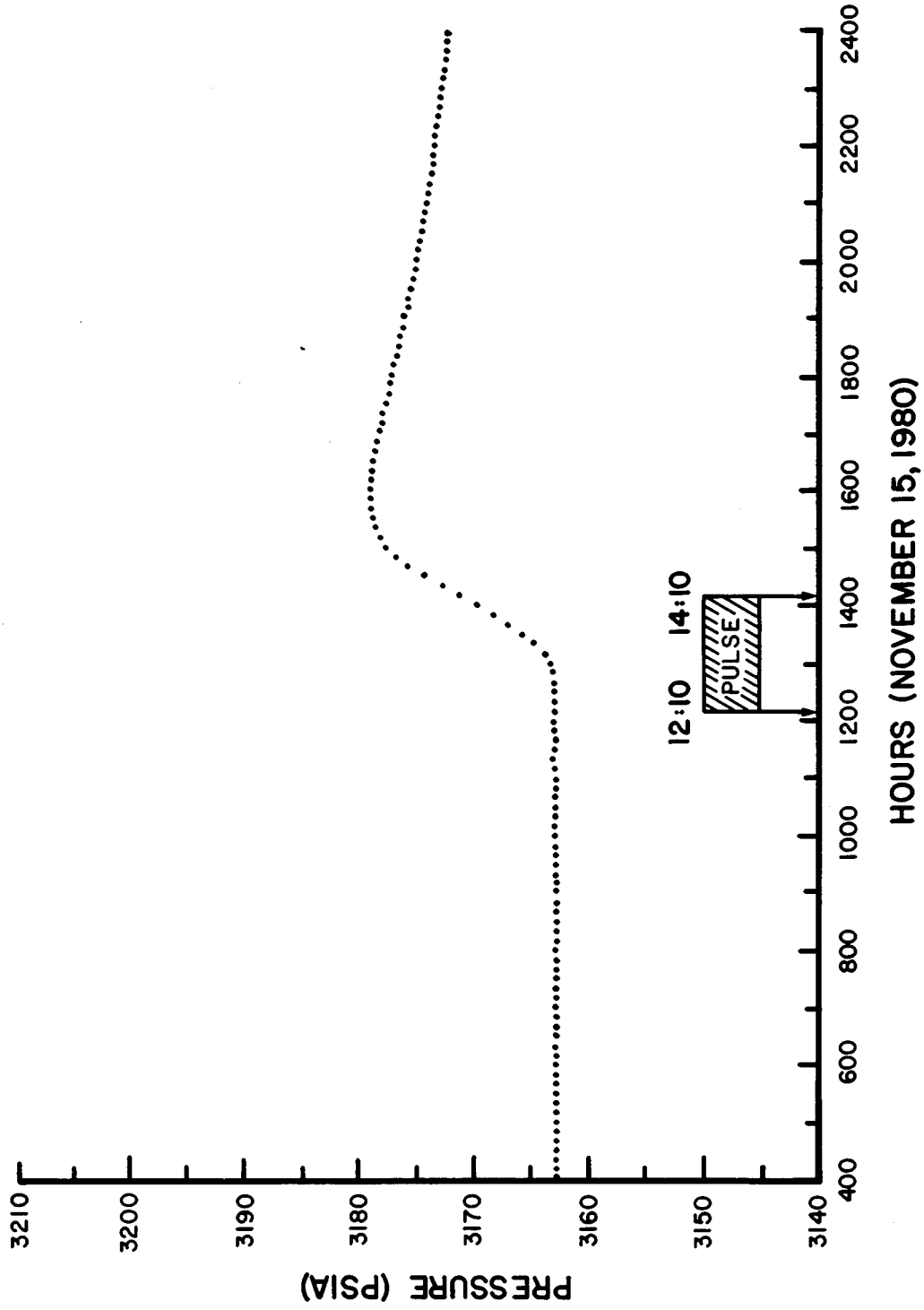


Fig. 18-Four well multi-well pulse test response recorded at Zabolotny Observation Well No. 3. Pressure (psia) at the surface recorded from the bottom PFS chamber (not helium corrected).

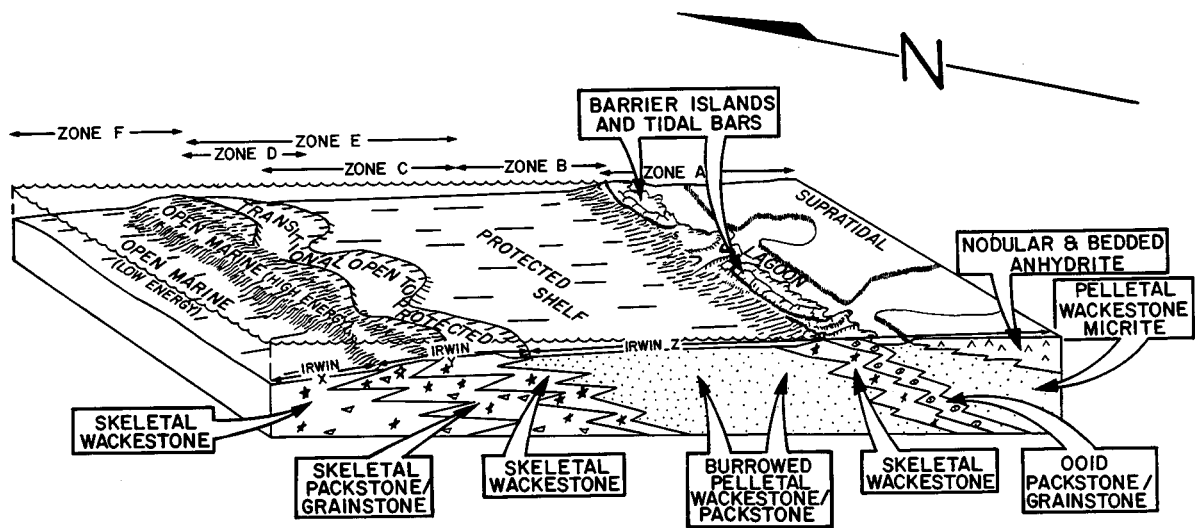


Fig. 19—Idealized depositional setting of Mission Canyon Formation at Little Knife Field. Informal log zonation A-F (top) and Irwin's²³ epeiric sea energy zones X, Y and Z (base) illustrate respective positions both occupied in the depositional system. Modified after Lindsay and Kendall²⁴.

ZABOLOTNY INJECTION #1

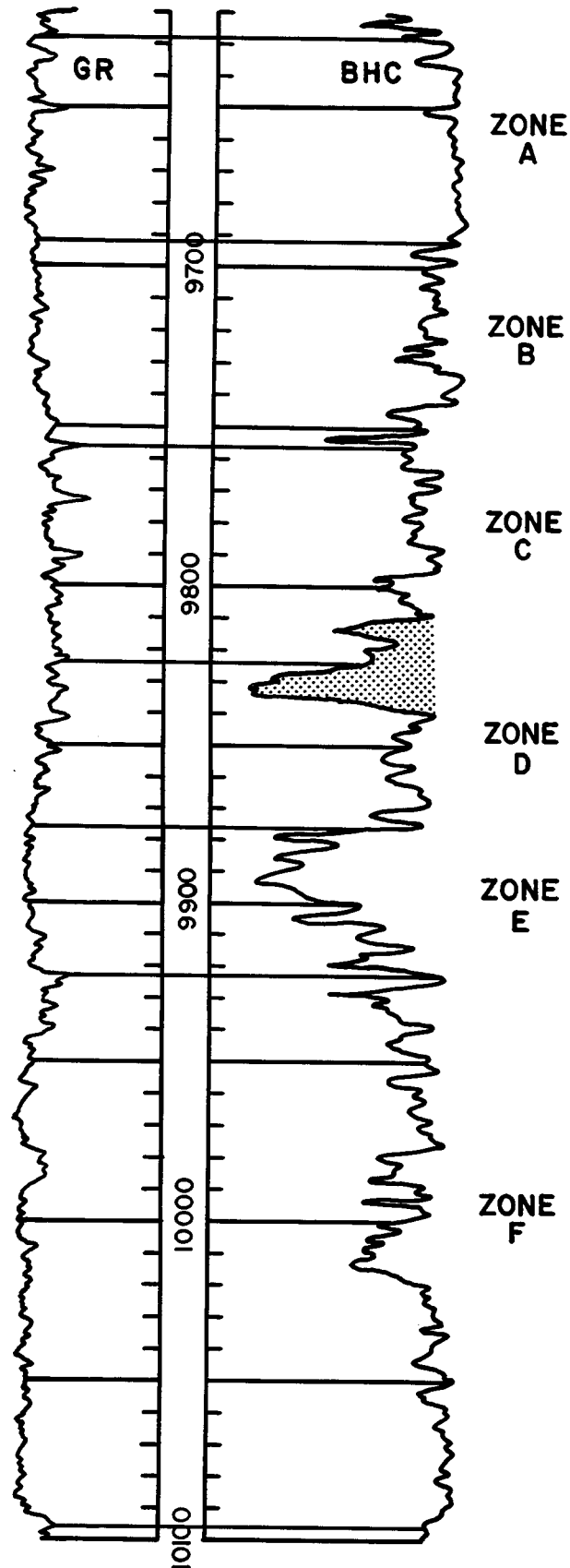


Fig. 20-Zabolotny Injection Well No. 1 sonic log (BHC), the central well within the CO₂ minitest. The complete Mission Canyon Formation is displayed, including the informal log zonations A-F. The project interval is the shaded portions in the base of zone C and the top of zone D.

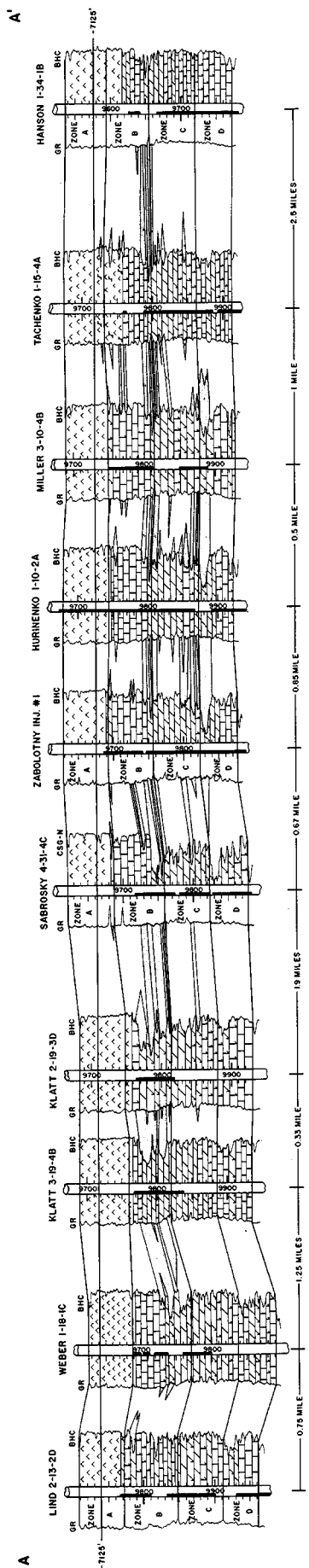


Fig. 21-North-south structural fence diagram of zones A, B, C and D of Mission Canyon Formation through cored wells in Little Knife Field. Black vertical bars represent cored intervals in each well. Shaded areas are porous hydrocarbon-bearing beds. Lithologies from core and log calculations illustrate rock types and their lateral and vertical relationship. Note thickening of anhydrite beds to the south (A') in zone A and uppermost portions of zone B. Also note changes in zone B and D porosity from porous beds of dolomite, northward, into dense beds of limestone to the south. Progradation is to the northwest, which is outward and toward the viewers left on approximately a 45° angle from the fence diagram. Position of the CO₂ minitest is in the center of the fence diagram, Zabolotny Injection Well No. 1.

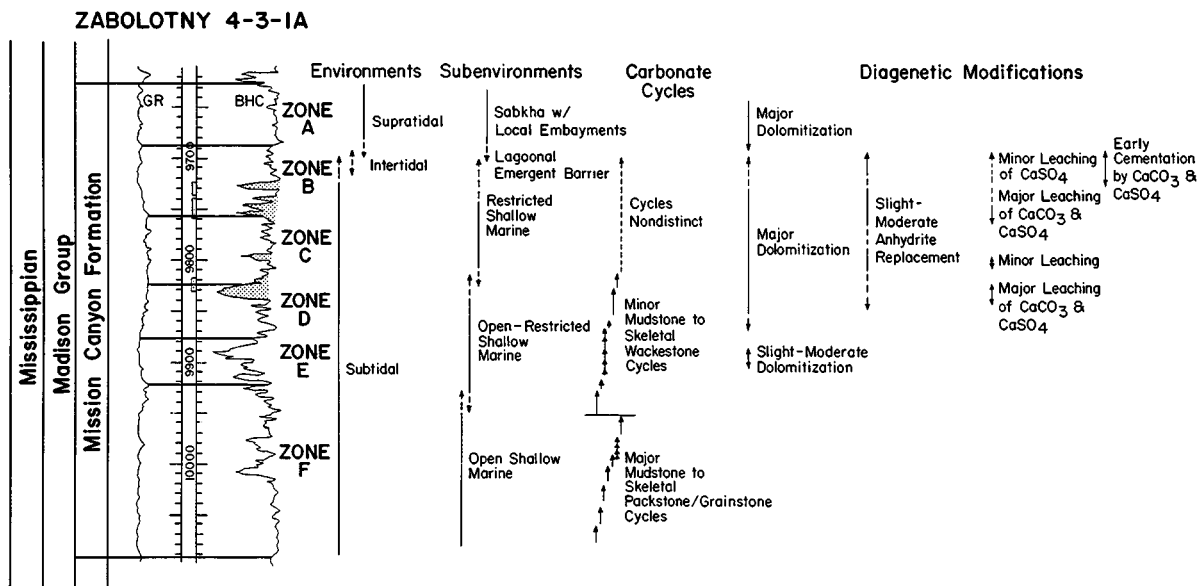


Fig. 22-Type log of Mission Canyon Formation at Little Knife Field, approximately 0.25 miles northwest from the minitest location. Informal log zonations A-F, for field correlation, are illustrated. Depositional environments, carbonate cycles and diagenetic modifications are from a composite section of several cores. Stipple area indicates where hydrocarbon bearing beds are located in this well. Modified after White and Lindsay¹.

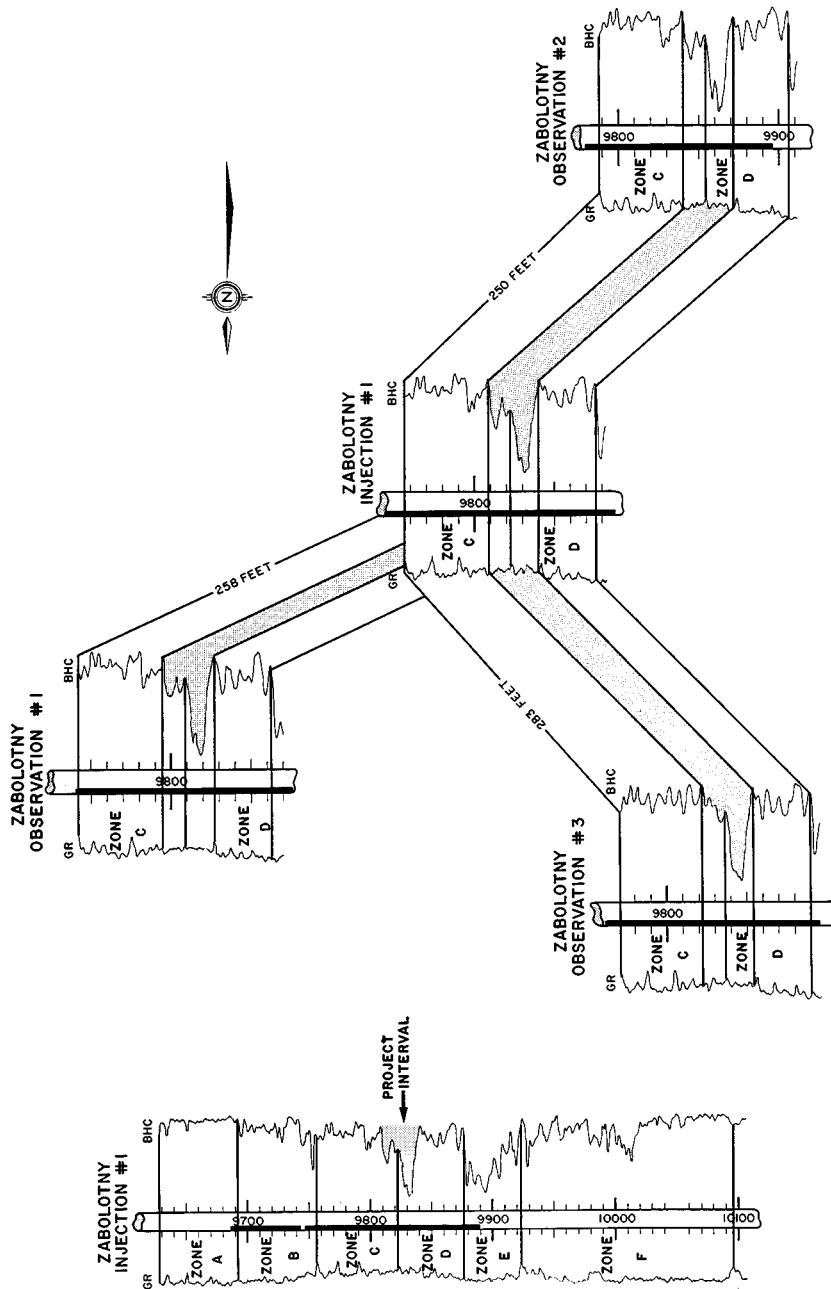


Fig. 23-Stratigraphic fence diagram of zones C and D through minitest wells. Shaded central portion of the fence diagram is the project interval. North is to the left. The central well, Zabolotny Injection Well No. 1, sonic log is illustrated on left to compare the location of the project interval beds to the complete Mission Canyon Formation. Black vertical bars in the center of each log represent the cored interval.

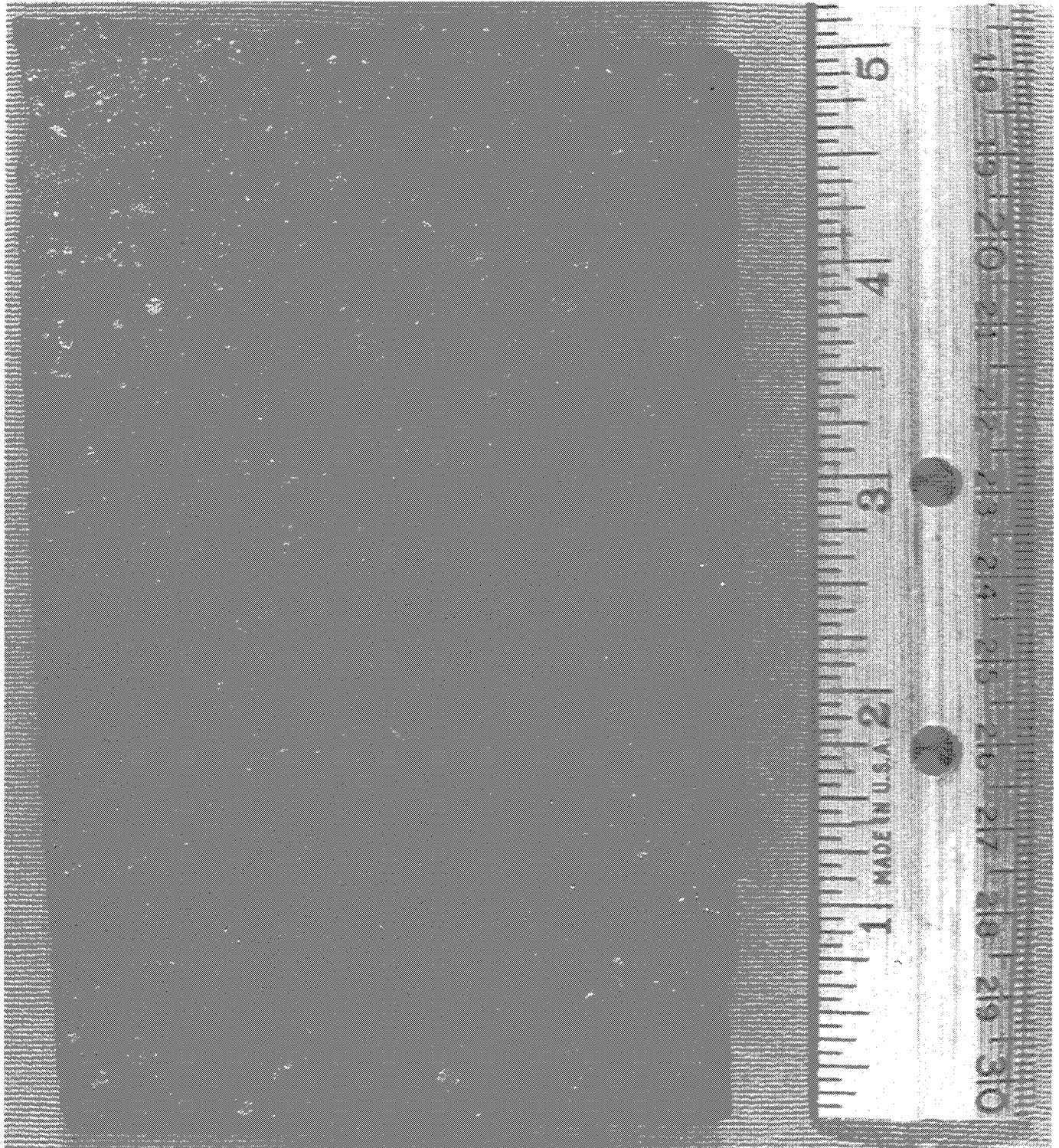


Fig. 24—Close-up view of an average sample of rock from the Little Knife CO₂ minitest. This rock is a partially dolomitized skeletal wackestone (skeletal limestone). The light particles scattered through the sample are skeletal fragments of crinoid columnals floating in the originally muddy matrix. Discontinuous horizontal and oblique laminations are the outlines of compacted burrows. The original muddy matrix has been dolomitized creating approximately 20% porosity in this sample. Dusty appearance of the sample is caused by reflection of light off of dolomite crystal faces. Scale is in inches and centimeters.

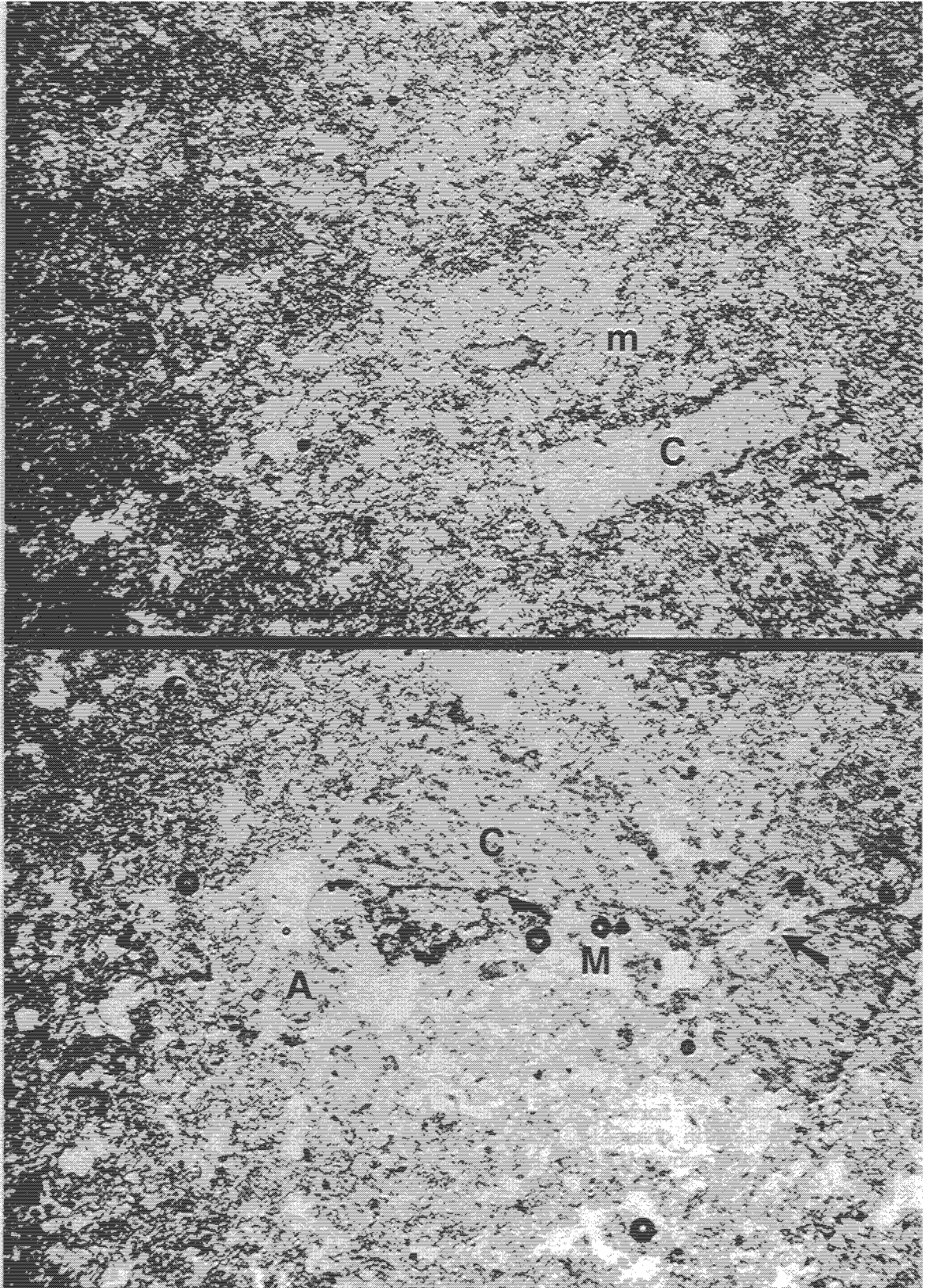


Figure 25

Fig. 25-Gulf Zabolotny Injection Well No. 1. Photomicrographs are from core taken in the CO₂ minitest project interval.

Upper photomicrograph (X-nicols and 1/4λ plate) is from 9829'11", 25X magnification, of a core sample of rock containing 18.4% porosity and 13 md permeability. It consists of a partially dolomitized (D) originally muddy matrix surrounding broken skeletal fragments (C) composed of crinoid columnals. Largest visible pores are moldic pores (M) set within the finely crystalline matrix. Scale is 500 microns.

Lower photomicrograph (X-nicols and 1/4λ plate) is from 9827'5", 25X magnification, of a core sample of rock containing 23.5% porosity and 88.7 md permeability. It is again a partially dolomitized skeletal wackestone with the muddy matrix, surrounding skeletal fragments (C), now dolomitized. Moldic pores (M), formed by solutioning of anhydrite replaced portions of skeletal fragments (A), are obvious and occasionally tend to form slight solution channels (arrow). Scale is 500 microns.

Fig. 26-Gulf Zabolotny Observation Well No. 1. Photomicrographs are from cores taken in the CO₂ minitest interval.

Upper photomicrograph (X-nicols and 1/4λ plate) is from 9808'4", 25X magnification, of a core sample of rock containing 20.5% porosity and 8.6 md permeability. It is a partially dolomitized (PD) skeletal wackestone (skeletal limestone), containing a dolomitized muddy matrix with skeletal fragments (C), crinoid columnals, floating in the original muddy matrix. Some skeletal fragments have been invaded (I) by dolomite crystals seeking a source of carbonate during dolomitization. Scale is 500 microns.

Lower photomicrograph (X-nicols and 1/4λ plate) is from 9815'3", 25X magnification, of a core sample of rock containing 24% porosity and 26 md permeability. Again, the sample has been partially dolomitized (D) throughout the originally muddy portions, with crinoid fragments (C) left floating in the muddy matrix. The dolomitized portions form a fine grained fabric. Moldic pores (M) and incipient solution channels, through the crinoid fragment (arrow), are areas where anhydrite has been leached away. Scale is 500 microns.

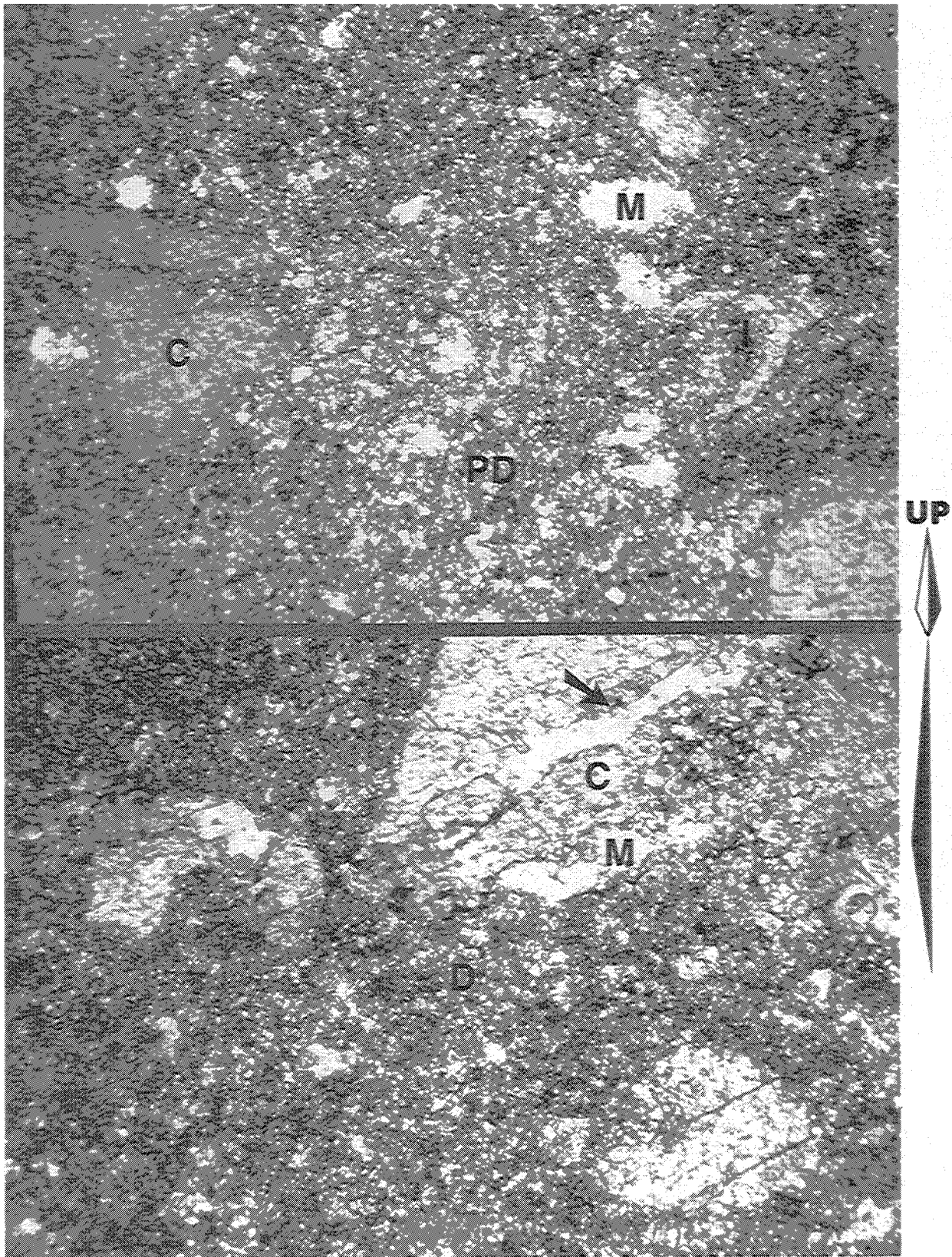


Figure 26

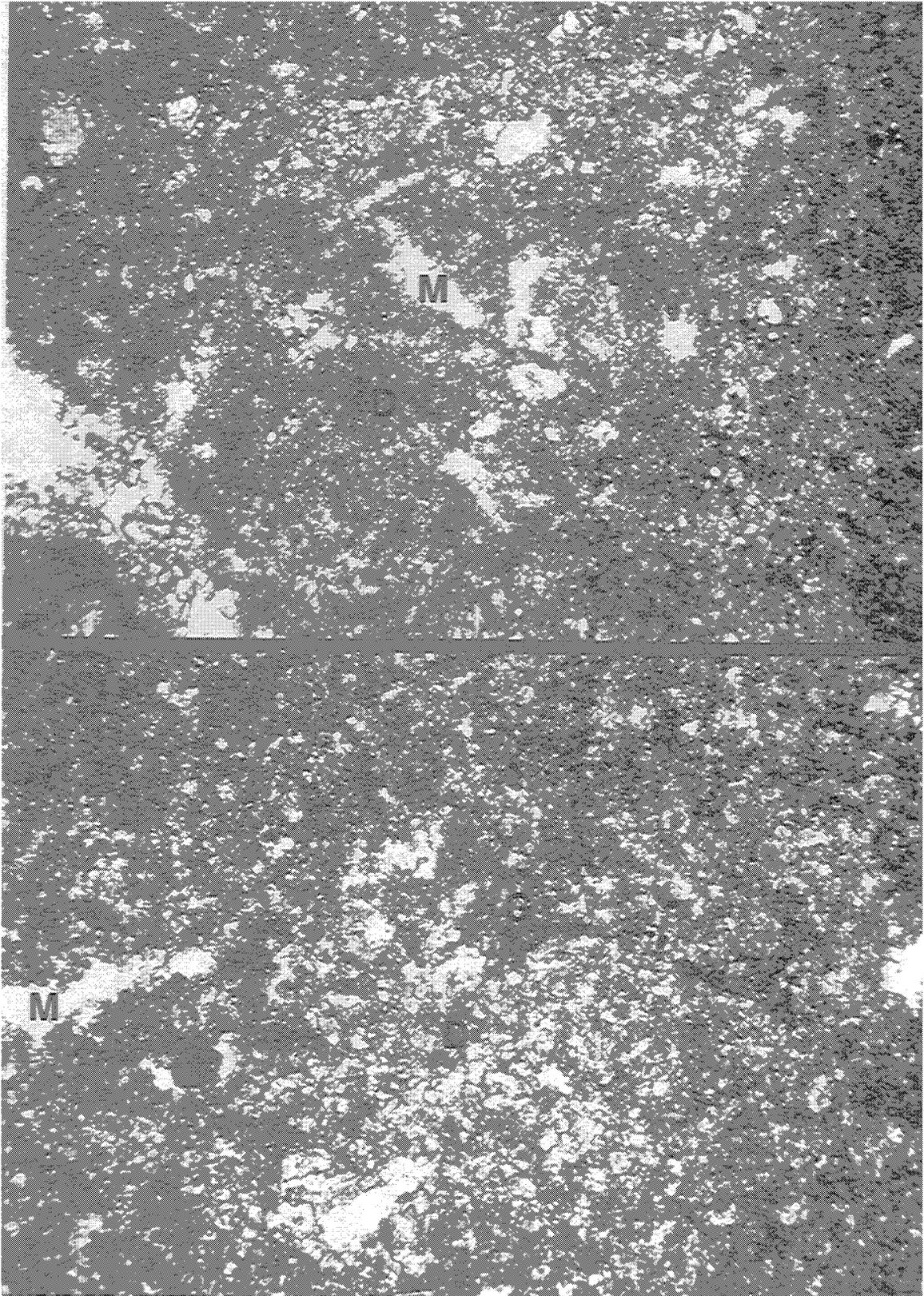


Figure 27

Fig. 27-Gulf Zabolotny Observation Well No. 2. Photomicrographs are from cores taken in the CO₂ minitest project interval.

Upper photomicrograph (X-nicols and 1/4λ plate) is from 9851'4", 25X magnification, of a core sample of rock containing 20.9% porosity and 15md permeability. This portion of the sample is well dolomitized (D) with skeletal ghosts, originally fragments of crinoids forming a skeletal wackestone, now forming moldic pores (M) after being replaced by anhydrite and later leached away. The dolomite maintains a fine grained saccharoidal fabric. Scale is 500 microns.

Lower photomicrograph (X-nicols and 1/4λ plate) is from 9859'5", 25X magnification, of a core sample of rock containing 27% porosity and high amounts of permeability. This sample is well dolomitized (D) with many ghosts (G), oval shapes, scattered throughout the field of view. Some elongate moldic pores (M) are present, with the much smaller intercrystal pores not visible on this scale of magnification. Note that the dolomite crystals are gradational in size, in this field of view, between a fine grained and medium grained fabric. Scale is 500 microns.

Fig. 28-Core slabs from Zabolotny Injection Well No. 1, at 9,817-19 feet. Crinkly line at upper left is stylolite created by pressure solutioning. Calcium carbonate from pressure solutioning (stylolite) has moved out laterally a few inches to reduce porosity down to 7.0% and create a marker on sonic logs in the section. This feature forms the top of Zone D throughout the CO₂ minitest area. Note the vertical fracture which cuts across the stylolite. Porosity away from the stylolite and down section increases from 7.0% at the stylolite to 13.3%, one foot below, and 20.9%, two feet below it. Scale is in inches and centimeters.

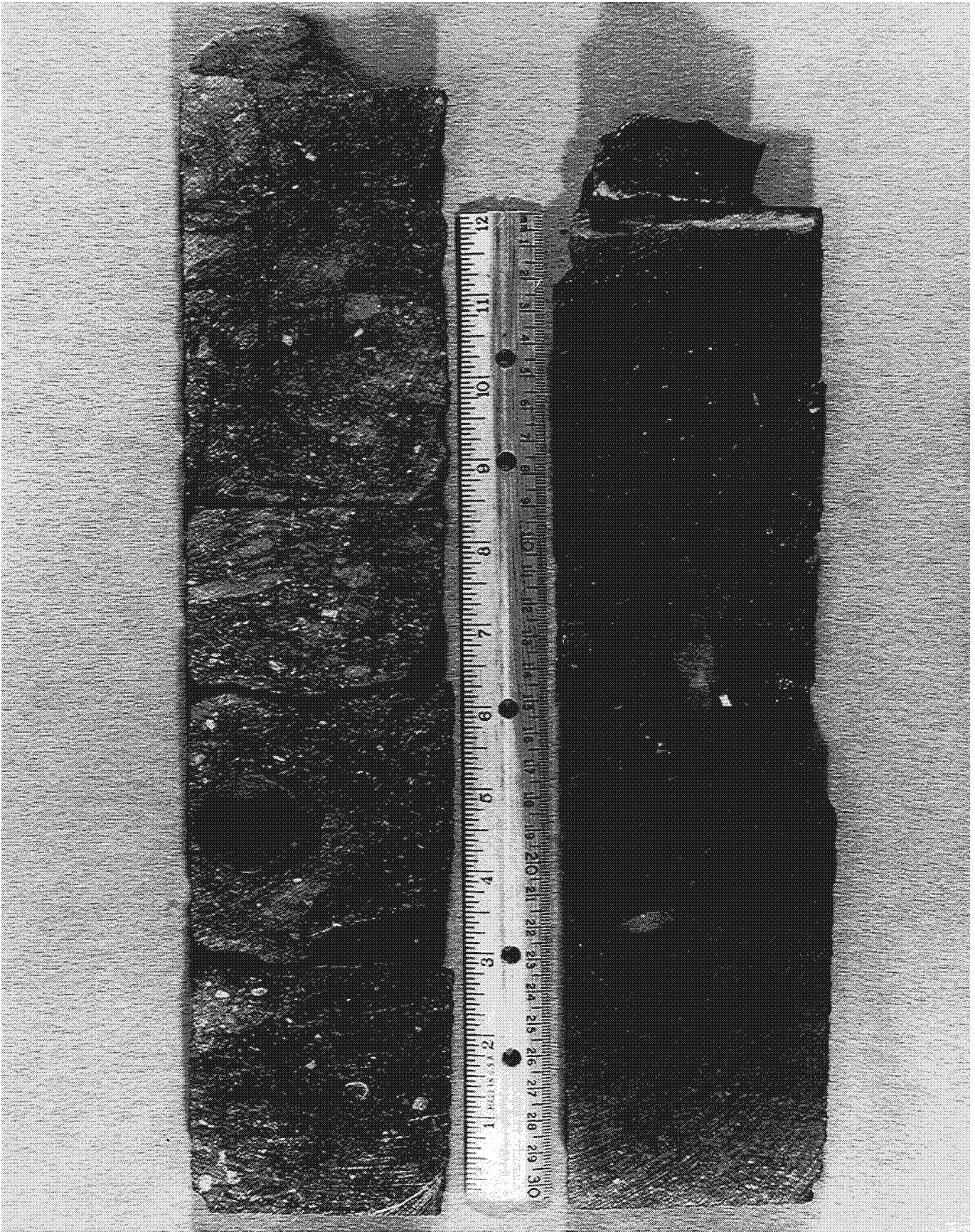


Figure 28

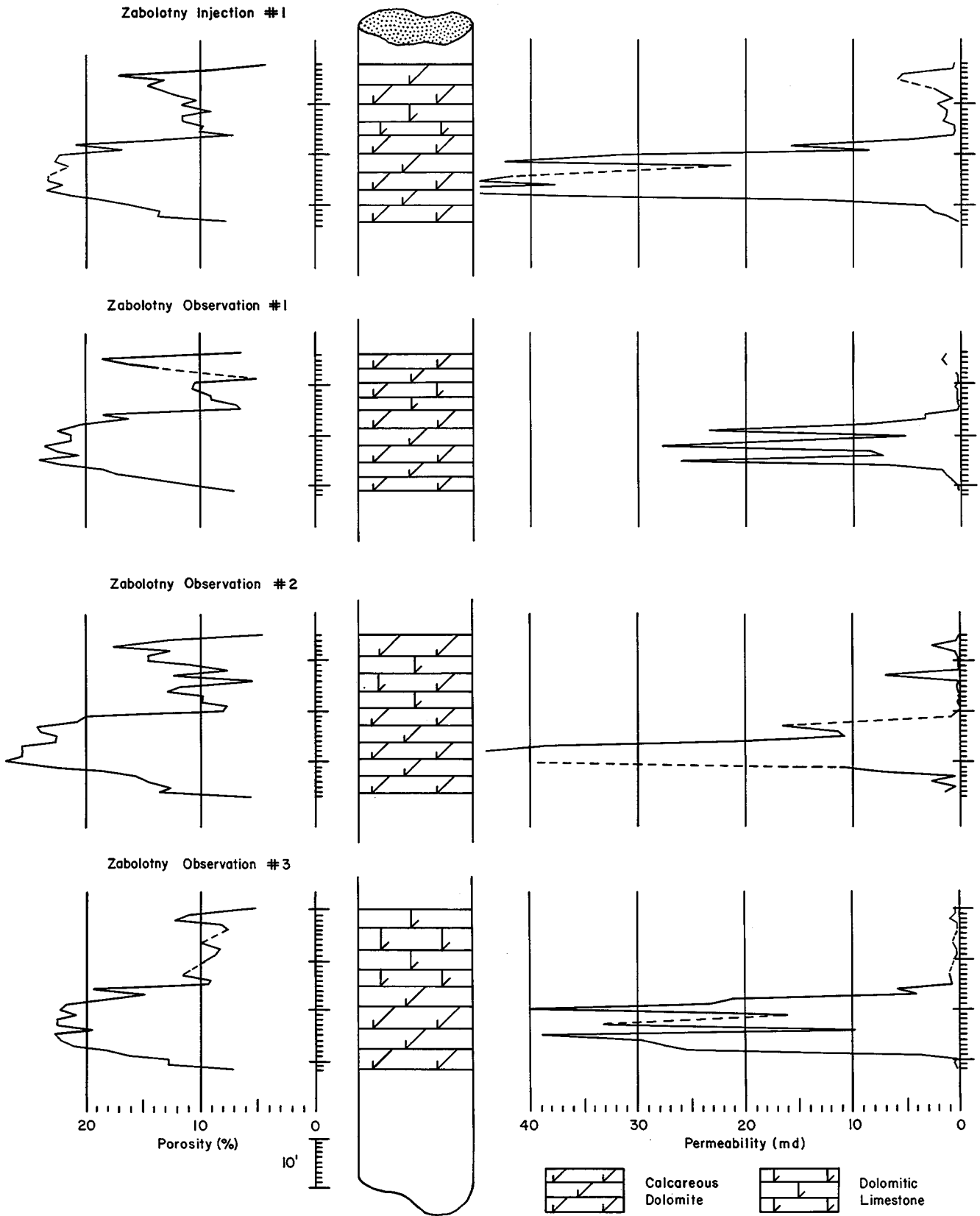


Fig. 29-Whole core porosity (%) and permeability (md) compared to lithology in each Little Knife CO₂ minitest well.

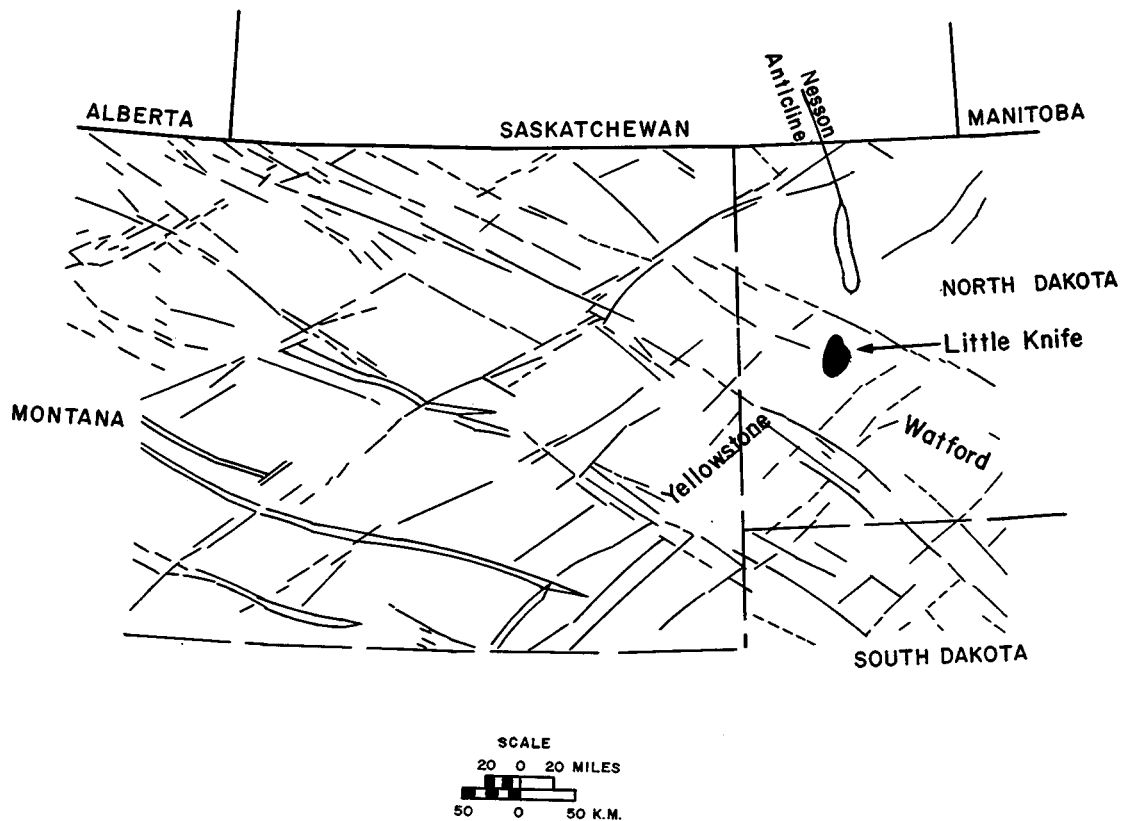


Fig. 30—Surface lineaments mapped through portions of Montana, western North Dakota and northwesternmost South Dakota. Little Knife Field is located within the intersections of the northeast trending Yellowstone Block and northwest trending Watford block. Location of Nesson Anticline, to the north, is compared to Little Knife Field. Scale is in miles and kilometers. Modified after Thomas¹⁰

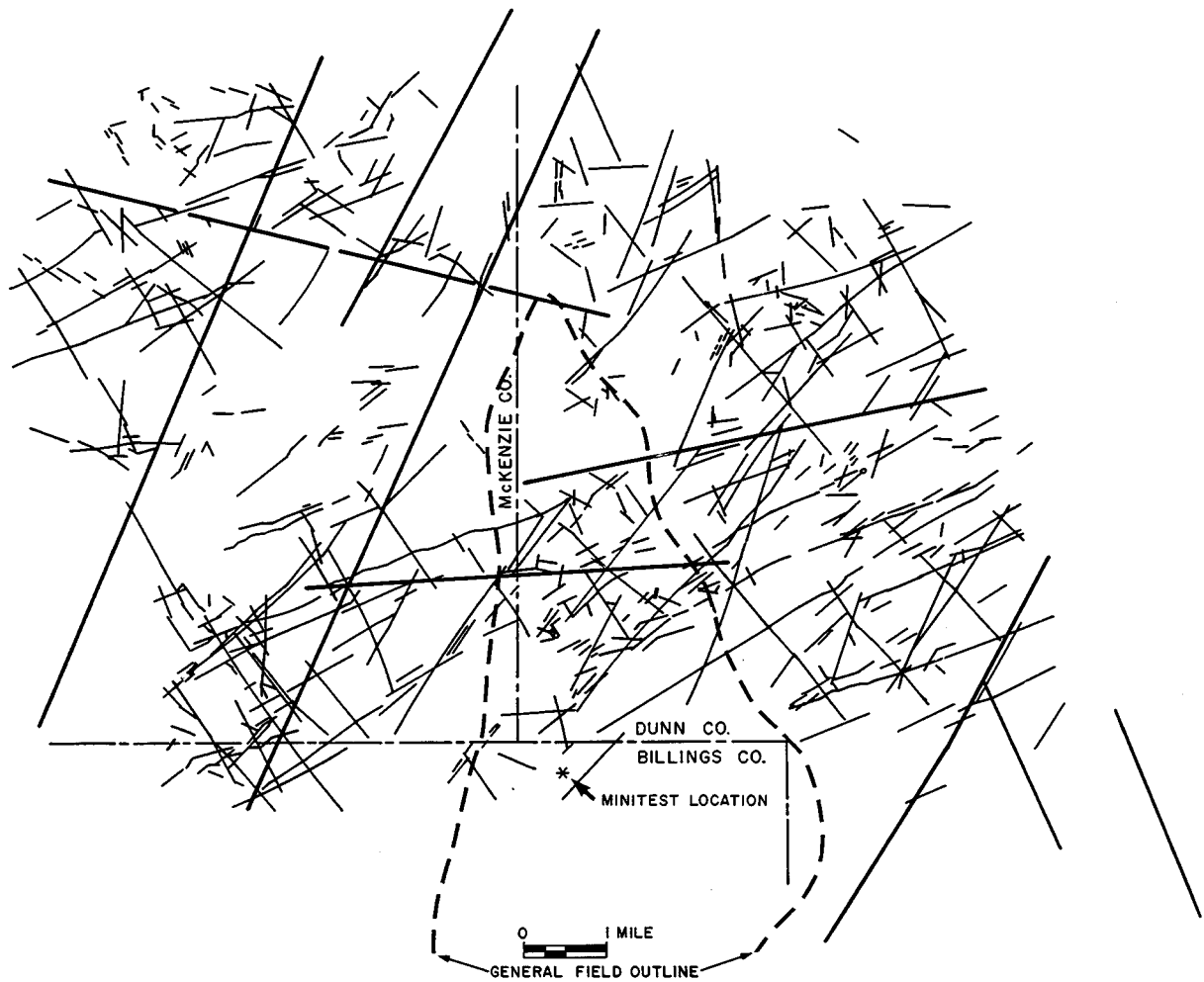


Fig. 31-Surface lineaments from Landsat photographs (thick lines) and aerial photographs (thin lines) in central and northern portions of Little Knife Field. Dashed line shows the field outline. Asterisk marks the position of the Little Knife CO₂ Minitest. Modified after Hodgson¹¹.

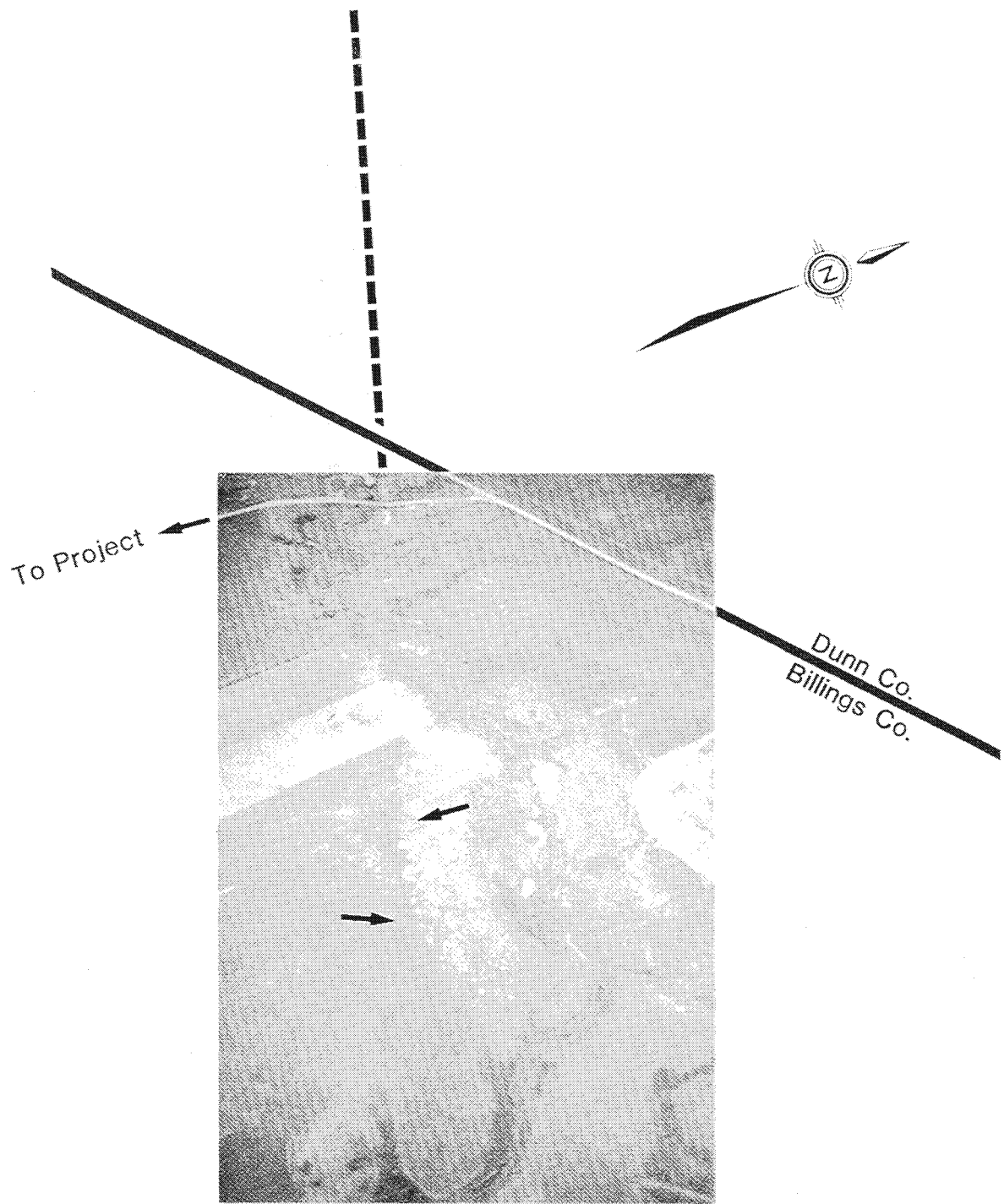


Fig. 32-Oblique, low angle aerial view of nearest surface lineament to the Little Knife CO₂ minitest. Note how lineament cuts across cultivated fields but is still recognizable. An intermittent stream follows this surface lineament. The CO₂ minitest is just to the left of the field of view, approximately 0.25 miles away. Most of the field of view is of Sec. 3, T144N, R98W, except for the uppermost right side.

Surface Linear

Surface Outcrop At Minitest Location

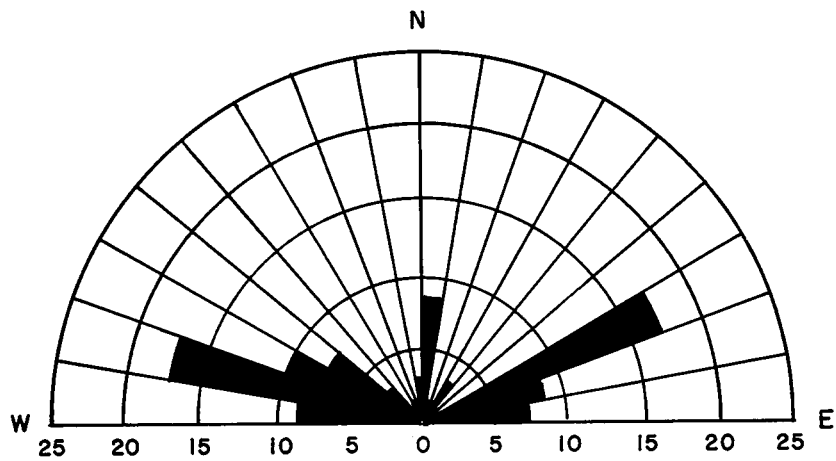


Fig. 33-Surface outcrop fractures measured next to Zabolotny Observation Well No. 3. Results of 69 apparent strike directions are plotted in 10 degree increments. Numbers along the bottom of the illustration are in percent.

Zabolotny Observation No. 3

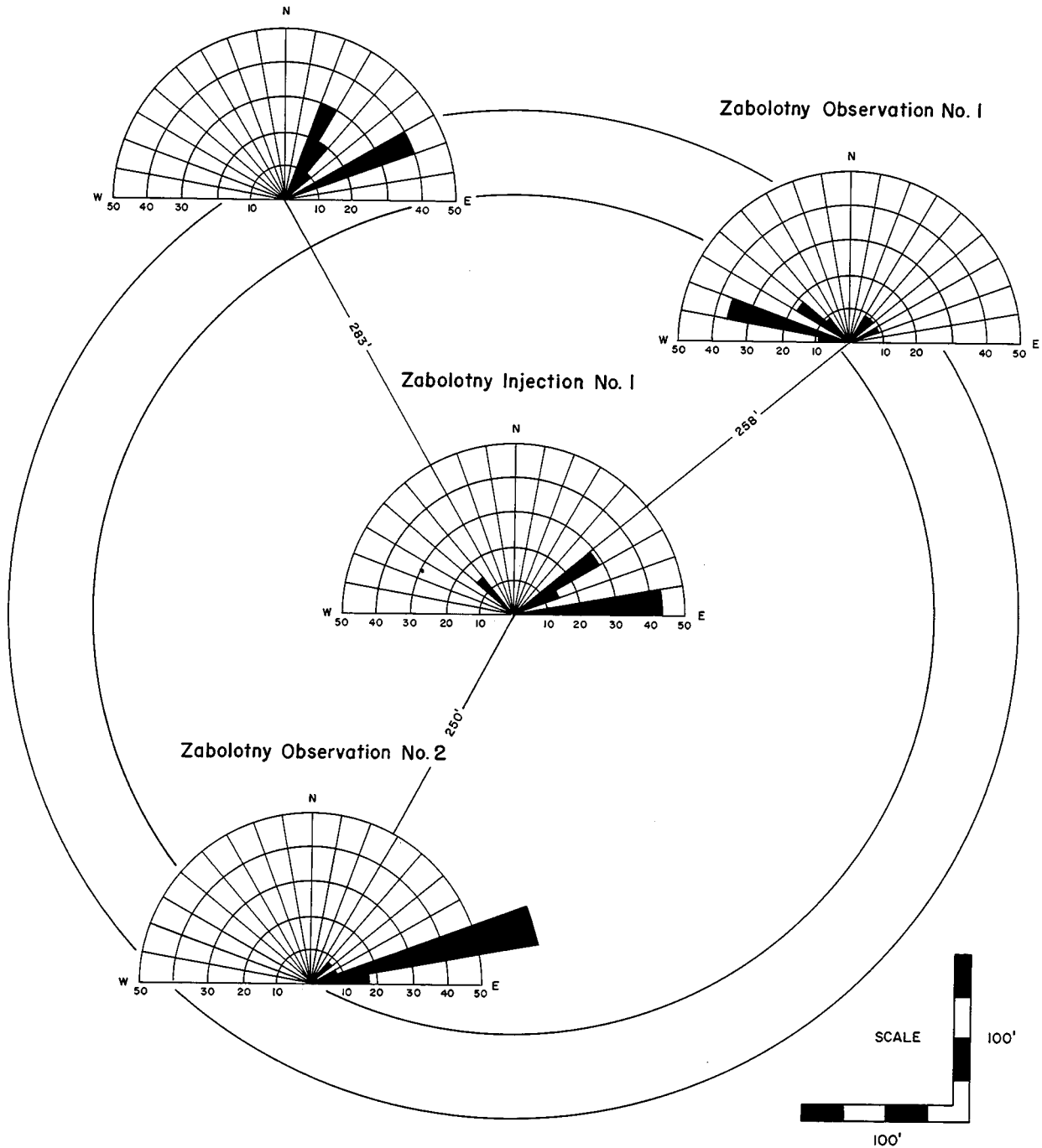


Fig. 34—Fractures measured from oriented cores in Little Knife CO₂ minitest beds. Sets of fractures are grouped in 10 degree increments and displayed as percentages. Exact reservoir bottomhole well locations are illustrated and their distance of separation within the CO₂ minitest. The outer circle is 600 feet in diameter and the inner circle is 500 feet in diameter.

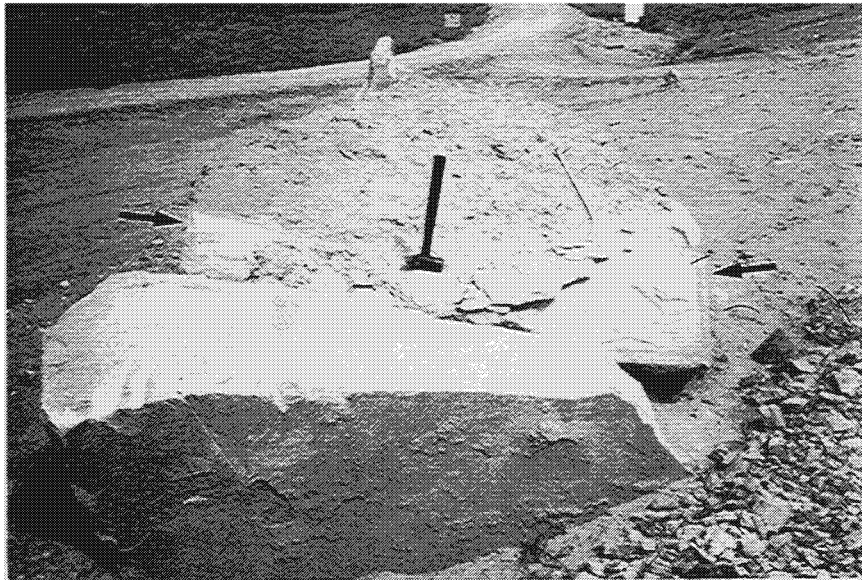
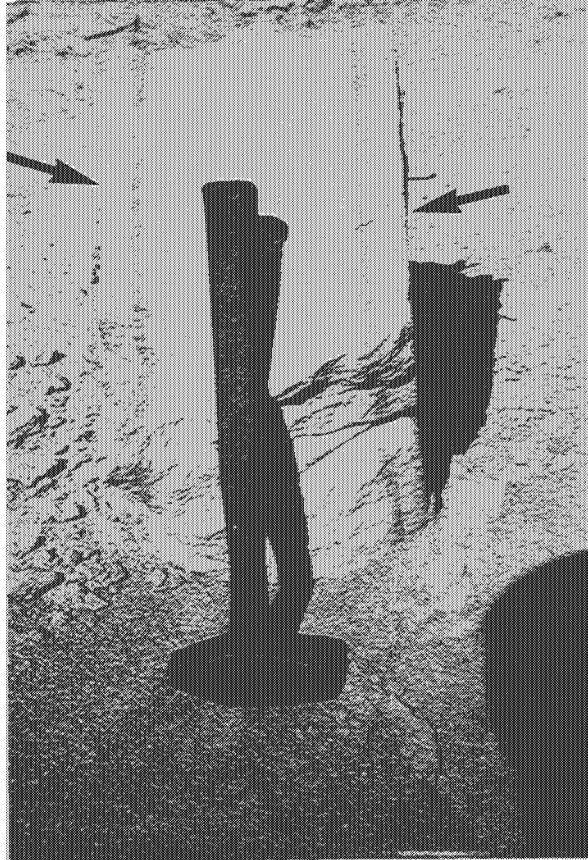
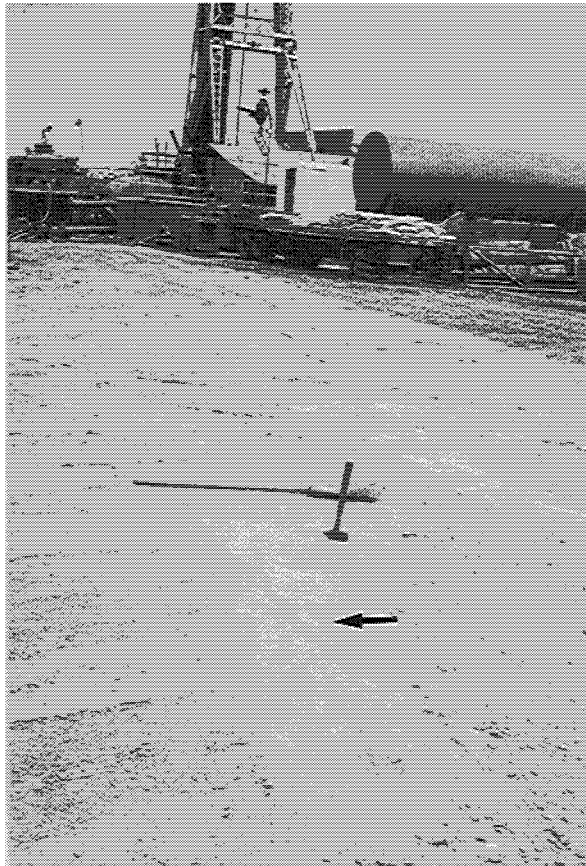


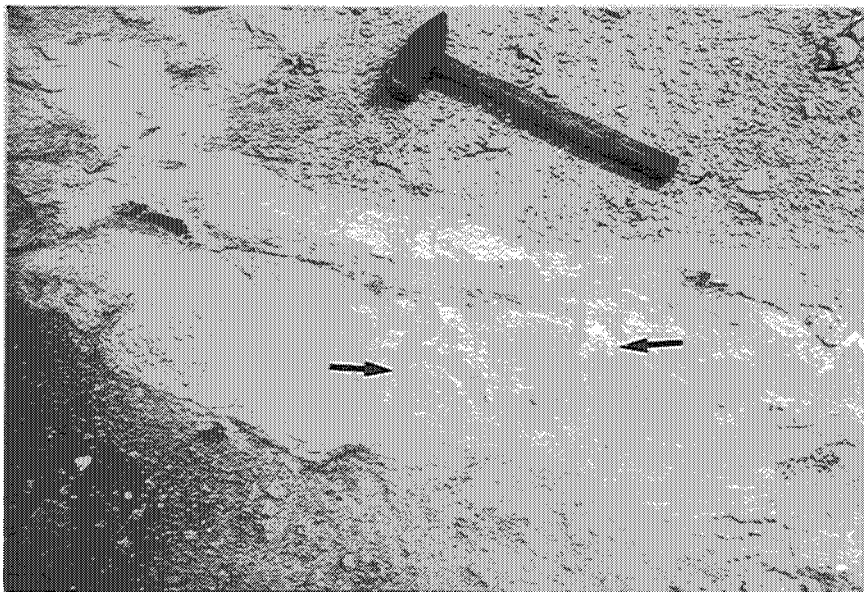
Fig. 35-Blocks of Sentinel Butte Formation, broken-up by bull dozing equipment along fractures, illustrating surface fracture (joint) separation. Separation is between 1-6 feet. Note how iron rich solutions migrating along the fracture (joint) have slightly invaded the sandstone to give it a banded appearance.

Fig. 36-Outcroppings of Sentinel Butte Formation, next to Zabolotny Observation Well No. 3, where surface fracture strike directions were measured. The rock type is a lithic sandstone.



Upper photograph illustrates cleared areas, next to the drillsite, where some of the fracture strike directions were obtained. Other such locations surrounding the drilling site were also cleaned off and the fracture strikes measured.

Lower photograph is a close-up of fractures (arrows) and their separation, and is the same area cleaned off in the upper photograph (arrow). Hammer is 18 inches in length. North is to the left.



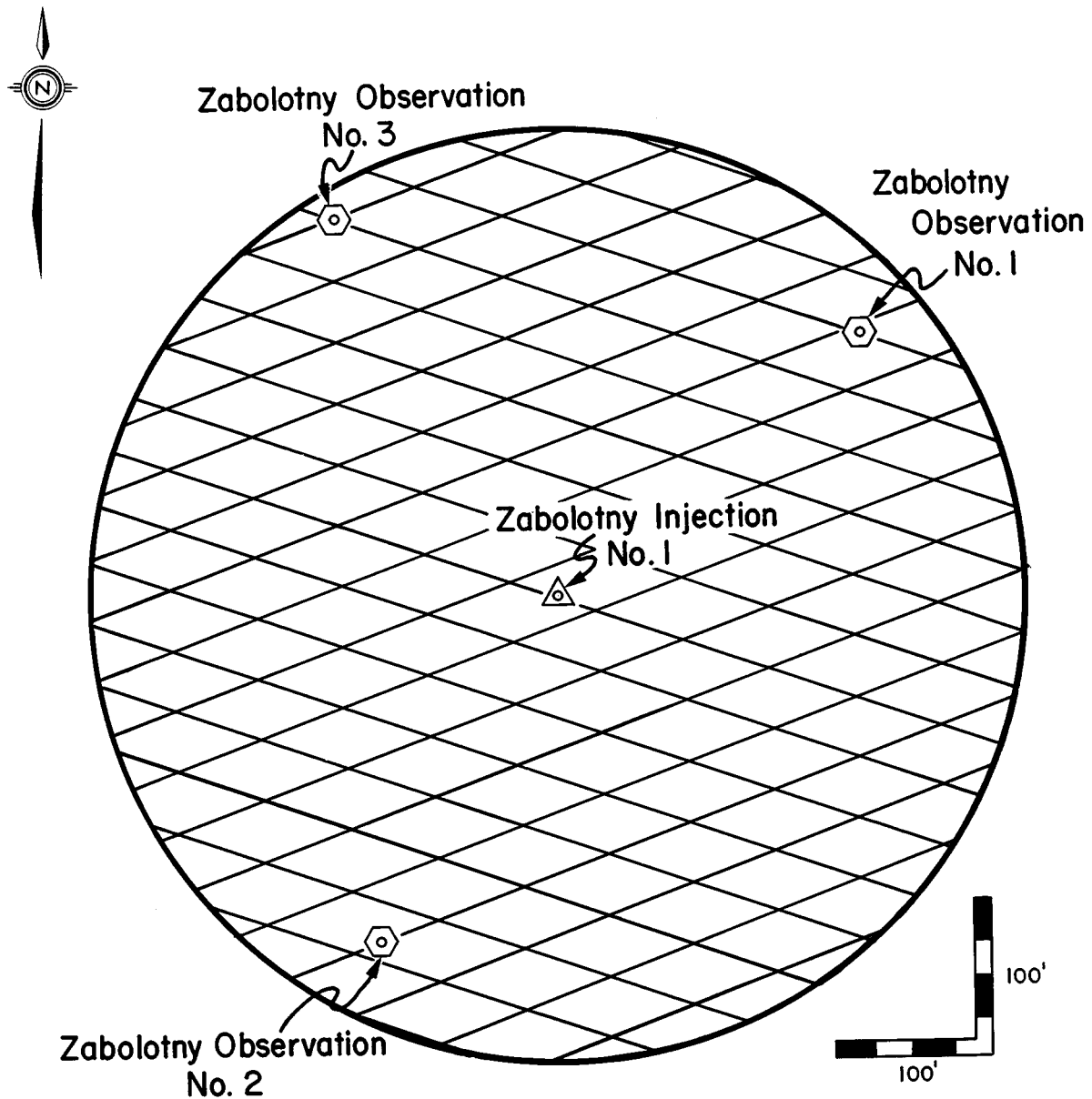


Fig. 37-Generalized illustration representing the average trends of fractures, not individual fractures, through the CO₂ minitest area. All fractures were found to be small, vertical, hairline, en echelon planes which are interpreted to have short lateral lengths. An average strike of these is in a northwesterly direction, N. 67 W., and a northeasterly direction, N. 69 E. Calculated permeabilities, from multiwell pulse testing, reveals no major contribution by fractures but calculates twice the average permeability, as compared to whole core analysis. This increased average permeability is uniformly distributed across the minitest area. This would signal that fractures may be dispersed in a somewhat uniform manner within the minitest area but that individual fractures are small and terminate abruptly.

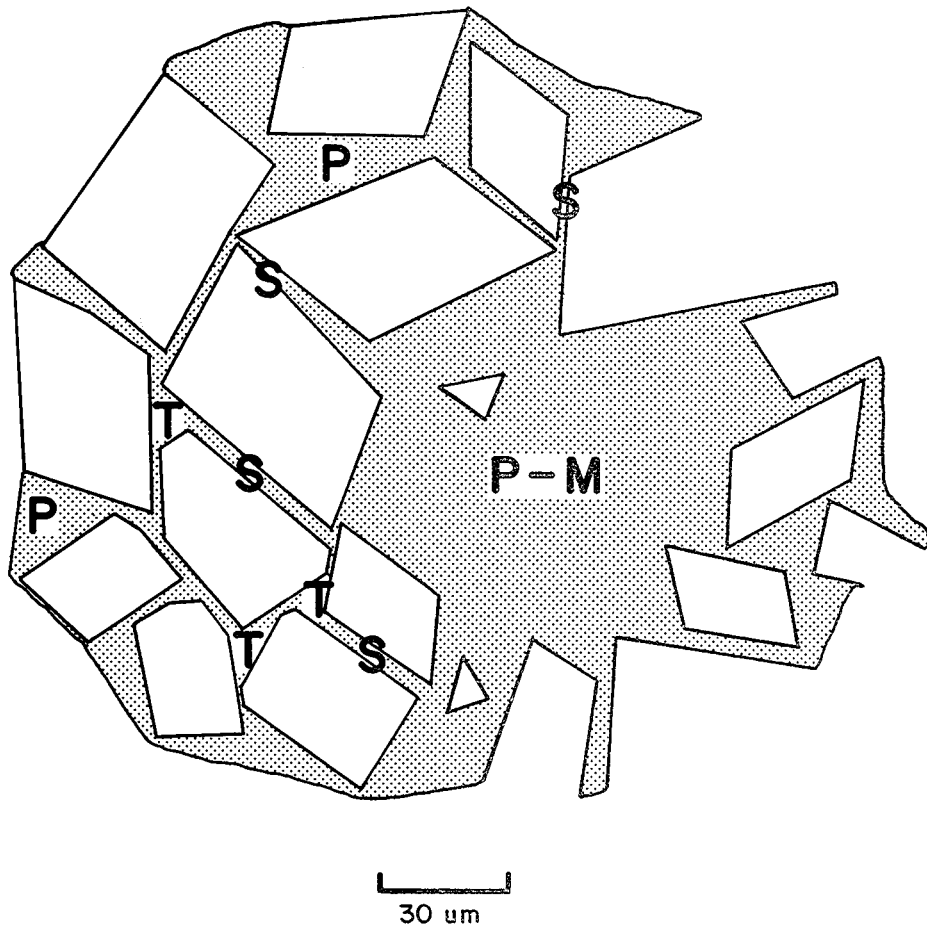


Fig. 38-Generalized illustration (cartoon) of the various pore types and throats in porous portions of the Mission Canyon. Stippled area is pore space surrounding dolomite crystals. A small moldic pore is transitioning, in size, to a large intercrystal polyhedral pore (M-P). Polyhedral pores (P) are the largest intercrystal pores and form a complex polyhedron shape between three or more dolomite crystals, in two-dimensional view. Tetrahedral pores (T) are intermediate sized intercrystal pores, formed where three dolomite crystals begin to impinge together forming a triangular shape in two-dimensional view. Interboundary-sheet pores (S) are the smallest intercrystal pores and form between closely spaced dolomite crystals. Scale is 30 microns.

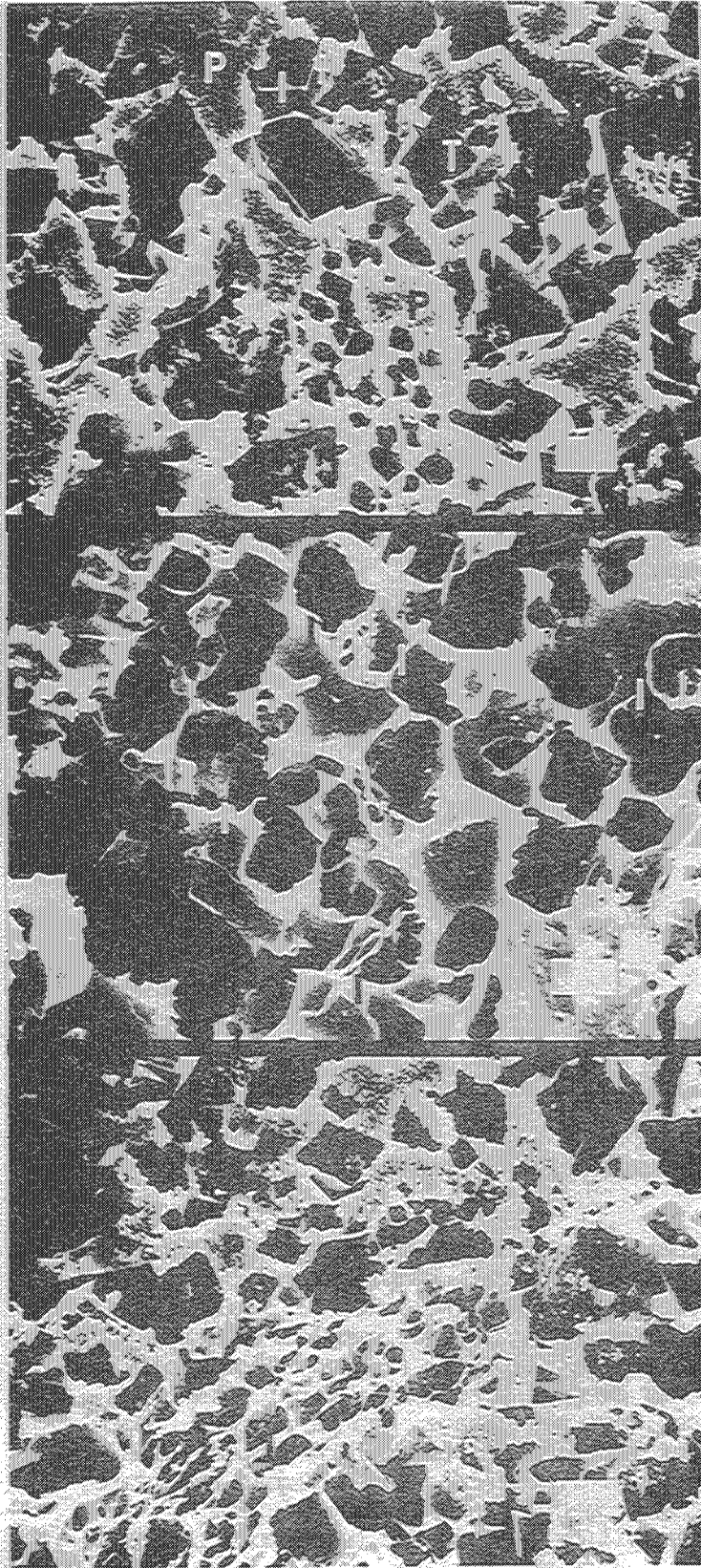


Fig. 39-Scanning electron micrographs (SEM) of relief pore casts of porous beds of Mission Canyon Formation at Little Knife Field. These casts were produced by impregnating the host rock with acid resistant resin and then completely dissolving the sample in dilute HCl, which left the pore and throat system standing in relief.

The uppermost SEM photo illustrates large polyhedral pores (P) giving way to smaller tetrahedral (T) and inter-boundary-sheet (I) pores. Both large and narrow throats connect the individual pores. Scale is 20 microns.

The middle SEM photo demonstrates how the narrow inter-boundary-sheet pores (I) actively effect permeability although the relative amount of pore space between dolomite crystals is highly reduced. Scale is 10 microns.

The bottom SEM photo illustrates how dolomite crystal growth can change laterally from crystal spacings associated with large pores and pore throats and grow much closer together to leave only very narrow pore/throats. This relief cast illustrates tortuosity to fluid flow in a dolomitized carbonate reservoir. Scale is 20 microns.

ZABOLOTNY INJECTION #1

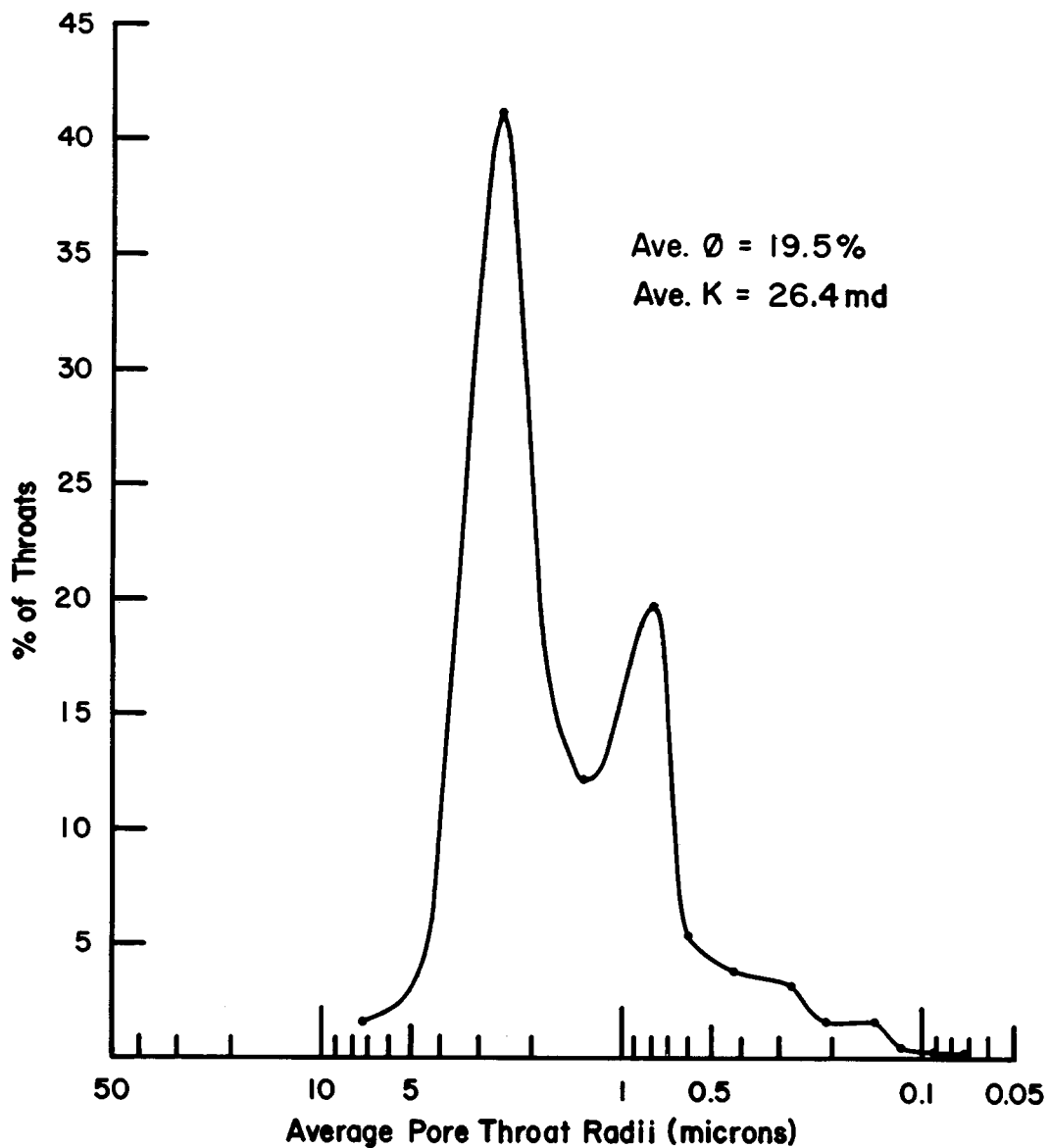


Fig. 40-Average calculated pore throat radii and percent of throats, from mercury capillary pressure tests, from core samples across the perforated interval in Zabolotny Injection Well No. 1. This is a generalized curve produced by averaging several samples together until the average porosity (19.6%) and permeability (26.4md) from whole core analysis matched. In this way average pore throat radii in microns, and their relative abundance, in a percentage, can be plotted. Note two general peaks of abundant throat sizes exist from samples with porosities of 19.5% in this well. These calculated throat radii are for the lower half of the CO₂ project interval where highest amounts of porosity and permeability are present (uppermost zone D).

ZABOLOTNY OBSERVATION #1

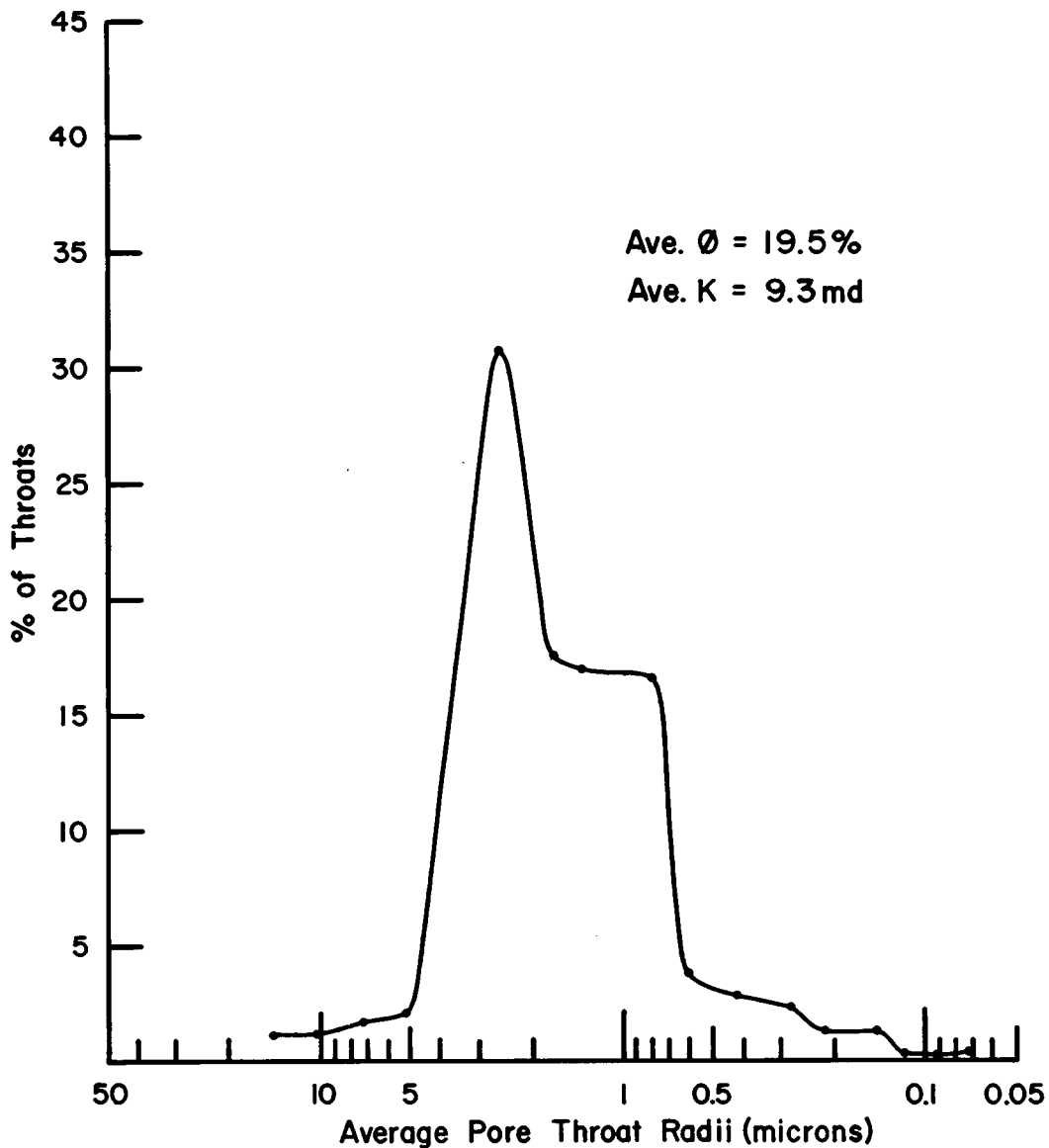


Fig. 41-Average calculated pore throat radii and percent of throats, by mercury capillary pressure tests, from core samples across the perforated interval, in Zabolotny Observation Well No. 1. This is a generalized curve produced by averaging several samples together until the average porosity (19.5%) and permeability (9.3md) from whole core analysis is closely matched. In this way average pore throat radii, in microns, and their relative abundance in a percentage can be plotted. Note how the two general peaks that were present in Zabolotny Injection Well No. 1 have merged into a single irregular shaped curve with a lower percentage of largest pore throats. These calculated throat radii are for the lower half of the CO₂ minitest project interval where highest amounts of porosity and permeability are present (uppermost zone D).

ZABOLOTNY OBSERVATION #2

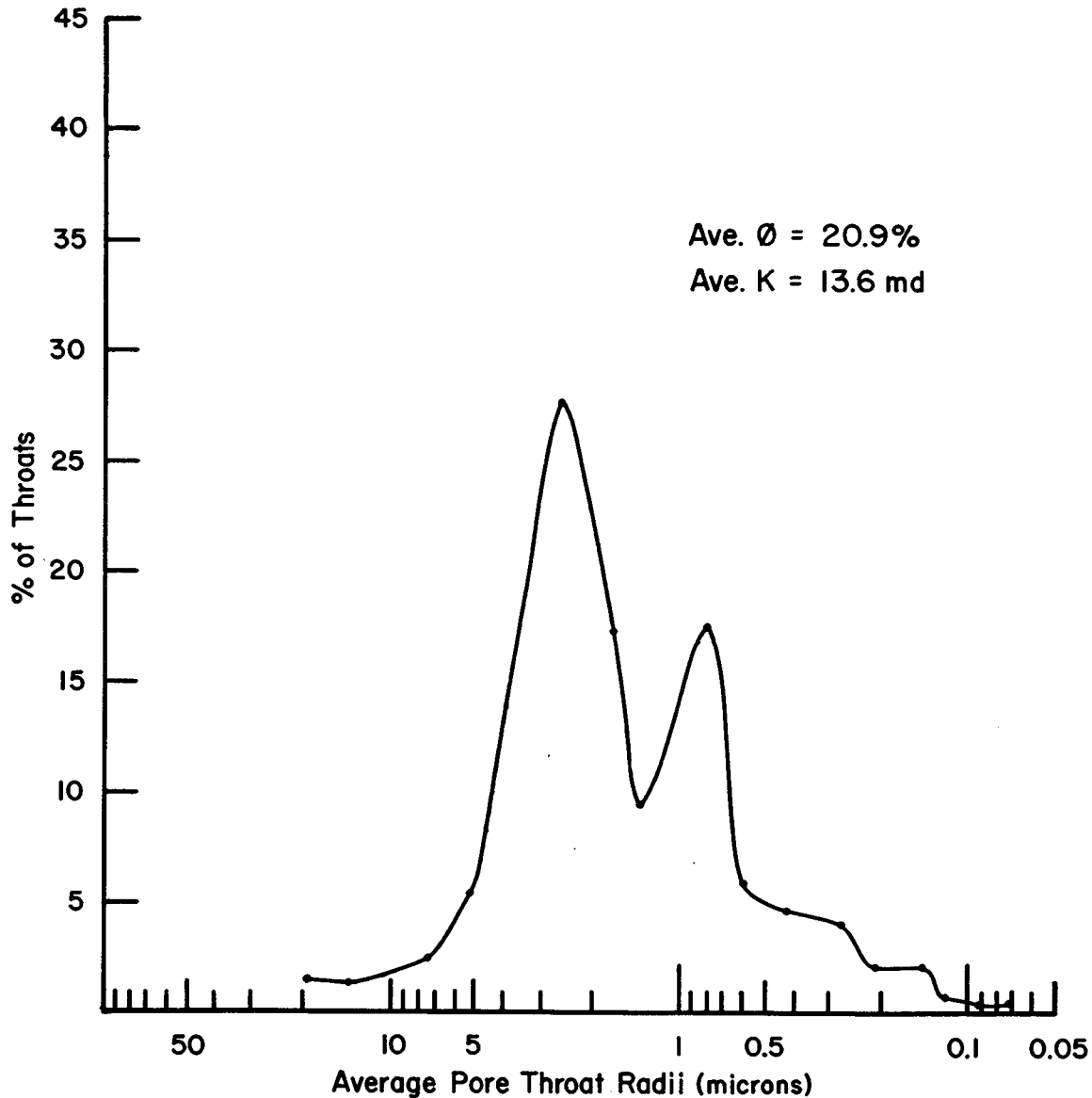


Fig. 42—Average calculated pore throat radii and percent of throats, from mercury capillary pressure tests, from core samples across the perforated interval, in Zabolotny Observation Well No. 2. This is a generalized curve produced by averaging several samples together until the average porosity (20.9%) and permeability (13.6md) from whole core analysis is closely matched. In this way average pore throat radii in microns, and their relative abundance, in a percentage, can be plotted. Note that in this well the two general peaks of abundant throat radii sizes are present, as in Zabolotny Injection Well No. 1, but that the percentage of larger throat radii is lowered. This lowered percentage of throats is slightly compensated for by a slight increase in larger pore throat radii, increasing the width of the curve slightly. These calculated throat radii are from the lower half of the CO₂ minitest project interval where highest amounts of porosity and permeability are present (uppermost zone D.)

ZABOLOTNY OBSERVATION # 3

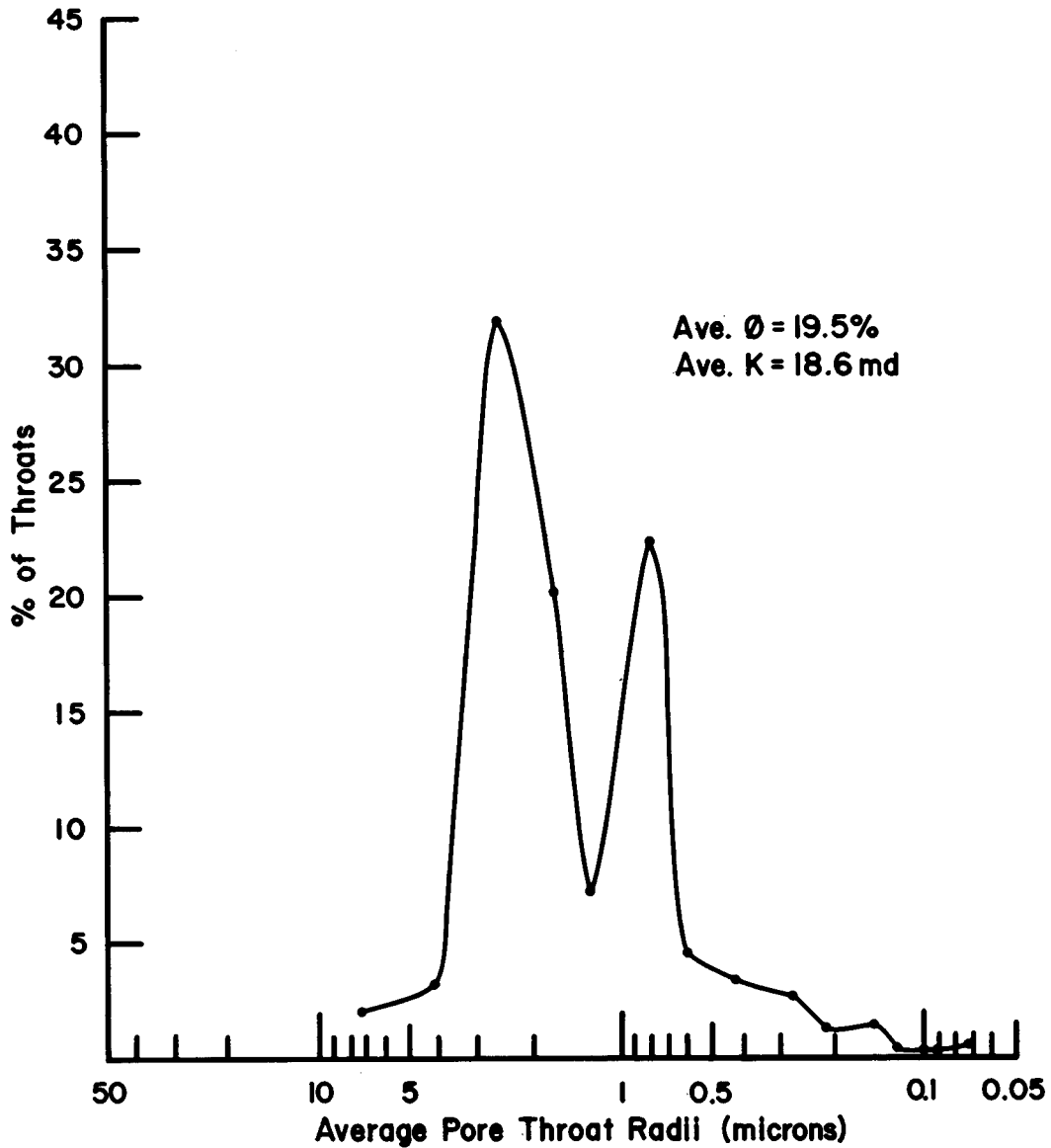


Fig. 43-Average calculated pore throat radii and percent of throats, by mercury capillary pressure tests, from core samples across the perforated interval, in Zabolotny Observation Well No. 3. This is a generalized curve produced by averaging several samples together until average porosity (19.5%) and permeability (18.6md) from whole core analysis is closely matched. Note in this well the two typical peaks of abundant throat radii sizes, similar to those in Zabolotny Injection Well No. 1 and Zabolotny Observation Well No. 2. These calculated throat radii are from the lower half of the CO₂ minitest project interval where highest amounts of porosity and permeability are present (uppermost zone D).

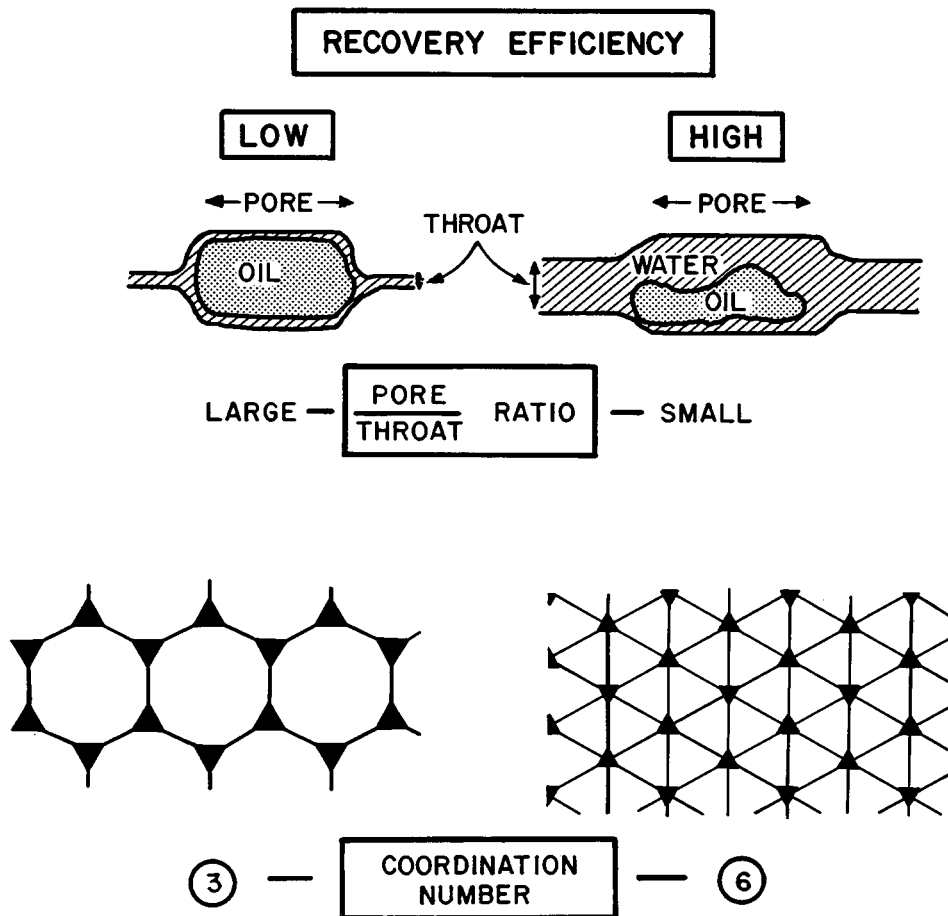


Fig. 44-Pore-to-throat size ratios for the Mission Canyon Formation are highly variable ranging from 40:1, when large moldic pores are well developed, down to 4:1. An average pore-to-throat size ratio is approximately 5-10:1. The average pore-to-throat coordination number, average number of throats connected to each pore in a two-dimensional view, is 3 to 5.

Fig. 45-Representative individual samples of pore throat radii, in microns, and percent of throats, calculated from mercury injection capillary pressure curves, in the Zabolotny Injection Well No. 1. five (5) characteristic pore throat radii vs. porosity and permeability relationships have been isolated into groups. The 5 pore throat radii curves illustrated are representative of these 5 groups:

- 1) The first group is from samples with the smallest pore throat radii measured, averaging 0.21 micron, with lowest amounts of porosity and permeability, average porosity 6.2% and permeability 0.16 md. These samples are from nonhydrocarbon bearing beds.
- 2) The second group is from samples with slightly larger pore throat radii, averaging 0.6 micron, with lowest amounts of producible porosity, average porosity 10.7% and average permeability 0.8 md.
- 3) The third group is from samples with more abundant pore throat radii, averaging 0.8 microns, with fair amounts of porosity and permeability, average porosity 13.6% and average permeability 3.5md.
- 4) The fourth group is from samples which contain 2 distinct sizes of average pore throat radii, at 0.8 and 1.8-2.5 microns respectively, and good amounts of porosity and permeability, average porosity 19.6% and average permeability 22.3 md.
- 5) The fifth and final group is from samples with abundant, large pore throat radii, at 2.5 microns, and highest amounts of porosity and permeability, average porosity 24.1% and average permeability 85.4 md.

ZABOLOTNY INJECTION #1

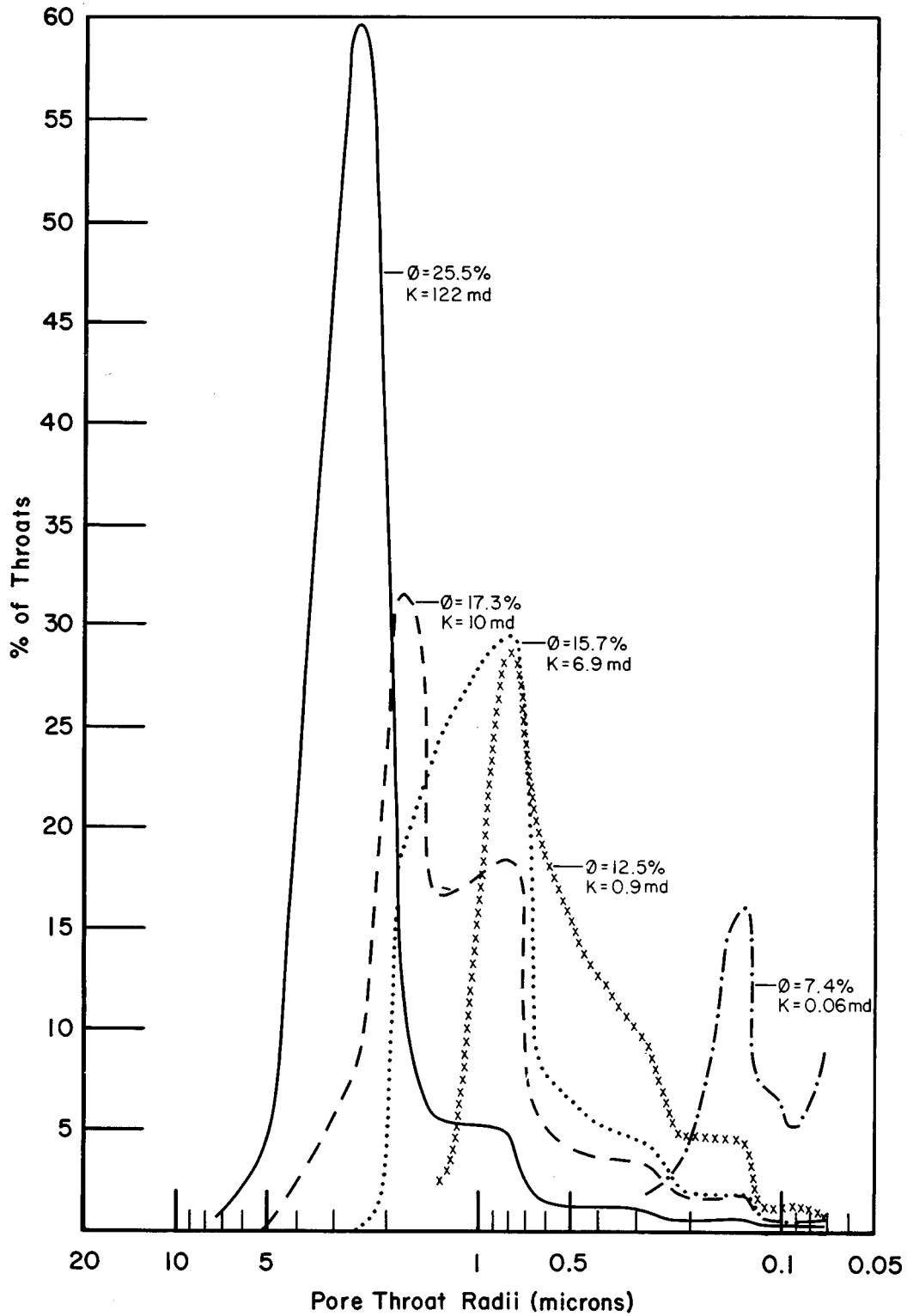


Figure 45

ZABOLOTNY OBSERVATION #1

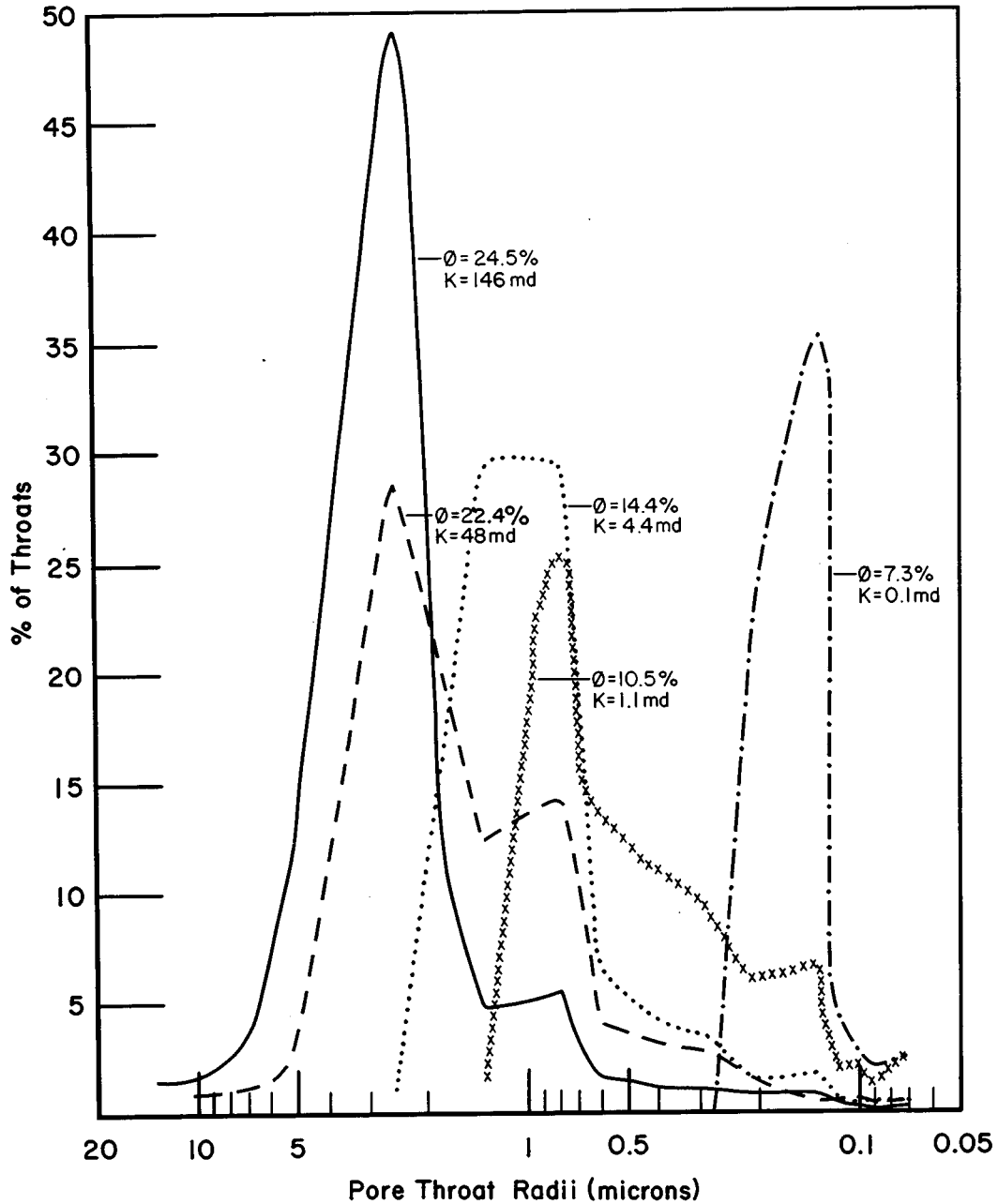


Fig. 46-Representative individual samples of pore throat radii, in microns, and percent of throats, calculated from mercury capillary pressure curves, in the Zabolotny Observation Well No. 1. Five (5) characteristic pore throat radii vs. porosity and permeability relationships as described in Fig. 45, have been isolated into groups.

ZABOLOTNY OBSERVATION #2

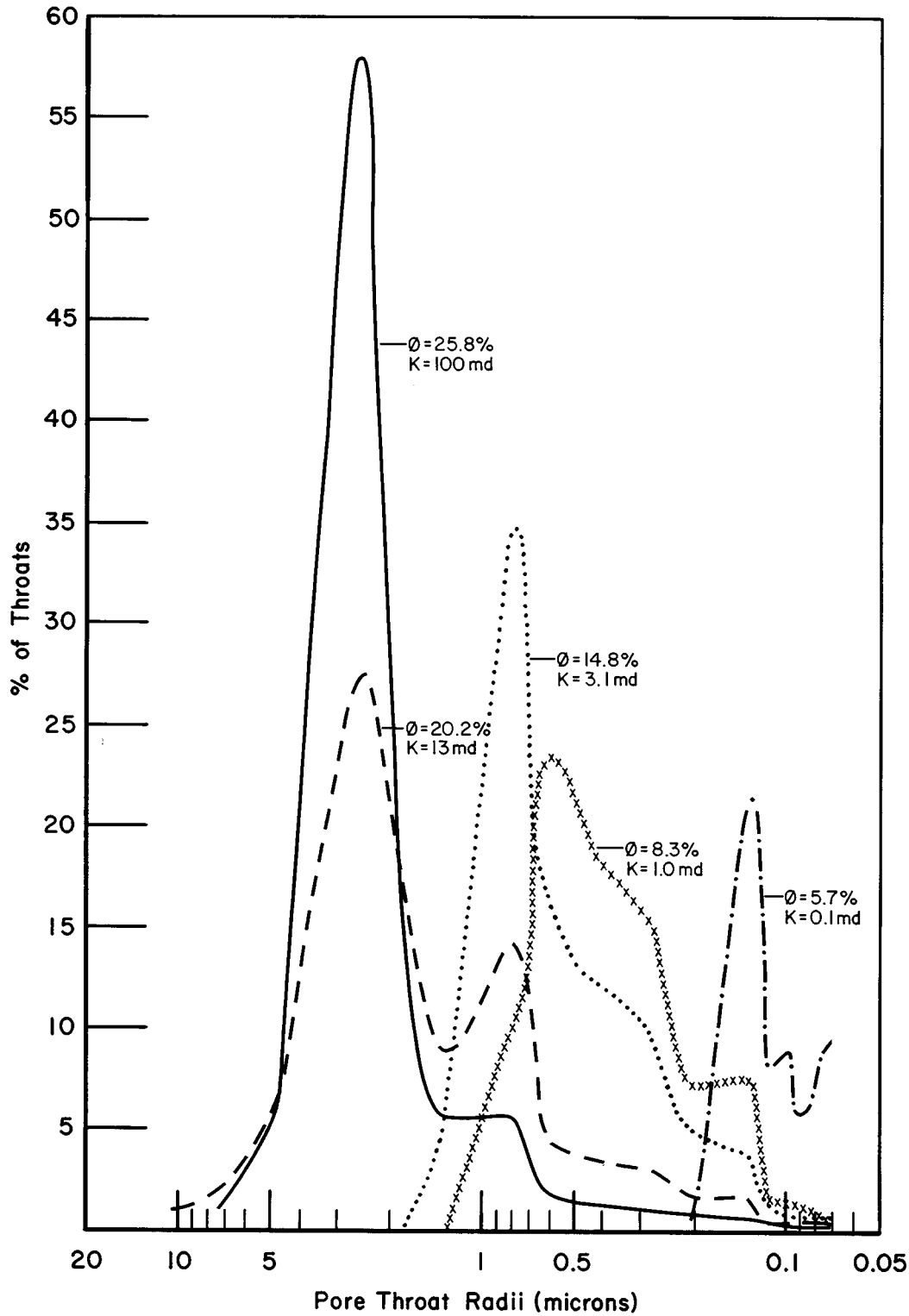


Fig. 47—Representative individual samples of pore throat radii, in microns, and percent of throats, calculated from mercury injection capillary pressure curves, in the Zabolotny Observation Well No. 2. Again, 5 characteristic pore throat radii vs. porosity and permeability relationships, as described in Fig. 41, have been isolated into groups.

ZABOLOTNY OBSERVATION # 3

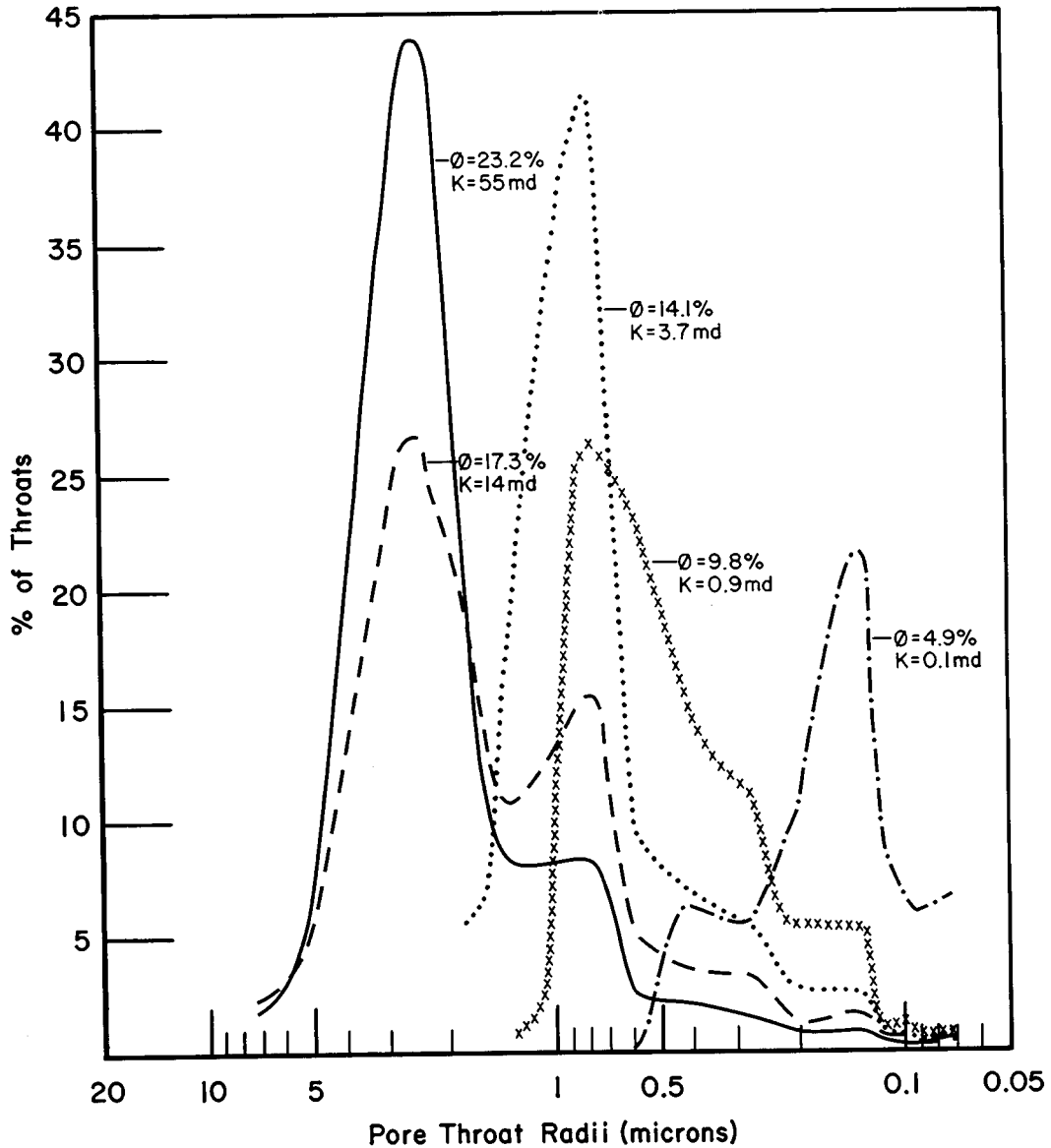


Fig. 48-Representative individual samples of pore throat radii, in microns, and percent of throats, calculated from mercury capillary pressure curves, in the Zabolotny Observation Well No. 3. The same five (5) characteristic pore throat radii vs. porosity and permeability relationships, described in Fig. 45, have been isolated into groups, as in the preceding wells.

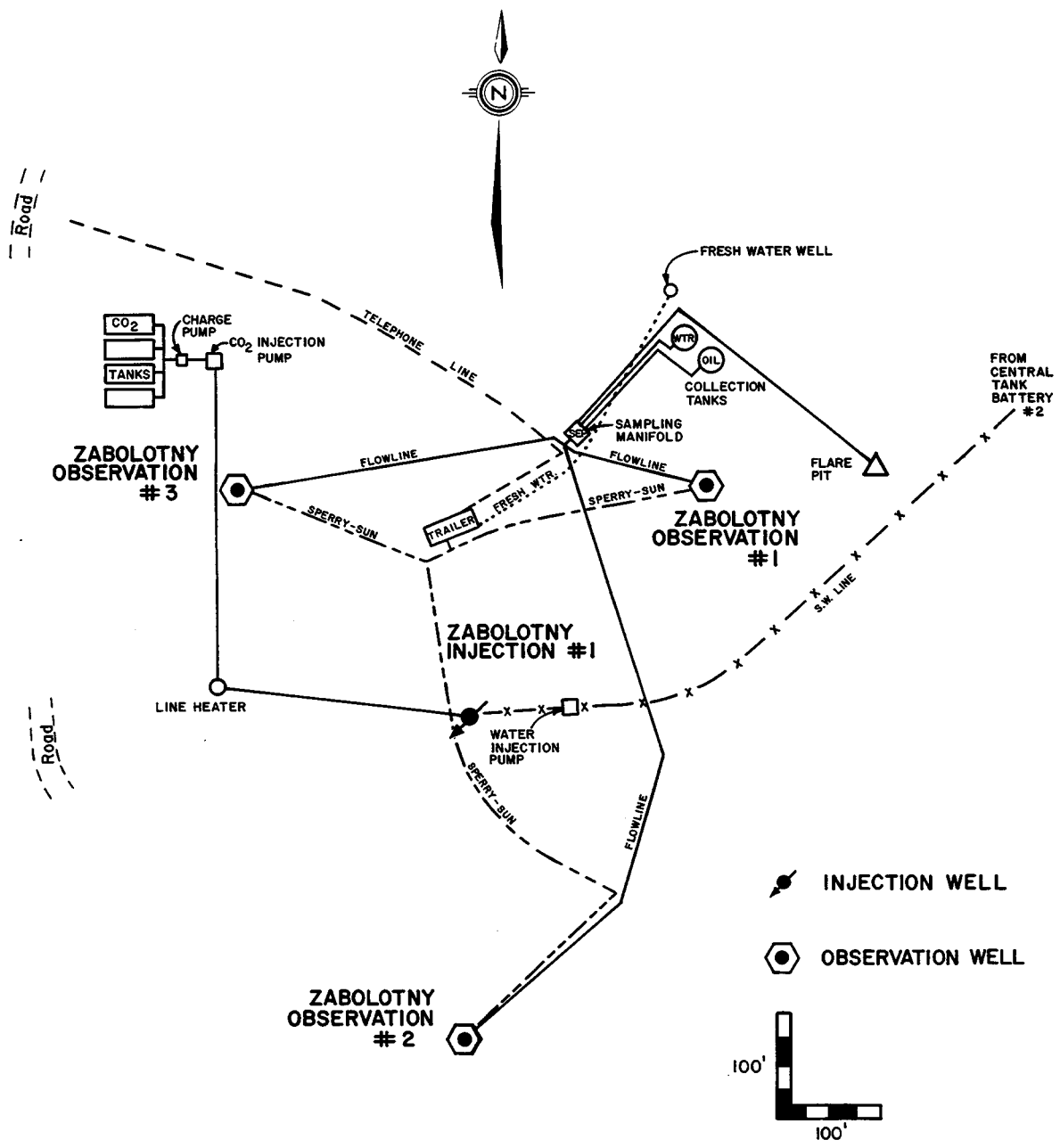


Fig. 49—Layout of surface equipment of the Little Knife CO2 minitest site. Modified after Nettle, Lindsay, and Desch²⁵.

CARBON DIOXIDE INJECTION SYSTEM

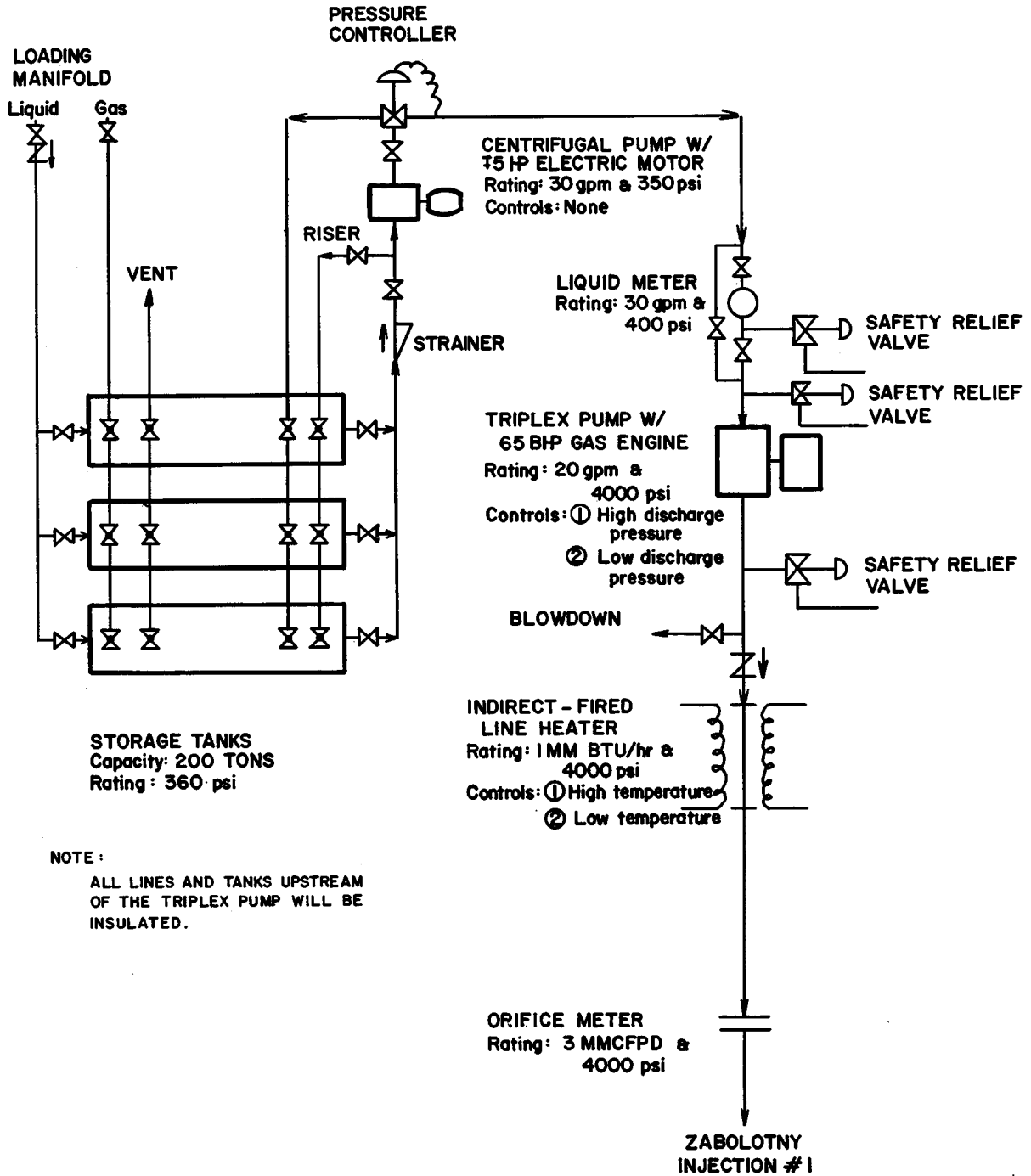


Fig. 50—CO₂ injection system for the Little Knife CO₂ minitest. It consists of storage, metering, pumping and vaporizing sections.

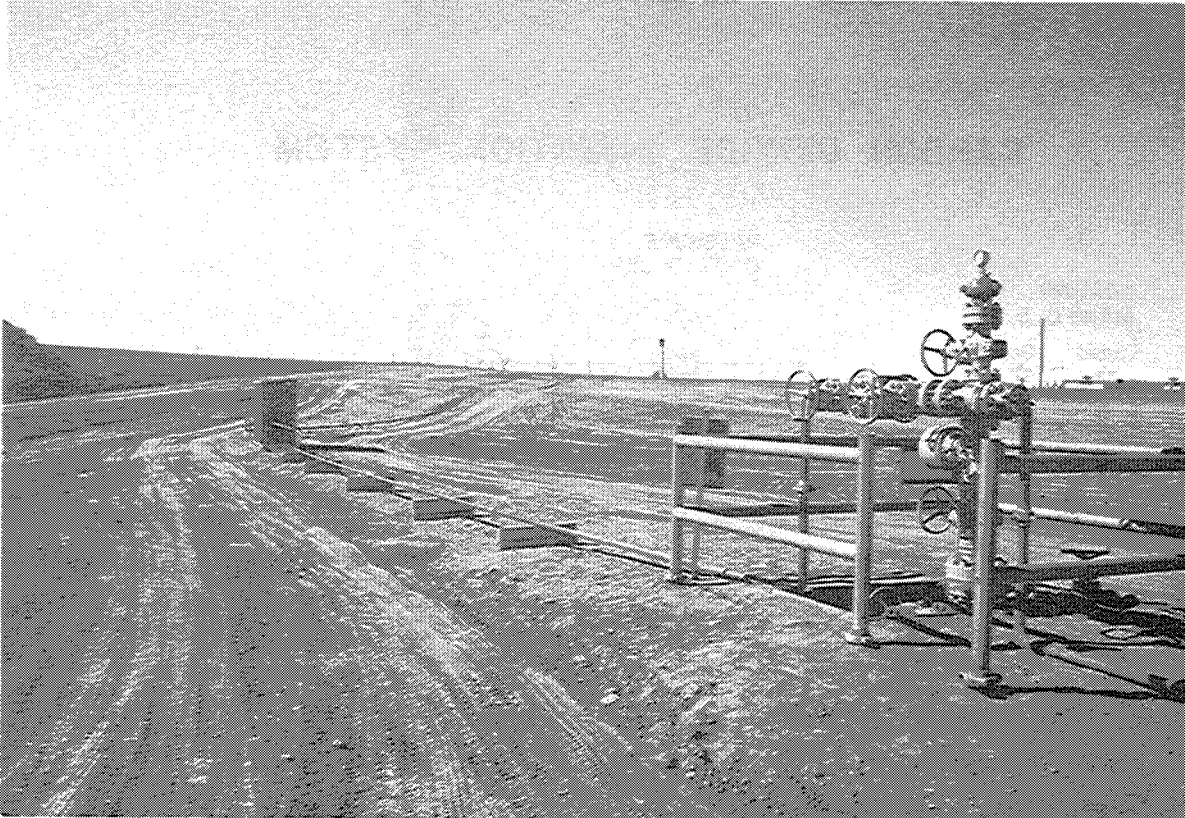


Fig. 51-Zabolotny Injection Well No. 1 with CO₂ injection line, gas meter shed, line heater and CO₂ storage tanks in the background.



Fig. 52-Fifty (50) ton capacity liquid CO₂ truck used to haul and store CO₂.

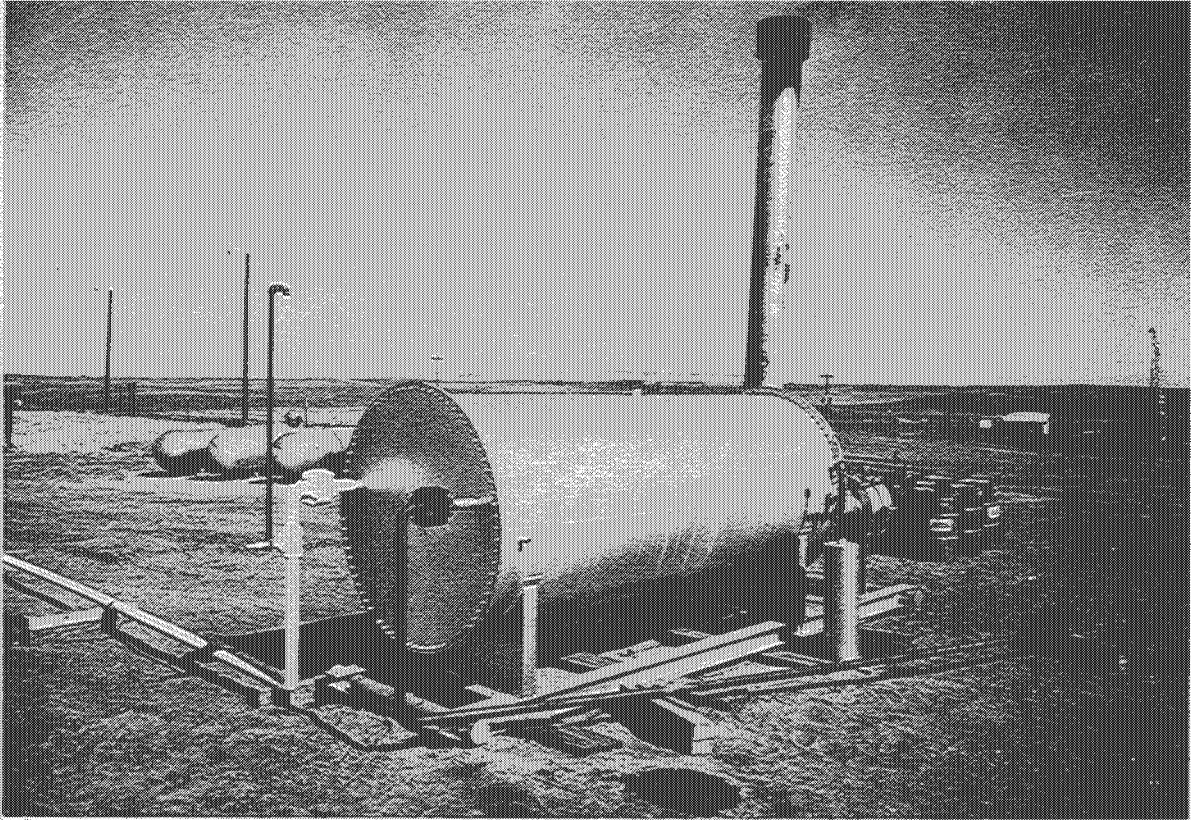


Fig. 53-Glycol indirect line heater which is downstream of the CO₂ injection pump. Propane fuel tanks are in the background.

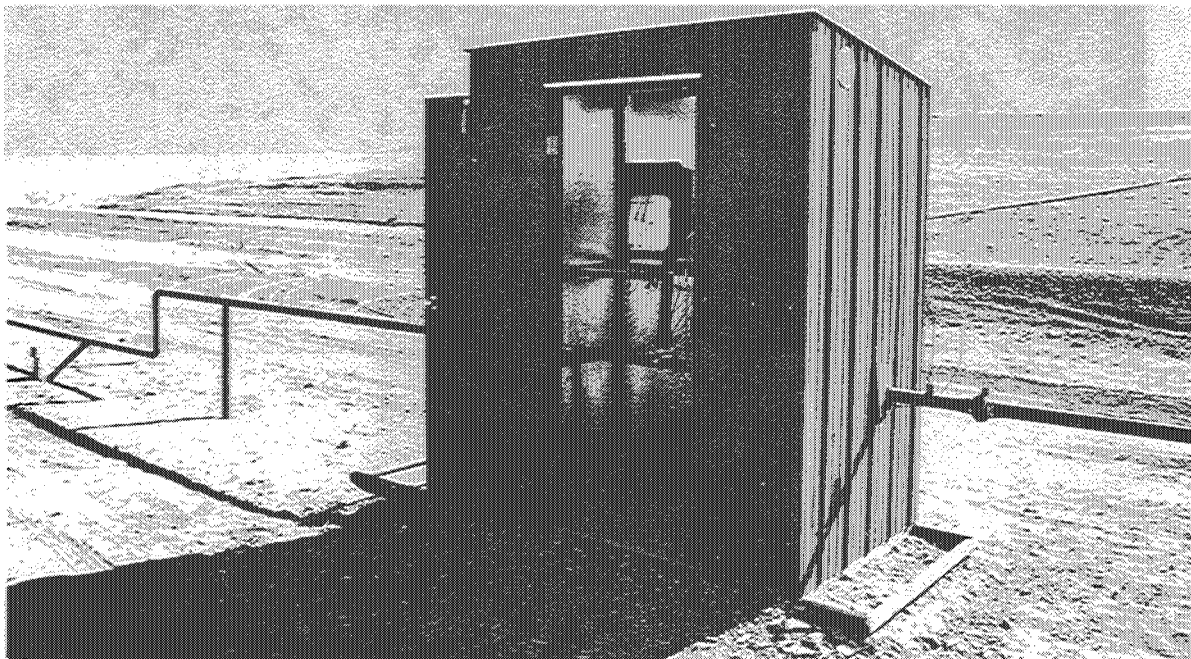


Fig. 54-CO₂ gas meter shed downstream of the line heater at Little Knife CO₂ minitest site.



Fig. 55—Manifold system at back of CO₂ storage tanks. The charge pumps for the CO₂ injection pump are located on the ground, in the middle of the four tanks.

WATER INJECTION SYSTEM

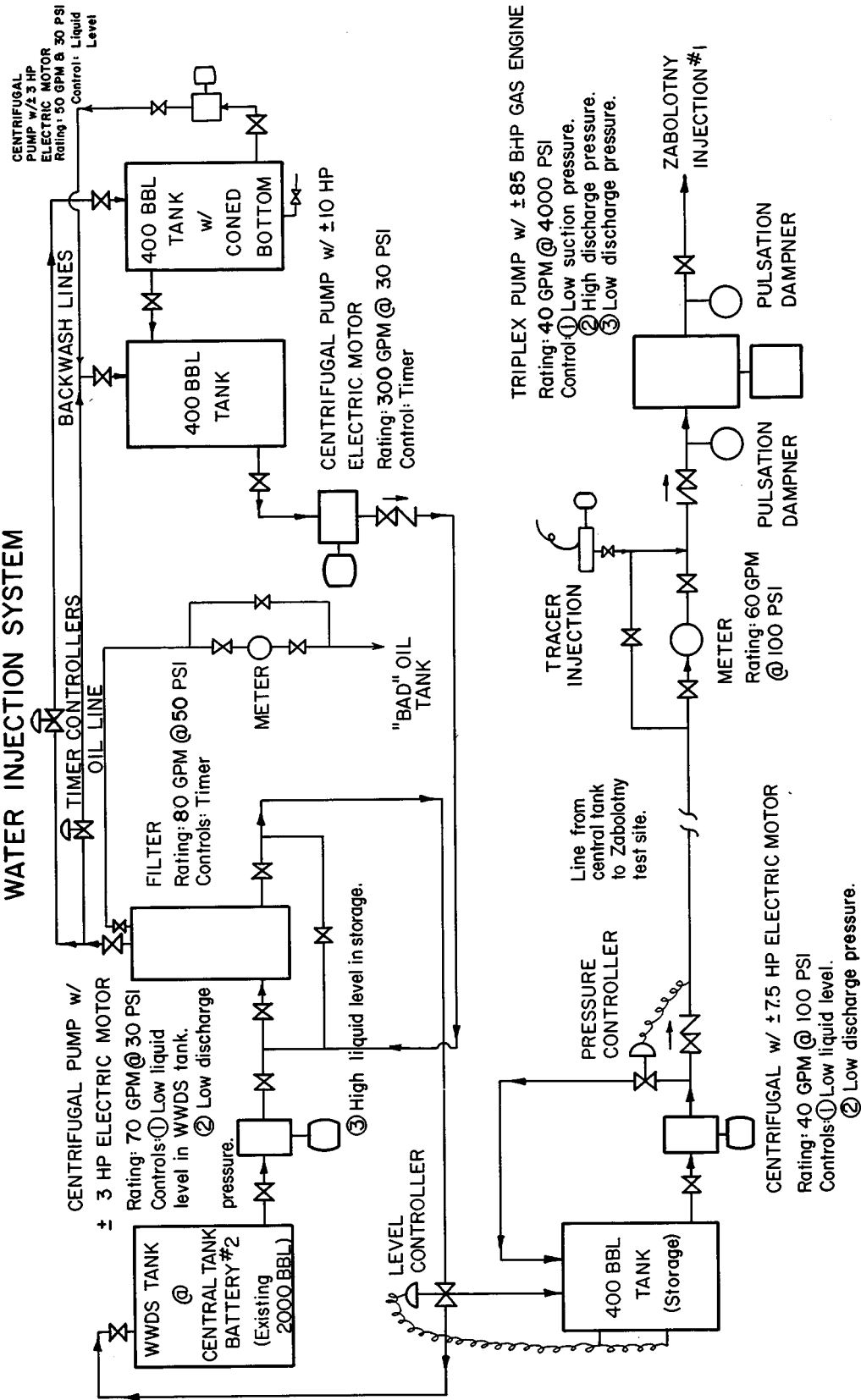


Fig. 56-Water injection system for the Little Knife CO₂ minitest. It will consist of two segments. One segment is the filtering system. The second segment is the injection pump.



Fig. 57-Salt water filter building with filtered salt water, flush, and sludge tanks.

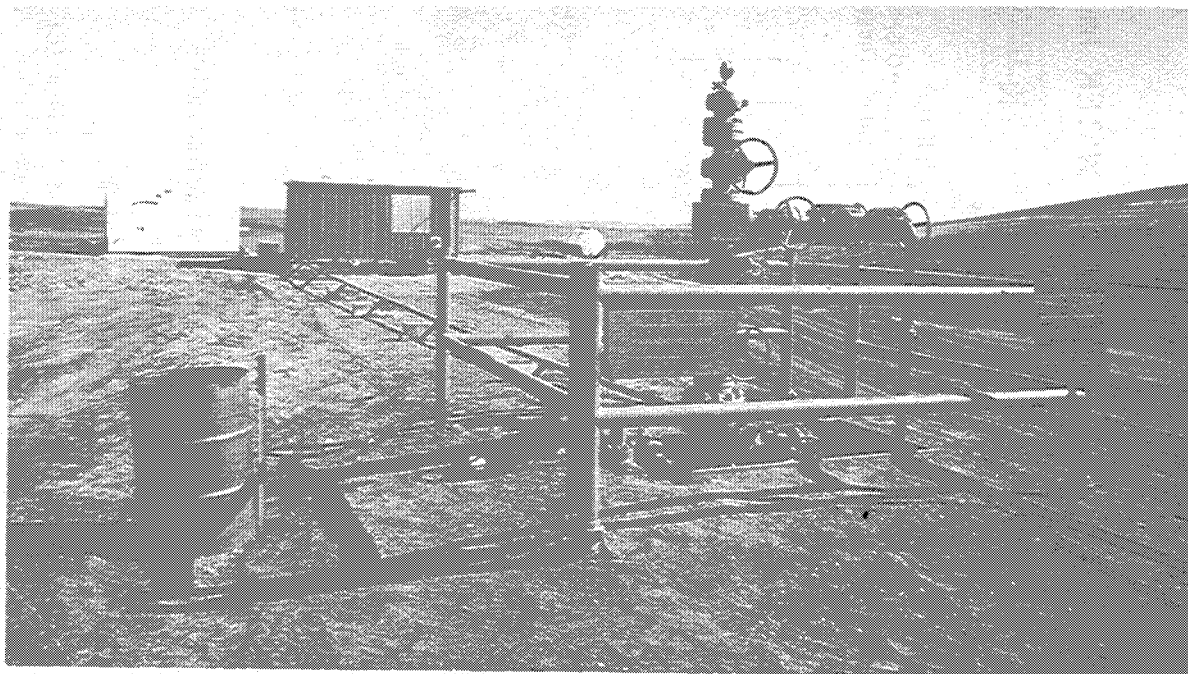


Fig. 58-Zabolotny Injection Well No. 1 with salt water injection line, salt water injection pump building and alcohol tracer storage tank in the background.

FLUID SAMPLING SYSTEM

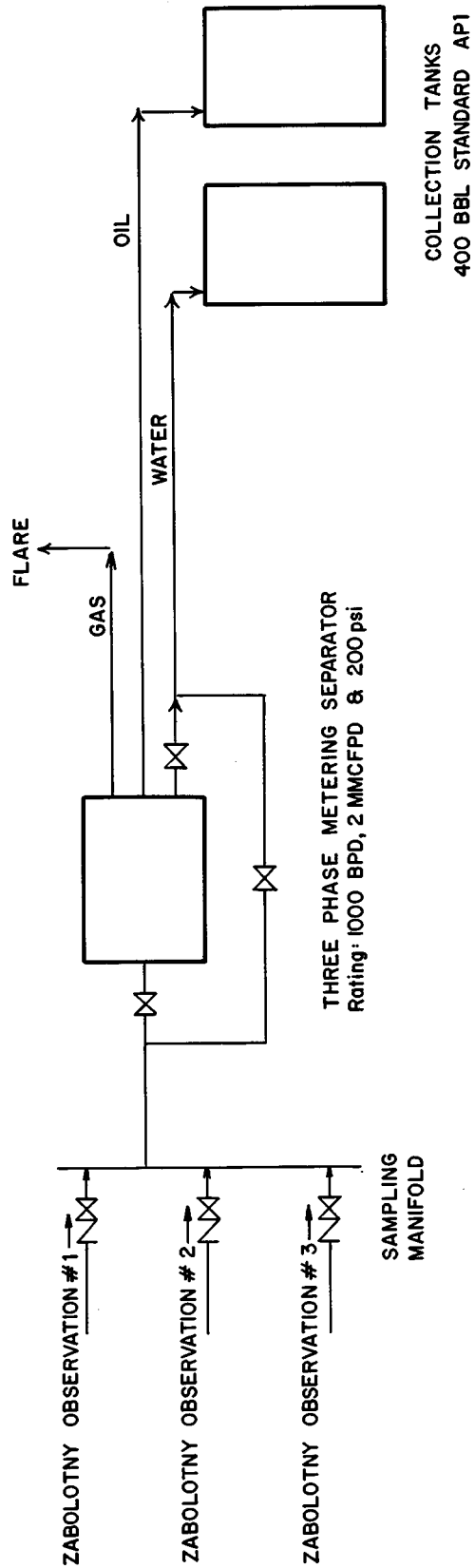


Fig. 59-Fluid sampling system for the Little Knife CO₂ minitest. It will consist of a three-phase metering separator. It will be equipped with standard instrumentation, along with level controls for both oil and water and meters for gas, oil and water.

